CHARACTERISTICS AND APPLICATION OF A LASER IONIZATION/EVAPORATION SOURCE FOR TANDEM MASS SPECTROMETRY

by

ROBERT JOHN PERCHALSKI

A DISSERTATION PRESENTED TO THE GRADUATE SCHOOL
OF THE UNIVERSITY OF FLORIDA
IN PARTIAL FULFILLMENT OF THE REQUIREMENTS FOR THE
DEGREE OF DOCTOR OF PHILOSOPHY

UNIVERSITY OF FLORIDA

1985

To my parents with love.

ACKNOWLEDGMENTS

I wish to express my sincere appreciation to Dr. Richard A. Yost for his direction and faith in this project. I am also grateful to the members of my committee: Dr. James D. Winefordner whose initial advice should have been given more serious consideration and whose instrumentation helped to make this project more successful; Dr. B.J. Wilder whose continuing personal and professional support over the last 13 years has been invaluable in the attainment of this goal; Dr. John G. Dorsey who offered advice and encouragement; Dr. L. James Willmore who offered counsel and expertise; and Dr. John Eyler who took over where Dr. Willmore left off. I also appreciate the generosity of Dr. Martin Vala who loaned us the laser.

Thanks are also due to Drs. Neal Brotherton and Dean Fetterolf who got me started, and to the members of the research group who freely gave advice and assistance. Special thanks are due to Dr. Jodie V. Johnson who kept the instrument running, and to Dr. Edward Voigtman for help with the laser and the storage oscilloscope experiments.

The LAMMA experiments were completed through the kindness of Dr. David M. Hercules of the Department of Chemistry, University of Pittsburgh. The assistance of Dr. Edward J. Hammond in the animal experiments and Dr. William Ballinger in the preparation of samples for LAMMA analysis is appreciated.

This project could not have been completed without the help and cooperation of my children, Matthew, Abby, Ben, and David.

Finally, for her support and patience, I thank my wife, Lynn.

TABLE OF CONTENTS

LIST OF TABLES

LIST OF FIGURES

Abstract of Dissertation Presented to the Graduate School of the University of Florida in Partial Fulfillment of the Requirements for the Degree of Doctor of Philosophy

CHARACTERISTICS AND APPLICATION OF A LASER IONIZATION/EVAPORATION SOURCE FOR TANDEM MASS SPECTROMETRY

By

Robert John Perchalski

May, 1985

Chairman: Richard A. Yost
Major Department: Chemistry

An instrument system is proposed that is based on tandem mass spectrometry (MS/MS) and a focused laser for vaporizing selected areas of samples within the ion source so that the molecular components of the sample can be identified and quantitated. This instrument is similar in principle to a commercially available laser mass spectrometer (LAMMA), but additional selectivity is possible with the proposed system because it has two stages of mass analysis, making molecular analysis feasible. The instrument used for this study consists of a triple quadrupole mass spectrometer and a single-shot, coaxial flashlamp-pumped dye laser, interfaced through a simple system of mirrors and a lens, mounted near the ion source, which serves as a vacuum seal and focuses the laser radiation on the sample.

The system is evaluated by observation of short-lived (< 1 ms) and long-lived (> 1 ms) events after the laser is fired. Ion signals lasting several seconds are observed when samples are irradiated in a heated chemical ionization (CI) source. These signals are a combination of a desorption event and a vaporization event, and desorption CI is used as a model to characterize the laser-initiated processes. The latter are called Laser-Induced or Laser-Enhanced Desorption CI. The current system proved unsatisfactory for quantitative analysis because the time limitations of the instrument combined with a concentration-dependent ion signal lifetime produced calibration curves with low correlation coefficients. Qualitative confirmation of the presence of a drug in rat liver was obtained, however, after laser vaporization of a small sample of intact tissue within the ion source.

Recommendations are made for overcoming the time limitations of the present system so that a microprobe capable of molecular analysis of heterogeneous and compartmentalized biological samples might be developed.

CHAPTER I

INTRODUCTION

The purpose of this work was twofold: first, to design, construct, and evaluate a laser evaporation/ionization source for a triple quadrupole mass spectrometer, and second, to determine the feasibility of developing a milli- or microprobe, based on a microscopically-directed sampling laser interfaced to a tandem mass spectrometer that is capable of molecular analysis of heterogeneous samples. Such an instrument could be used for chemo-morphological mapping of geological, metallurgical, environmental and astronomical samples, and of intact plant and animal tissues by direct, in situ elemental and molecular analysis. The major use of this instrument, however, is anticipated in the biomedical sciences, in which samples and their chemical constituents are highly compartmentalized from the organism to the ultrastructural level.

Overview of Current Technology

Much of the work of medical, agricultural, biochemical, and pharmacological research involves experiments designed to provide insight into the chemical and physical processes occurring at the cellular and subcellular levels. Elucidation of these processes is

sought to define, in molecular terms, the normal chemical condition of organisms of interest from microscopic flora and fauna to man, abnormalities in this chemical condition that are evident as disease or deficiency, and effects and mechanisms of action of the various curative measures employed to produce and maintain an optimal state of being. The experiments are conducted in five general areas: morphology, physiology, pharmacology, histochemistry, and chemistry. Morphological studies relate shape and structure with physical function. Physiological and pharmacological studies define organism and substructure reaction to endogenous and exogenous (both therapeutic and anti-therapeutic) chemical species, respectively. Histochemical studies relate, usually indirectly and qualitatively, chemical species, and anatomical structure. Chemical analysis also relates chemical species with structure but has greater potential for quantitation through direct determination of the compounds of interest. Each of these methodologies, when used in this context, is site-specific at various levels of spatial resolution, and depends wholly or in part upon microscopy (1, 2).

Methodologies for Physical and Chemical Analysis

Morphology is generally the initial subject of interest and is pursued at three levels, delineated by the instruments used. Macrostructural surveys include all work done with the unaided eye and therefore are limited to gross anatomical correlations in large organisms and organ systems with dimensions measured in meters to millimeters. Microstructural studies are conducted with the light

microscope in its various forms and can delve deeply into organ systems in large species or give information of more general nature for one- or few-celled organisms. Dimensions are measured in millimeters to micrometers. Ultrastructural investigations are conducted with the electron microscope and give information at the cellular and subcellular levels with dimensions normally measured in micrometers to nanometers.

Physiology and pharmacology are usually restricted to micro- to macrostructural studies, since the probes used to measure or observe the chemical or physiological response are incapable of spatial resolution below the cellular level (5 to 10 μm) in a living organism, or in a normally functioning tissue or cellular preparation. These studies include clinical evaluations of drug effects on animals and humans (pharmacological), and nutritional studies designed to evaluate effects of and requirements for biomolecules such as vitamins, amino acids, hormones, and transmitter substances necessary for proper nervous system function (physiological). In many cases, subject response coupled with chemical analysis of easily obtained body fluids (blood or urine) can give the information sought, since all foreign substances and most biomolecules present in an organism are in dynamic equilibrium with the circulatory system. At the lower limits of spatial resolution for these studies, test chemicals are usually applied by microiontophoresis (3) and responses are monitored by potentiometric (4) or voltammetric (5) microelectrodes.

The gross chemical analyses which necessarily precede physiological studies and coincide with pharmacological studies can be carried out by

usual methods (chromatography, ultraviolet, visible and infrared spectrophotometry, nuclear magnetic resonance and mass spectrometry, atomic absorption, emission and fluorescence spectroscopy) applied to physiological fluids and tissue homogenates. As the work progresses, however, to the stage at which a more exact localization of active substances is desired, more spatially selective techniques must be used which usually place more stringent requirements on the analytical techniques, particularly with regard to sensitivity. The techniques that are most used for localization studies are based on three general methodologies, histochemistry, autoradiography, and direct chemical analysis of microdissected tissue samples or subcellular fractions obtained by density gradient centrifugation.

The histochemical methods rely upon chemical, enzymatic or immunological reactions which involve the molecule of interest, an enzyme specific for the molecule of interest, an inhibitor of that enzyme, or an antibody created to bind specifically to the molecule of interest, as reagents to give, either directly or indirectly, a product visible with a light or electron microscope (6). The method is devised so that all reactions occur rapidly in succession, and the final visible product is synthesized at and does not diffuse from the location of the reactant of interest. Potential for qualitative analysis is predicated on the specificity of the chosen reagent, enzyme or antibody for the molecule of interest. Insuring this specificity presents the most challenging problem during method development. Quantitative analysis is possible by densitometry if normal stains are used, or by fluorometry if

the final product is naturally or can be made fluorescent with a fluorogenic reagent or fluorescent-labeled enzyme or antibody (7-9). The introduction of raster beam microscopes, coupled with computerized data acquisition and imaging techniques, have contributed greatly to improving the accuracy of these methods (10).

Autoradiography is a direct method of localizing radioactively-labeled molecules of interest at the light and electron microscope levels (11). The system under investigation is sacrificed and sectioned at an appropriate time after the labeled compound is introduced. The sections can be treated as usual for the microscopic method of choice (staining) and are then coated with a thin layer of silver halide emulsion (gelatin). Resolution is determined by the homogeneity of the emulsion, the size of the particles, and the thicknesses of tissue and emulsion layers. After exposure of the emulsion for a suitable period of time, which depends upon the half-life of the nuclide (normally several weeks to a few months), the emulsion is developed and the sample is subjected to microscopy.

Direct chemical analysis of anatomical structures isolated by microdissection or density gradient centrifugation can sometimes be performed using scaled-down versions of normal analytical methods. Typical methods for microdissection of brain, however, allow differentiation of more than 220 cell types and areas of a rat brain (whole brain wet weight: 1.5 g) with samples measuring 200 - 500 μm square x 100 μm thick, a volume of 4 - 25 nL (12), and methods for isolation and analysis of single brain cells (20 - 50 pL) have been

reported (13). As sample size is decreased to effect a more exact localization, enzymatic cycling methods must be used (14) which take advantage of the chemical amplification (10^4-10^8) afforded by the continuous recycling of enzymes in a reaction. This catalytic effect increases the concentration of the substance chosen as an indicator to the point where it can be accurately measured. These methods have generally been applied to determination of endogenous substances, biomolecules and enzymes, rather than exogenous substances.

Microbeam and Probe-Type Instruments

Another methodology that has been developed is the use of microbeams of electrons, ions or light, not only to visualize microstructures, but also to obtain a simultaneous chemical analysis of the surface by analysis of emissions of electromagnetic radiation, electrons and ions resulting from the interaction of the incident beam with the sample. The first such instrument, patented in 1947 and commercially available in the late 1950s, was the electron microprobe (15) which uses a focused (0.1 to 3 μm) beam of electrons to produce X-rays characteristic of the elements in the sample. Other probe-type instruments that followed include those based on Auger electron spectroscopy, ion backscattering spectrometry, electron spectroscopy for chemical analysis (ESCA) and secondary ion mass spectrometry (SIMS) (16, 17). The SIMS instruments gave rise to the ion microprobe and ion microscope, which differ in the method of obtaining an image of the sample. The microprobe uses a focused beam of ions to scan in raster fashion over the sample surface. The microscope uses a flood beam about

250 to 300 μm in diameter to image an area of the surface. Final images of the secondary ions emitted maintain a direct relationship to the point of origin at the sample surface (18).

Laser-based instruments. Shortly after the introduction of the laser in 1960 (19), it was incorporated into a microprobe instrument based on emission spectrography (20), and emission of electrons, ions and neutral atoms was observed from conductors, semiconductors and insulators irradiated in a mass spectrometer (21). Several reviews discuss the early work in both of these fields, concentrating primarily on emission spectroscopic instruments, laser characteristics, and interactions of laser radiation with solid surfaces (22-24). The most recent spectroscopy-based instrument to be introduced commercially was the laser Raman molecular microprobe (MOLE) (25). Point or global illumination was possible to allow recording of a complete Raman spectrum of a particular portion of a sample or mapping of a larger area by selecting a Raman line characteristic of an analyte of interest. Although this instrument was capable of identifying some molecular species, the complexity of the identifiable molecules and of their environment was limited. Most applications to date have shown identifications of inorganics, or simple organics deposited in biological systems in concretions of essentially pure crystals. This system is no longer commercially available, but work is still continuing in this area (26). Another microprobe instrument based on nitrogen-pumped dye laser-excited atomic fluorescence of analytes after site-

specific sample evaporation by a second microscopically-directed laser (ruby) has also been reported (27).

Laser-based mass spectrometers. Lasers have been applied extensively in mass spectrometry (MS) over the past 20 years as a means of rapid vaporization and ionization of samples in the ion source. Conzemius and Capellan (28) have reviewed much of the work conducted prior to 1980, including instrument system characteristics (lasers and mass spectrometers) and applications. This review has been updated to include all work published through 1982 (29). In 1975, Hillenkamp et al. (30) reported the use of a LAser Microprobe Mass Analyzer (LAMMA) which was designed primarily for in situ determination of physiologically significant elements in intact biological samples. The instrument, introduced commercially in 1977 (LAMMA 500), is based on a time-of-flight mass spectrometer with a Q-switched, frequency-multiplied Nd-YAG sampling laser and a He-Ne spotting laser, both directed and focused through a high quality microscope. The system has been described (31), and two reviews have covered sample requirements, performance characteristics (32), and applications to structural analysis (33). Proceedings of a symposium on analysis with LAMMA have been published (34) and include articles on characteristics of laser spectra of various molecular classes (35, 36), preparation of biological specimens (37-39), and techniques for quantitative standardization (40, 41). A second generation instrument (LAMMA 1000) has been introduced (42-44) which allows for analysis of bulk samples rather than restricting the analyst to the use of thin sections, as did the LAMMA 500.

Molecular analysis with current probes. The characteristic that links all of the above microprobe instruments is their almost exclusive application to elemental analysis. This is not to say that they have not been used to obtain spectra of molecules; however, there is an almost complete lack of applications for which the microprobe capability has been used in real, heterogeneous samples for qualitative or quantitative determination of molecules. In fact, in a search of the literature, only four such applications were found (two for the MOLE and two for the LAMMA). In three of these (25, 39, 45), the analysis succeeded because the spatial resolution of the laser beam allowed sampling of microcrystals or pure concretions of analyte, and not because of the resolution or chemical specificity of the spectrometric method. The only application that succeeded in identifying a molecular species in an intact, heterogeneous sample involved detection of a fungal metabolite, glyceollin, in plant tissue with LAMMA (46). In this study, two ion masses indicative of the metabolite were observed as the infection boundary was crossed. Part of the problem is that these instruments were never really designed to do molecular analysis. It is not, however, unrealistic to expect that the considerable selectivity necessary for molecular analysis is obtainable with appropriate combinations of currently available methodologies. In fact, several review articles on mass spectrometry and tandem mass spectrometry that have come out of the laboratory of R.G. Cooks in the past four years have included some reference to a "molecular microscope" (47-51),

although no specific instrument has been described. The current project grew out of a desire to begin working toward this ideal.

Projections for a molecular probe. Of the three instruments described above that are capable of localized molecular analysis, the laser mass spectrometer was thought to be the most promising. Due to the non-exclusive nature of the electromagnetic spectra of molecules (i.e., all organic molecules contain essentially the same types of bonds which give rise to signals contained within a limited portion of the electromagnetic spectrum for any given method), the selectivity and specificity of a microprobe instrument based upon optical (Raman) spectroscopy would be seriously limited. The molecular reordering that occurs during surface bombardment with energetic ion beams (50) would ultimately limit the resolution obtainable with an instrument based upon SIMS. The primary deficiency that precludes molecular analysis of heterogeneous samples with the LAMMA is the lack of confirmation of the identity of an ion corresponding to a specific mass peak. Elemental analysis is possible because molecular interferences can be eliminated by using a high power density (greater than 10^9 W cm^{-2}) and confirmation can be based on relative isotopic abundances for the analyte. This deficiency might be corrected by substituting a tandem mass spectrometer for the current single stage mass spectrometer to allow online verification of the identity of selected ions by sequential fragmentation and mass analysis steps.

Tandem mass spectrometry. Modern tandem mass spectrometry (MS/MS) was developed in the laboratories of Cooks (52) and of McLafferty (53)

using reversed-geometry, double-focusing instruments for Mass-analyzed Ion Kinetic Energy Spectrometry (MIKES). The introduction of the triple quadrupole mass spectrometer by Yost and Enke (54) simplified the automation of tandem mass analysis, increased the allowable speed of data acquisition, and brought the technique within reach of laboratories other than those specializing in design and construction of unique MS systems (similar instruments are now available from several manufacturers). A recently published volume (55) summarizes the developments and applications of this relatively new field. A tandem mass spectrometer consists of an ionization-fragmentation region followed in space (tandem sector and quadrupole instruments) or time (Fourier transform ion cyclotron resonance instruments (56)) by a mass selector-analyzer region. Therefore, a molecular ion or fragment produced in the ion source can be selected by the first mass analyzer, fragmented, usually by collisionally activated dissociation (CAD), and a complete spectrum of the fragments can be obtained by scanning the second analyzer. Carrying this process to its limit, a single pure compound can be totally characterized by obtaining CAD spectra for the molecular ion and each fragment produced in the ion source; or a mixture may be characterized by using a soft ionization technique producing primarily molecular ions with little fragmentation, and obtaining a CAD spectrum for each component. Used in this way, the instrument is analogous to a chromatograph/mass spectrometer system; however, the relatively lengthy chromatographic separation is replaced by a nearly instantaneous mass separation. This decreases analysis and method

development time, but more importantly, allows additional modes of operation that require simultaneous presence of signals from all analytes of interest. An example of full use and an explanation of these special MS/MS operating modes are given in a report describing a rapid, general method for detection and structural elucidation of drug metabolites (57).

The recording of mass spectra is a statistical process in that the reproducibility of relative ion intensities is dependent upon the length of time the ion signals are present, and the length of time available for monitoring each mass of interest. Therefore, the primary problem associated with interfacing a laser with a mass spectrometer is a temporal one, since the ion signal resulting from interaction of a pulsed laser (pulsewidth = 10^{-8} to 10^{-6} s) normally has a lifetime of less than a millisecond. Zackett et al. (58) used a laser pulsed at 10 Hz to obtain MS and MS/MS spectra of sucrose deposited on a silver foil. They reported that a 10 ns pulse gave ions for 300 μs in a chemical ionization (CI) source maintained at 0.1 torr with isobutane and for 1.5 ms at a source pressure of 0.5 torr. The same group identified a naturally occurring quaternary amine in cacti using laser desorption MS/MS after extracting the plant material and evaporating the extract on a silver or platinum foil (59). They used a CI source maintained at 0.5 torr with isobutane, and concluded that the CI conditions contributed only to increasing the ion signal lifetime by causing more efficient extraction of ions from the source, and not to the actual ion formation process. Cotter (60), however, has used an

auxiliary chemical ionization source to take advantage of the abundant and relatively long-lived neutral species desorbed by the laser as discussed by Ready (61). A molecular ion for guanosine was recorded with a lifetime of 4 ms after a 40 ns laser pulse.

Overview of Present Work

The scope of the present work will include all aspects of interfacing a single shot-laser with a tandem quadrupole mass spectrometer, and prolonging the signal obtained upon interaction of the laser radiation with a solid sample. Chapter II will cover the work that has been done to develop an understanding of the interaction of laser radiation with matter and the processes leading to ion formation in laser desorption mass spectrometry. Chapter III will describe the instrumental systems and procedures used in this study. The capabilities of a commercially available laser microprobe (LAMMA 500) will be evaluated along with those of the triple quadrupole mass spectrometer for localization of species of interest (Chapter IV). The characteristics of the new system will be studied with respect to short-lived (Chapter V) and long-lived (Chapter VI) processes, so that recommendations can be made for future research efforts (Chapter VII) in the development of a microprobe capable of site-specific molecular analysis of heterogeneous and compartmentalized samples. Finally, an attempt will be made to answer a question which may make the development

of a molecular microprobe-microscope for analysis of biological samples somewhat academic; that is,

> Although a molecule may be present in tissue, is it in a form that is recoverable by direct vaporization or is it incorporated into membranes, proteins and anatomical structures in such a way as to make it unrecognizable?

This question may not have a single answer covering all species of interest; however, it is important to show that discrete molecular structures can be identified by vaporization from intact tissue.

CHAPTER II

CHARACTERISTICS OF LASER-INDUCED PROCESSES IN MASS SPECTROMETRY

This chapter is primarily a literature review covering the most notable work directed toward developing an understanding of the laser-induced processes leading to ion formation. The initial discussion of absorption of laser radiation at solid surfaces covers the physical basis for prediction of the extent of temperature increase at the target surface upon laser impact. This treatment assumes that no vaporization or melting of the target material occurs, and is applicable to experiments conducted on bulk samples or substrates at power densities at which little visible surface evidence exists of laser impact. The second section deals with the investigation of the laser vaporization-ionization processes. The primary questions that have been asked include (1) what is the energy spread of particles of mass spectral significance emitted (ions, atoms, neutral and ionized molecules), and does the system exist in a state of thermal equilibrium? (2) how does the nature of the laser-induced surface emission change with time? and (3) what are the mechanisms of laser-induced ionization? The chapter ends with a discussion of the techniques used to enhance the analytical usefulness of laser-initiated processes.

Effects of Absorption of Laser Radiation at Solid Surfaces

The unique properties of laser light include a high degree of brightness, directionality and monochromaticity, these features resulting from the coherence of the emitted radiation. The laser is, therefore, a versatile source of spatially and temporally controllable spectral and thermal power. In laser desorption mass spectrometry (LDMS), it is the thermal power that is of primary interest because of the need for sample evaporation and ionization. The advantages of laser-induced vaporization over more common methods involving resistive heating lie in the high rate of heating which can approach 10^{10} °C/s and the extreme localization of the effects to areas as small as 10^{-8} cm^2 (62).

Experimental systems used for LDMS are of two basic types: (1) those in which samples are mounted on thin substrates such as electron microscope grids and sample and substrate are completely vaporized by the laser (MS instruments based primarily on time-of-flight); and (2) those in which samples are mounted on relatively thick substrates (thin foils to bulk metal stages) and are partially or totally vaporized with no apparent effect on the substrate (studies employing time-of-flight, quadrupole and sector instruments). Because the latter process is viewed as an effect on the substrate which is transferred to the sample, much effort has been expended in determining the temperature rise induced in the sample substrate by the laser radiation, and the time-course of laser-induced thermal effects.

Ready (63) has developed equations for predicting temperature variations in metallic substrates for lasers having pulse widths greater than 10^{-8} s. An assumption of local equilibrium at the site of impact is based on the premise that the energy is absorbed by electrons whose collision frequency is 10^{13} s^{-1} (the Debye frequency) so that distribution of the energy to other electrons and the lattice is instantaneous with respect to the duration of the laser pulse. A generalized (dimensionless) equation was presented by Ready to allow calculation of curves applicable to any material. This treatment was used by van der Peyl et al. (64) to calculate the time-dependent temperature variation for a stainless steel surface irradiated by a pulsed (200 ns) CO_2 laser, whose pulse profile was experimentally determined. A comparison of stainless steel (m.p. 1808°C) and quartz (m.p. 1883°C) indicated that a lower energy was required to bring quartz to its melting point (2.4 mJ) than was required for stainless steel (5.6 mJ). Lincoln and Covington (65) used a specially designed time-of-flight mass spectrometer (66) which allowed variation of specimen distance from the ion source (30 or 100 cm) and monitoring of ions or neutrals. They calculated surface temperatures for two different types of graphite having different thermal conductivities by measuring the expansion velocity of the vapor plume and calculating the vaporization temperature from gas dynamic models for the vapor expansion process. Both of these studies indicated a more rapid increase in surface temperature for materials with lower thermal conductivities, the rationale being that materials of low thermal conductivity do not allow

for rapid redistribution of the absorbed energy to the bulk substrate. Knox (67) has reviewed some of the earlier work in which surface temperatures were determined experimentally. Results for normal pulsed lasers with power densities of 10^6 to 10^8 W cm^{-2} were 2200°C to 9700°C for metals, and were relatively reproducible. Q-switched lasers with power densities of 10^8 to 10^{11} W cm^{-2}, however, gave widely variant results for similar materials.

Laser-Induced Vaporization and Particle Emission

This discussion will focus on the vaporization processes that occur when laser radiation strikes a target. The initial section will cover vaporization from the point of view of the substrate, primarily with respect to spatial and temporal characteristics. The second section will cover vaporization from the point of view of the vapor plume, and will summarize most of the work that has been done to elucidate the mechanisms of laser-induced ion formation.

Laser-Induced Vaporization

Ready (68) again appears to be the jumping-off place for discussion of the vaporizing actions of normal-pulsed and Q-switched lasers. Data have been given for depths of holes produced in a number of thick metal targets. For a normal-pulsed laser (700 μs pulsewidth), the depth was dependent on thermal conductivity of the substrate at low laser power density, but became independent of this property at higher power density and dependent on latent heat of vaporization of the metal. Therefore,

at low power, the material having the greater thermal conductivity redistributes the energy to the bulk phase rapidly, experiencing relatively little vaporization, whereas at higher power, energy is absorbed too fast for redistribution, regardless of the thermal conductivity, and deeper holes are produced in the material having the lower heat of vaporization. The power density, F (W cm^{-2}), at the point where heat of vaporization becomes dominant is given approximately by Eq. 2.1:

$$F \geq 2L\rho\kappa^{\frac{1}{2}}t^{-\frac{1}{2}} \tag{2.1}$$

where L is the latent heat of vaporization (J g^{-1}), ρ is the density (g cm^{-3}), κ is the thermal diffusivity (cm^2 s^{-1}), and t is the laser pulse length (s). This view is consistent with the types of laser interactions outlined by Kovalev et al. (69) and Furstenau (70), who described interactions for metals, semiconductors and dielectrics based on a model in which the extent of the interaction was determined by the concentration of free charge carriers (electrons) in the substrate and the difference between the valence band-conduction band energy gap and the photon energy of the laser radiation.

For Q-switched lasers ($F \geq 10^9$ W cm^{-2}), vaporization is not a simple matter of ablation of material at its boiling point at a front that advances into the substrate. Other processes occur, including exertion of pressure on the target by the vapor plume, allowing superheating of the surface and leading to explosive ejection of

material, and absorption of incoming laser radiation by the plume. In general, much less material is removed by short (ns), very high power density pulses than by longer pulses of lower power density.

Scott and Strasheim (71) have studied the spatial and temporal characteristics of vapor plume generation by normal-pulsed (850 μs), semi Q-switched (30 μs) and Q-switched (50 ns) lasers. Metal substrates were used and impressive photographic evidence was presented in each case. In the normal mode, vapor emission began at about 30 μs after initiation of laser action and ended at about 400 μs, even though lasing continued. This was thought to be due to scattering of incoming light by particles emitted from the surface. The vapor expanded at 8.3×10^3 cm s^{-1} with the solid angle of ejection decreasing as the crater became deeper. The semi Q-switched laser provided radiation at a higher power density and emission began after about 20 μs. No particle ejection was observed and the plume expanded at a rate of 3.2×10^5 cm s^{-1}. For the Q-switched pulse, a small spherical plasma was visible for about 20 μs. The expansion rate was greater than 10^6 cm s^{-1} and no particle ejection was seen. In all cases, the vapor plume expanded in a direction normal to the target surface regardless of the angle of incidence of the laser beam (33, 72).

Laser-Induced Particle Emission

The primary mathematical relationship found in articles dealing with LDMS is the Langmuir-Saha equation (Eq. 2.2):

$$i_+/i_0 = (g_+/g_0)\exp[(\Phi - I)/kT] \qquad (2.2)$$

where i_+ and i_0 are the positive ion and neutral molecule fluxes leaving the surface at temperature T. The quantities g_+ and g_0 are the statistical weights of the ionized and neutral states, k is the Boltzmann constant, Φ is the work function of the surface (eV), and I is the ionization potential (eV). The equation gives the temperature dependence of the degree of ionization of surface emissions (73). For substances for which I is greater than Φ, evaporation occurs at a temperature less than that required for efficient ionization (74). Datz and Taylor (75) reported that the alkali metals, the species most commonly implicated in laser-induced ionization processes, follow this equation when adsorbed on platinum and tungsten. From a review of the literature, Conzemius and Capellan (28) divided ionization efficiency into two general regions based on power densities of lasers employed. Below 10^8 W cm^{-2}, ionization efficiency was low, about 10^{-5}. Above 5×10^9 W cm^{-2}, emissions were almost completely ionized.

Energy- and Time-Resolved Studies

Measurement of the energies and time-course of emission of desorbed ions and neutrals is useful for elucidation of the mechanisms of laser desorption-ionization, and also for providing a firm basis for increasing the analytical potential of the technique. Cotter (76, 77) has recently reviewed the area of energy- and time-resolved studies, some of the most notable work having been done in his own laboratory. Numerous reports of energy spreads of elemental and molecular ions have offered conflicting evidence. The review by Ready (78) cited ion energies up to 5 keV and typical values of up to 400 to 500 eV. Bernal et al. (79),

using a Q-switched CO_2 laser (775 ns pulsewidth; 7 x 10^6 W cm^{-2}), reported time-resolved energy spreads during the 1.3 us ion pulse as 0 to 60 eV initially and rising to about 200 eV. Ion energies of up to 20 eV have been reported for the LAMMA 500 for thin non-metallic samples, and up to several hundred eV for bulk metallic samples (31). Hardin and Vestal (80), using a quadrupole instrument with samples being introduced continuously on a moving belt, reported energies of 6 to 25 eV for potassium iodide clusters and protonated and cationized guanosine ions and fragments. They reported that the observed time-of-flight distributions were dependent on laser power density, and the relative concentrations of sample and alkali salt on the belt. All work was performed at a power density of about 10^7 W cm^{-2}. Energies as low as 0.26 eV were reported by van der Peyl et al. (81) for Na^+ in a double-focusing instrument.

Cotter and coworkers have published a series of papers in which they report results obtained on a versatile time-of-flight instrument designed to allow observation of ions produced directly by the laser, or laser-produced neutrals ionized by a pulsed electron beam (82-85). An ion-drawout pulse was provided to sample the contents of the ion source at any time up to 500 μs after the laser was fired. They have used this system to resolve the convoluted profiles of laser-desorbed ions into separate contributions from prolonged vaporization envelopes and finite energy spreads. The energy spread for K^+ was 15.3 eV at 10 μs after the laser pulse, and decreased to 0.31 eV at about 44 μs. This is probably

the most accurate work that has been done to date, and while it does not negate the value of the previous work, it certainly offers a much improved method for solving the problems.

Mechanistic Studies

Early work in laser-assisted mass spectrometry was concerned mostly with elemental analysis or pattern recognition after pyrolysis of large molecules or molecular aggregates. Vastola et al. (86, 87) introduced the concept of using laser radiation for volatilization and ionization of molecules that could not be vaporized intact by the usual methods of ohmic heating. Until 1978, laser desorption continued to take a back seat to field desorption (FD), secondary ion mass spectrometry (SIMS) and the newly introduced (88) plasma desorption (PD) in the field of molecular analysis. The commercial introduction of the LAMMA 500 and the report by Posthumus et al. (89) in particular provided impetus to define the optimum conditions for laser desorption and the mechanisms of ion formation. In this work, laser desorption spectra were presented for important biomolecules which were generally considered intractable, including oligosaccharides, cardiac glycosides, steroid conjugates, antibiotics, nucleotides, nucleosides, amino acids, peptides, and chlorophyll. All gave abundant molecular ions as alkali metal ion adducts ($M+Na^+$, $M+K^+$), indicative of a process called "cationization". This study, along with others (88, 90, 91), indicated that a rapid heating rate was important for molecular ion production in preference to fragmentation and decomposition. Although most researchers have used laser power densities of 10^5 to 10^8 W cm^{-2}, Stoll and Rollgen (92)

observed the cationization process and desorption of quaternary ammonium ions (preformed ions) using a CW CO_2 laser at a power density of about 20 W cm^{-2}; however, after scrupulously cleaning the copper substrate and purifying a sucrose sample to eliminate traces of alkali metals, no molecular ions or protonated or cationized molecules were detected, even though the sucrose did evaporate.

In an effort to determine the mechanism of the cationization reaction which is predominant in laser desorption, van der Peyl et al. (93-95) performed experiments using several different instrumental configurations in which thermionically produced alkali metal ions originated in a different area of the ion source than the test compound (sucrose). Temperatures of both thermionic emitter and sample holder were monitored during resistive heating and laser heating cycles and plotted along with ion intensity curves. They proposed a model in which the laser serves to produce a steep temperature gradient at the surface with alkali metal ions thermionically emitted from the hot central zone of the laser spot (greater than 427°C) and neutral sample molecules vaporized from the relatively cooler periphery. Ion formation occurs in the gas phase as an ion-molecule reaction producing a stable, even-electron species with a positive charge on the alkali metal atom. Stoll and Rollgen (96, 97) arrived at a similar conclusion using a system in which the thermionic emitter was not completely isolated from the sample.

Heinen (98) and Hercules et al. (33) have reviewed the types of ions formed from molecules containing various functional groups. Hillenkamp (99, 100) has summarized the work reported by the most

prominent LDMS research groups, and listed some features of LD mass spectra. These features include (1) in contrast to the normal situation with resistive heating, polarity and ionic character promote desorption and ionization; (2) ions are generally even-electron species; (3) cationization by alkali and other singly-charged metal ions is common; (4) anionization has been observed but not frequently reported; (5) positive and negative ions are produced in approximately equal amounts, with less fragmentation of negative ions; (6) cluster ions are frequently seen; (7) matrix effects are observed; and (8) extent of fragmentation is dependent on laser power density. Cooks and Busch (101) have compared the various desorption ionization techniques (SIMS, FD, PD, LD) and have developed a general model for the ionization-fragmentation events that occur. The model is based on the fact that these techniques, which differ in the types of energy put into the sample result in the production of similar ion types.

Analytical Usefulness of Laser Desorption Mass Spectrometry

The utility of a laser desorption/evaporation source in mass spectrometry derives from the characteristics of the laser beam, i.e., it can be focused to sub-micrometer diameter spot sizes, contains a high thermal power, can desorb or vaporize large, polar molecules intact, and can ionize them directly or present them to the instrumental system in a state suitable for ionization by other means. The primary tasks associated with coupling a laser with a mass spectrometer are (1)

prolonging the laser-induced events so that they persist for the time required for the mass spectrometer to acquire statistically relevant data; or (2) designing the mass spectrometer so that it can acquire such data during the lifetime of laser-produced ions. Ion lifetimes have been extended by operating the ion source in the chemical ionization mode (102). This not only takes advantage of the neutral species that are desorbed, but also increases the lifetime of ions produced directly by the laser. Using a renewable surface with a pulsed or CW laser provides a continuous signal, but this is not ideal for microprobe work, because the intrinsic nature of the investigation precludes the assumption of a renewable surface (i.e., why use a microprobe if the sample is homogeneous enough for the surface to be considered renewable). A variation of this approach involves pulsing the laser in synchronization with mass scanning so that only one mass is monitored for each laser pulse (repetitive laser desorption (103)). McCrery et al. (104) used ion storage in a Fourier Transform mass spectrometer and were able to digitize and average twelve decay transients for each laser pulse. Adapting the mass spectrometer to the laser duty cycle has been done in the LAMMA instruments with time-of-flight mass analysis. Other workers have used sector instruments with photoplate or array detectors to simultaneously detect ions over a certain mass range. Since the objective of this work is to evaluate a tandem mass spectrometer system for application to laser microprobe mass spectrometry, emphasis was be placed on obtaining as much information as possible from a single laser shot.

CHAPTER III

EXPERIMENTAL

This chapter describes the instrumentation and procedures used in this three-part study. The first experiments, performed in the laboratories of D. M. Hercules at the University of Pittsburgh, were done to gain familiarity with a commercially available laser microprobe and to illustrate the problems inherent in using a single stage mass analyzer for analysis of heterogeneous samples. The second study was done to evaluate the capabilities of the Triple-Stage Quadrupole Mass Spectrometer (TSQ) for quantitative analysis of drugs in small (2-10 mg) samples of rat brain in preparation for anticipated laser/MS/MS analysis at some later date. The objectives of the final series of experiments were (1) to design and construct a laser interface for the triple quadrupole mass spectrometer; (2) to evaluate the instrument system with respect to short-lived and long-lived events produced directly or indirectly by the laser; and (3) to determine the feasibility of and make recommendations for construction of a laser/tandem mass spectrometer-based milli- or micro- probe capable of molecular analysis of heterogeneous samples.

Laser Microprobe Study

Apparatus

Laser microprobe mass analyzer (LAMMA 500). The LAMMA 500 (Leybold-Heraeus GmbH, Federal Republic of Germany) has been described in detail (31). The instrument consists of a time-of-flight mass spectrometer with an open ion source, coupled with a Q-switched, frequency-multiplied Nd-YAG laser through a high quality microscope. A He-Ne laser aligned coaxially with the Nd-YAG laser is used for site selection and aiming. The laser light is incident on the sample at 90° to the sample rear surface and ions are extracted into the mass spectrometer at 90° to the sample front surface (the instrument operates with a 90°/-90° configuration, according to the convention established by Conzemius and Capellan (28)). For this reason, samples are restricted to thin films, or if granular forms are used, the laser must be aimed so as to strike a grain edge. An ion reflector is employed to minimize the effect of the initial ion energy spread on mass resolution and to increase resolution by allowing a longer flight path without greatly increasing instrument size.

Procedure

Preparation of animals. An epileptic focus was created in an adult male Sprague-Dawley rat by sub-dural deposition of powdered cobalt (105). After 2 weeks, the lesioned animal along with a control (non-lesioned) animal were sacrificed. The brains were removed (106) and fixed in phosphate-buffered glutaraldehyde for 48 hours. The lesioned

area of the test animal and a corresponding area from the brain of the control animal were dissected out and embedded for sectioning. Thin sections (1 μm) from each sample were mounted on electron microscope grids for use in the LAMMA, and serial sections were mounted on glass microscope slides for pre-test selection of analysis sites by optical microscopy.

Analysis. A calibration mixture of Ni, Mo, and Pb was made by grinding together $NiSO_4$, MoS_2, and $PbSO_4$, and dusting the fine particles onto an EM grid. Spectra were acquired with a 0.020 μs sampling interval and a 1100 channel delay time. Delay time is the time in sampling intervals that the transient recorder waits after the laser is fired before beginning to accumulate data and store it in the 2048 channels available. Sampling interval is the time between each sample, or channel width in μs, and determines the upper limit of the mass range. The delay time multiplied by the sampling interval determines the low mass recorded. The delay time plus 2048 multiplied by the sampling interval is the total flight time that is covered in a run. Laser energy before filtering (energy incident upon the sample is selected very roughly by neutral density filters) is read in mJ after each shot from a digital panel meter which receives a signal from a photodiode. Energy from shot to shot is variable and uncontrolled. Energies varied from 9.7 mJ to 32.5 mJ, but were usually between 10 and 20 mJ. Mass calibration was obtained from the Ni-Mo-Pb calibrant spectrum by identification of mass peaks from the isotopic patterns and correlation of flight times with chart distances. Numerous spectra were

recorded from the lesion sample and the control sample with delay times of 1000 channels and a sampling interval of 0.020 μs.Specimens were observed in the LAMMA with the 32X objective (total magnification 320X). The mass range covered was m/z 20-219.

Preliminary Triple Quadrupole Mass Spectrometry Study: Regional Distribution of Phenobarbital and Phenytoin in Rat Brain

Apparatus

Finnigan triple stage quadrupole (TSQ) mass spectrometer. The TSQ (Finnigan MAT, San Jose, Calif.) (Fig. 3.1), consisting of an electron impact (EI)/chemical ionization (CI) ion source followed in series by a mass selector-analyzer quadrupole (Q1), an ion-focusing fragmentation quadrupole (Q2), a second mass selector-analyzer quadrupole (Q3), and a continuous dynode electron multiplier, has been described (107, 108). Finnigan INCOS software (TSQ revision C) was used for instrument control, and data acquisition, storage, and manipulation. The center quadrupole (Q2) functions as a second fragmentation region when pressurized with an inert gas (N_2, Ar), operating by collisionally activated dissociation (CAD) as described by Yost et al. (119). Table I shows the primary operating modes of the instrument along with the corresponding configurations of the mass analyzer and collision quadrupoles.

Figure 3.1

Analyzer section of Finnigan TSQ mass spectrometer.

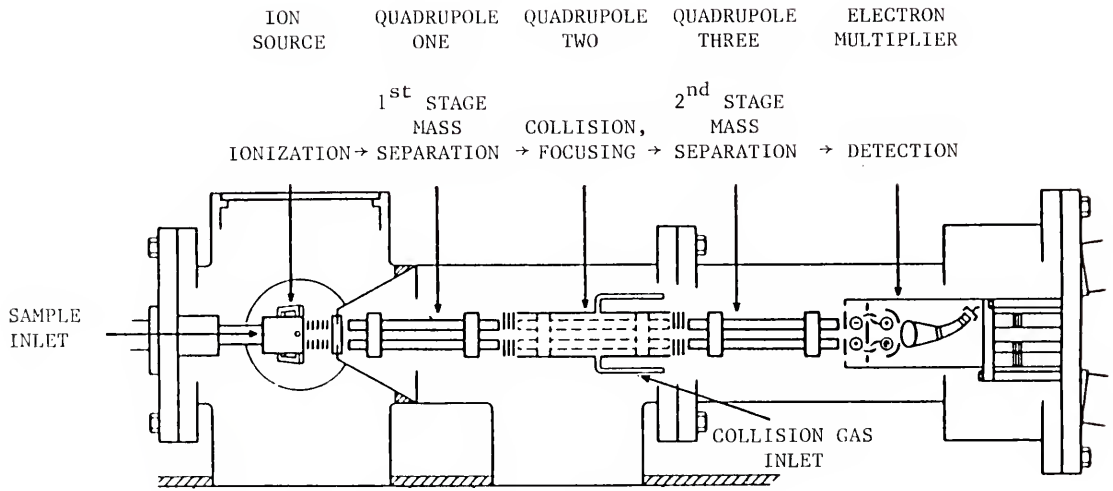
ION SOURCE
QUADRUPOLE ONE
QUADRUPOLE TWO
QUADRUPOLE THREE
ELECTRON MULTIPLIER
1st STAGE MASS SEPARATION
COLLISION, FOCUSING
2nd STAGE MASS SEPARATION
IONIZATION
DETECTION
SAMPLE INLET
COLLISION GAS INLET

Table I. Common Operational Modes of the Triple-Stage Quadrupole Mass Spectrometer

mode	quad 1	quad 2	quad 3	spectrum
(1) single stage mass spectrometer	a) pass all m/z b) scan m/z	no collision gas; pass all m/z	a) scan m/z b) pass all m/z	normal mass spectrum (CI, EI, positive and/or negative ion)
(2) parent ion experiment	scan m/z	collision gas,[a] pass all m/z	select m/z	spectrum of all ions that fragment to give selected m/z
(3) daughter ion experiment	select m/z	collision gas,[a] pass all m/z	(a) scan m/z or (b) select daughter ions for each ion passed through quad 1[b]	spectrum of all ions that arise from fragmentation of selected m/z
(4) neutral loss experiment (linked scan)	scan m/z	collision gas,[a] pass all m/z	scan m/z at same rate as quad 1 but with a constant mass difference	spectrum of all daughter ions that result from loss of selected mass difference

a) If no collision gas is present, the unimolecular dissociation products (metastable ions) will be observed.
b) Selected reaction monitoring. Only daughter ions or ions characteristic of parent ion fragmentation are monitored.

Procedure

Preparation of animals. Rats were given phenobarbital or phenytoin (20 mg kg^{-1} twice daily) for 5 days. Animals were sacrificed, the brains were removed, and various structures (cerebellar gray and white matter, sensory motor cortex, basal ganglia, hippocampus, corpus callosum, occipital cortex, pontine white matter) were separated by vacuuming into weighed glass pipets plugged with glass wool.

Analysis. The pipets containing the brain samples were reweighed to obtain sample weight, and the section of pipet containing the sample was crushed in a screw cap culture tube (Teflon-lined screw cap) for analysis. Whole blood was also collected and plasma was analyzed. Methylated analogues of the drugs [5-(p-methylphenyl)-5-ethyl barbituric acid, 5-(p-methylphenyl)-5-phenylhydantoin] were used as internal standards. Samples were homogenized by sonication in 300 µL of 1 M phosphoric acid. After addition of 300 µL of 1 M phosphoric acid containing the internal standard, samples were extracted with 3 mL of chloroform. The chloroform residue was dissolved in 100 µL chloroform and 1 to 2 µL was placed in a probe vial for MS. The mass spectrometer was operated in the selected reaction monitoring (SRM) mode by sequentially passing the drug and internal standard molecular ions resulting from methane CI through Q1, fragmenting those by CAD in Q2 (pressurized with nitrogen at 2.3 mtorr; collision energy of 18 eV) and selecting the major daughter ions for each in Q3. Thus, phenobarbital (mol. wt. 232) was monitored by selecting the m/z 162 daughter ion in Q3 while passing m/z 233 through Q1. Quantitation was based on the ion

intensity ratio of m/z 162 to m/z 191, the daughter ion of the phenobarbital internal standard parent ion m/z 247. Phenytoin (mol. wt. 252) concentration was calculated from the ratio of the m/z 182 daughter ion of the phenytoin molecular ion, m/z 253, to the m/z 196 daughter ion of the internal standard (parent ion, m/z 267).

Laser-Triple Stage Quadrupole Studies

Apparatus

Laser. The laser was a coaxial flashlamp-pumped dye laser (Model SLL-625, Candela Corporation, Natick, Mass.) operated primarily with Rhodamine 6G (4×10^{-5} M in absolute ethanol) with driver voltages between 16 kV and 20 kV. The output coupler was a sapphire window without reflective coatings. Pulsewidth was 1.5 to 2 μs. The laser could be operated only in the single shot mode with a maximum firing rate of 3 shots min^{-1}. An iris diaphragm, calibrated in 2 mm increments between 2 mm and 18 mm, was inserted into the laser cavity between the dye cell and the output coupler to reduce the diameter of the laser beam and focal spot. Pulse energy, measured with a volume absorbing energy meter (Gen-tec, Ste-Foy, Quebec, Canada), was 0.65 J, 1.49 J, and 1.64 J for driver voltages of 16 kV, 18 kV and 20 kV, respectively.

Laser-mass spectrometer interface. The side flange of the TSQ was machined according to the specifications of Fig. 3.2.a to accommodate a 1.5" diameter fused silica lens (focal length: 12.5 cm). Three spacers (Fig. 3.2.b) were also machined to allow adjustment of the point of

Figure 3.2

Diagrams for machining (a) blank side flange of TSQ to hold 1.5" diameter fused silica lens, and (b)spacers for adjusting focal point of lens within ion source. Measurements marked are: (A) 4.5 in.; (B) 1/4 in.; (C) 7/8 in.; (D) 5/8 in.; (E) 1 in.; (F) 1/4 in. (G) 1/8 in., 3/16 in., and 1/4 in. (3 spacers).

a) FLANGE

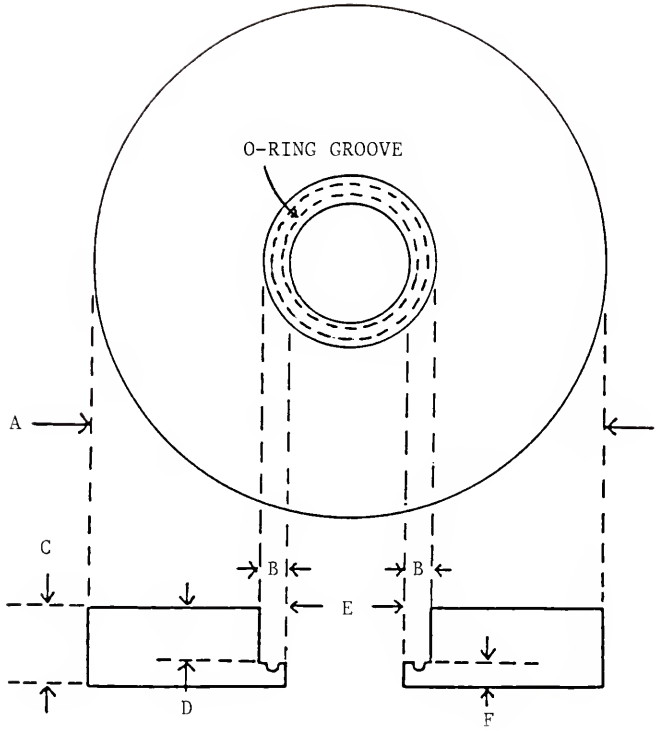

b) SPACER

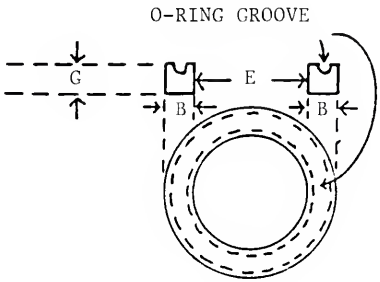

focus over a 9/16" range in 1/16" steps. As it happened, the focal point was about 1/16" from the reagent gas inlet side of the ion volume with no spacers. Vacuum was maintained with O-ring seals. To allow entrance of laser light into the ion source, a 1/8" hole was drilled into the ion volume (EI and CI) directly opposite the reagent gas entry hole. Extensions to the solids probe were machined out of stainless steel according to the specifications of Fig. 3.3 to allow insertion of samples on electron microscope (EM) grids and angles of laser incidence of 90° and 45°. The 45° tip was later modified to allow grids to float in the ion volume with no backing. This tip was used for the desorption CI experiments. The dye laser was aligned (Fig. 3.4) by directing a He-Ne laser (L1) through the dye cell (L2) with the retroreflector (M0) removed, through the output coupler (W1) to a plane mirror (M1) which reflected the beam to another plane mirror (M2) mounted on the TSQ, then to plane mirror (M3) mounted on a gimbal mount on a line axial with the focusing lens (W2). Final adjustments in laser aiming could be made by slight adjustments of M3 while determining the point of impact on an electron microscope grid inserted into the ion source.

Detection systems. Short-lived events were monitored with one of two MS detection systems. In the first, a storage oscilloscope (Model 549, Tektronix, Inc., Beaverton, Ore.) was connected directly to the electron multiplier of the TSQ through a Type D high gain differential amplifier plug-in, and was triggered by a TTL pulse from a photodiode-to-TTL interface connected to the output of a fast photodiode (FND100, EG&G Electro-Optics, Salem, Mass.). The laser light (about 8% of total

Figure 3.3

Diagrams for machining (a) 90° and (b) 45° stainless steel solids probe extensions. The 45° extension was later modified for desorption chemical ionizaton (DCI) by grinding the tip until it was flat (dotted line). Measurements shown are: (A) 9/32 in.; (B) 1/4 in.; (C) 0.0765 ± 0.0005 in.; (D) 1/16 in.; (E) 0.215 ± 0.001 in.; (F) 1/64 in.; (G) 0.133 ± 0.001 in.; (H) 13/32 in.. Depression is 7/64 in. in diameter and between 1/64 in. to 1/32 in. deep. A small leaf spring tightened by a screw is used to hold the tabbed EM grid on the 90° tip, and a cylinder made to just fit over the end of the 45° tip is used to secure the grid on that probe extension.

a) 90° SOLIDS PROBE EXTENSION

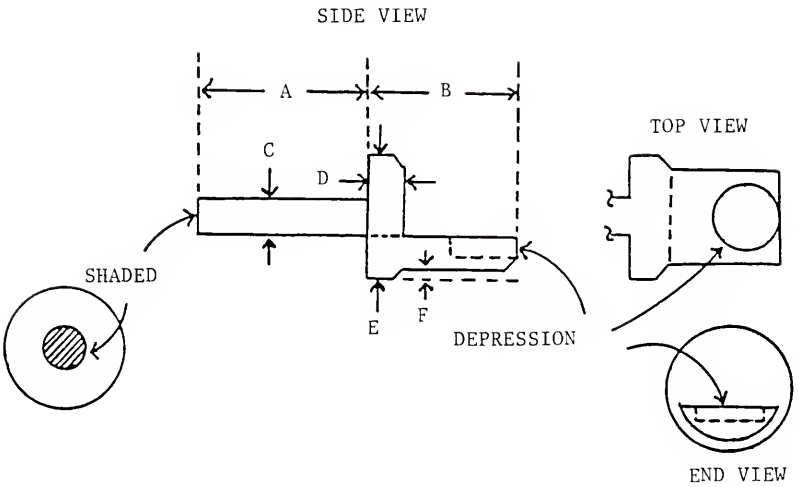

b) 45° SOLIDS PROBE EXTENSION WITH DCI MODIFICATION

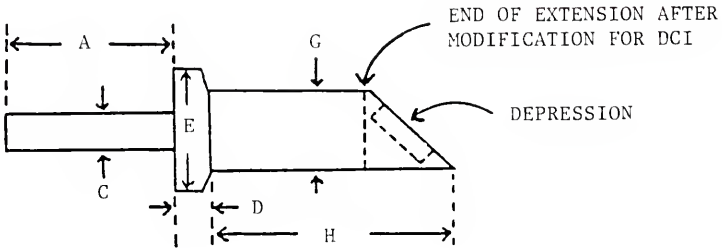

Figure 3.4

Layout of lasers and beam directing optics in relation to TSQ ion source. Components are: (L1) He-Ne alignment laser; (L2) dye cell of dye laser; (M0) 100% reflecting plane mirror for laser back reflector; (M1, M2, M3) plane mirrors for beam steering with M3 on gimbal mount; (S1) iris diaphragm calibrated in 2 mm increments from 2 mm to 18 mm; (W1) sapphire window for laser output coupler; and (W2) fused silica lens with 12.5 cm focal length for focusing laser light inside ion source.

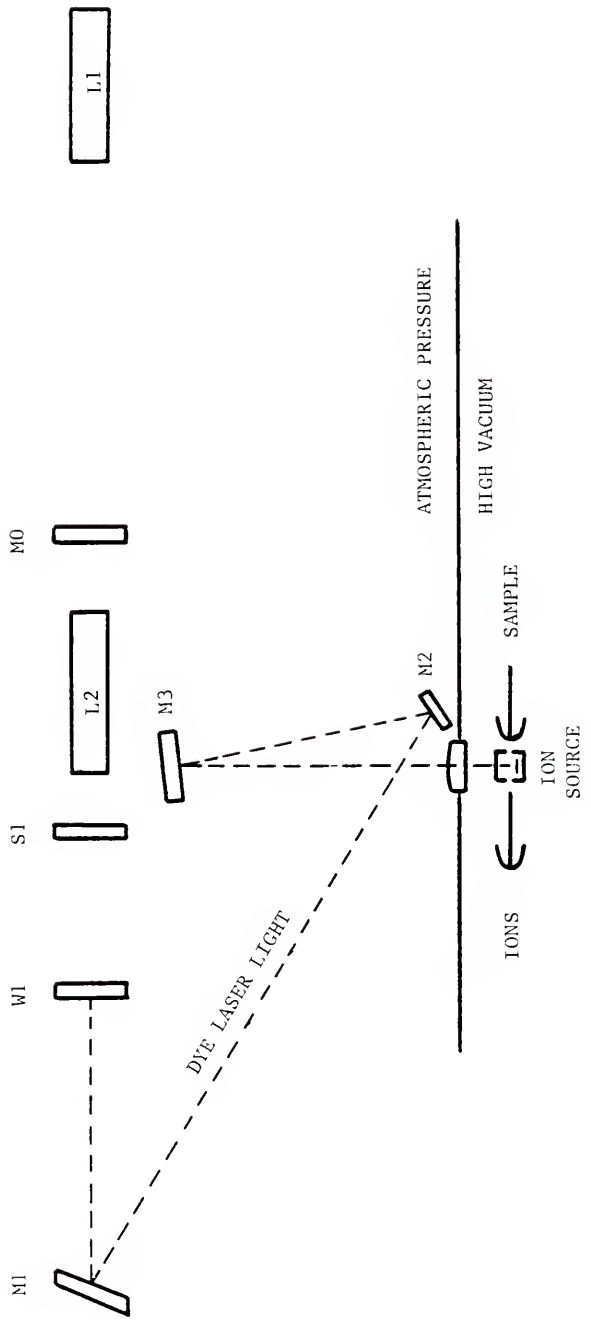
M1
W1
S1
L2
M3
M0
L1
DYE LASER LIGHT
M2
ATMOSPHERIC PRESSURE
HIGH VACUUM
SAMPLE
ION SOURCE
IONS

output) was reflected to the photodiode from a microscope slide placed in the light path. Comparison of the TSQ instrument oscilloscope with the storage scope indicated a sensitivity of 1.6×10^{-7} A V^{-1} for the latter. The storage scope could not be run from the amplified instrument signal, because the output of the amplifier contained the instrument scope trigger signal and mass marker signals which disrupted the storage scope signal and triggering. In the second detection system, the TSQ data system was used for monitoring fast signals by acquiring data in profile mode. In this mode, time resolution of 25 μs was obtained because the instrument acquires data at the maximum analog-to-digital conversion (ADC) rate of 40 kHz. A single long scan (20 s) of profile data was acquired during which time the laser was fired. By setting the mass of interest with the unscanned quadrupole and turning off the DC voltage to the scanned quadrupole, a signal of ion current vs. time was obtained. This operation will be described in more detail in Chapter V. The beginning of the scan was monitored by connecting an oscilloscope (Model 2213, Tektronix, Inc.) to the positive Y-axis input (Y+) at the rear of the TSQ scope and observing the scan signal (TSQ scope set for multiple mass marker display) with a fast time base. Long lived events were monitored with the TSQ data system operated normally, but with the centroid sampling interval set at less than the normal 200 μs. The centroid sampling interval is the number of ADC readings (1 to 8) summed to produce a single datum point. Therefore, with an ADC rate

of 40 kHz, the centroid sampling interval can be varied, in 25 μs increments, from 25 μs to 200 μs with the latter being the default setting.

High performance liquid chromatograph. A high performance liquid chromatograph was used for quantitation of test drugs in animal samples and to determine the quantities of sample vaporized in the ion source by the laser. A high pressure syringe pump (Model 4100, Varian Associates, Palo Alto, Calif.), 6-port rotary injection valve (Valco Instrument Co., Houston, Tex.), and a fixed-wavelength (214 nm) ultraviolet absorbance detector (Model 1203, Laboratory Data Control, Riviera Beach, Fla.) were used with a 4.6 mm i.d. x 250 mm stainless steel column, packed with a 5-μm particle diameter octadecyl silica gel stationary phase (Biosphere-ODS, Bioanalytical Systems, Inc., West Lafayette, Ind.) and maintained at 52°C with a circulating water bath (Neslab Instruments, Inc., Portsmouth, N.H.). The mobile phase was pumped at 80 mL/h, and consisted of acetonitrile:tetrahydrofuran:water (28.5:0.5:71) with potassium dihydrogen phosphate added at a concentration of 2.7 g L^{-1}.

Procedure

Laser system evaluation. The laser system was evaluated with Coumarin 2 and Rhodamine 6G laser dyes (Eastman Kodak, Rochester, N.Y.). The coumarin lased at about 450 nm, however, the intensity was low and the useful life of the dye was only a few shots. Rhodamine 6G lased at about 590 nm with high pulse energy and a single dye solution allowed

operation for several hundred shots. Pulse shapes were measured for various laser cavity diameters at 16 kV, 18 kV and 20 kV by monitoring the signal directly from the fast photodiode.

Laser-TSQ evaluation. The laser-mass spectrometer system was evaluated with respect to short-lived and long-lived laser-initiated processes. The short-lived events (μs to ms) were observed with an open electron impact ion source at high vacuum, while long-lived processes (ms to s) occurred with a closed chemical ionization source with reagent gas present at greater than 0.35 torr. Phenytoin, a relatively nonvolatile (m.p. 295 - 298°C) drug, which was also used in the animal experiments, was used in most of the system evaluations, since it was readily available as the free acid and the sodium salt, and proved to be a suitable test substance. A series of compounds (Appendix) having various functional groups and molecular weights was also tested under desorption chemical ionization conditions (110) in which only the source block was heated in most cases, under normal direct probe conditions, and under laser vaporization conditions to determine the versatility and utility of the present system. In all cases, samples were inserted into the source as solids packed into a depression in the stainless steel probe tip or as residues from solutions evaporated on copper, nickel or silver electron microscope grids (Ted Pella, Inc., Tustin, Calif.).

Preparation, collection and analysis of animal samples. To provide animal tissue samples suitable for laser analysis, two adult male rats were given a loading dose (150 mg/kg) of phenytoin intraperitoneally

75 min before decapitation. At the time of sacrifice, the animals were ataxic and lethargic, indicating substantial drug absorption. Brains and livers were removed and washed in isotonic phosphate buffer. One set was frozen at -20°C. The other set was fixed for 72 h in phosphate-buffered glutaraldehyde (KCl, 0.0834 M; KH_2PO_4, 0.0127 M; K_2HPO_4, 0.0846 M; 25% aqueous glutaraldehyde; 925 mL water). Samples from fixed and frozen brains and livers were analyzed by high performance liquid chromatography (111). Aliquots of homogenized weighed tissue samples were deproteinized with acetonitrile. The aqueous acetonitrile phase was washed with iso-octane and then poured into a tube containing granular KCl. Vortexing caused the acetonitrile to be salted out of the water, at the same time extracting the phenytoin and internal standard. The acetonitrile layer was transfered to a clean tube, evaporated to dryness, and the residue was dissolved in mobile phase for injection into the HPLC system. Sections of the fixed tissues were frozen in isotonic phosphate for later MS analysis.

CHAPTER IV

PRELIMINARY STUDIES AND INSTRUMENT CHARACTERISTICS

This chapter includes discussions of (1) the LAMMA experiments with thin slices of rat brain tissue taken from the cobalt lesion site in one animal and a corresponding site from a non-lesioned animal, (2) the determination of the regional distributions of phenytoin and phenobarbital in rat brains by triple quadrupole MS/MS, and (3) the basic characteristics of the laser-TSQ system, including laser pulse shape and variation of diameter of laser spot size with target position and cavity diameter.

LAMMA Experiments

The LAMMA instruments, initially the Model 500 and, more recently, the Model 1000, were designed ideally to monitor atomic mass spectra during the brief lifetime of laser-induced emissions from thin film and bulk samples. The time-of-flight (TOF) mass spectrometer operates within the time restrictions of Q-switched, single shot lasers and the lifetimes of the ions which they produce, so that a complete mass spectrum covering a significant mass range can be acquired in less than 100 us. After the laser fires, kinetic energy is imparted to the ions in the source area by a high voltage accelerating pulse. This is

translated into an ion motion according to eqn. 4.1,

$$(1/2)mv^2 = zeV \tag{4.1}$$

where m and v are the ion mass and velocity, respectively, z is the ion charge, e is the electron charge, and V is the accelerating voltage. The time of ion flight is determined by the length of the flight tube (L) and the ion velocity (eqn. 4.2).

$$t = Lm^{1/2}/(2zeV)^{1/2} \tag{4.2}$$

Since m is equal to the molecular weight divided by Avogadro's number (6.023×10^{23}) and the voltage in electron volts (eV) is the accelerating voltage times the charge per molecule (ze), for singly charged molecules with time measured in seconds, eqn. 4.2 becomes,

$$t = 7.199 \times 10^{-7}(L/V^{1/2})m^{1/2} \tag{4.3}$$

or

$$t = cm^{1/2} \tag{4.4}$$

where c is the instrumental constant, incorporating unit conversion factors, length of the flight path and instrument accelerating voltage. Table II gives the masses, their square roots and abundances for the

Table II. Masses and Flight Times for Nickel, Molybdenum and Lead Isotopes in LAMMA Calibrant

Isotope	Ion Mass (u)	Ion Mass$^{1/2}$	% Abundance[a]	d_p[b]	t[c]	d_t[d]
^{58}Ni	57.933	7.6115	68.3	101.5	32.579	312.6
^{60}Ni	59.931	7.7415	26.1	106.4	33.089	317.5
^{92}Mo	91.907	9.5868	14.8	176.4	40.385	387.5
^{94}Mo	93.905	9.6905	9.3	180.2	40.781	391.3
^{95}Mo	94.906	9.7420	15.9	182.1	40.979	393.2
^{96}Mo	95.905	9.7931	16.7	184.1	41.188	395.2
^{97}Mo	96.906	9.8441	9.6	186.1	41.396	397.2
^{98}Mo	97.905	9.8947	24.1	188.0	41.594	399.1
^{100}Mo	99.907	9.9953	9.6	191.9	42.001	403.0
^{206}Pb	205.974	14.352	24.1	356.8	59.187	567.9
^{207}Pb	206.976	14.387	22.1	358.0	59.312	569.1
^{208}Pb	207.977	14.421	52.4	359.0	59.416	570.1

a) % Abundance of naturally occurring isotopes.
b) d_p = Chart distance from recorder start to peak in mm.
c) t = Total flight time in us.
d) d_t = Total chart distance (d_p + delay distance) in mm.

calibrant isotopes (Ni, Mo, Pb), and the distance and time data derived from the calibration spectrum. The flight times (t) were calculated as the sum of chart time (t_c) plus the delay time (t_d) with

$$t_c = nt_s(d_p/D) \tag{4.5}$$

and

$$t_d = n_d t_s \tag{4.6}$$

where n and n_d are the total number of chart channels (2048) and the number of delay channels, respectively, t_s is the sampling interval, and d_p and D are the chart distance to the peak and total chart distance covered by 2048 channels (393.0 mm at 0.020 μs sampling interval), respectively. Regression analysis of flight time (μs) vs. the square root of the ion mass indicated a 2.563 μs lag (Y-intercept) between the start of recorder timing and the ion acceleration pulse. The slope of this plot (Fig. 4.1) gave the instrument constant, 3.944 μs $u^{-1/2}$. Using this value with eqns. 4.3 and 4.4 gave a flight path length of 300.2 cm.

Figure 4.2 shows the calibration spectrum (A) with spectra acquired from the lesion site (B) and the control site (C). Although the peak at m/z 59 (*) is higher in the lesion site than in the control sample, it is impossible to say if this signal is actually due to cobalt. The presence of large peaks at almost all masses throughout this range

Figure 4.1

Plot of flight time vs. the square root of ion mass for LAMMA calibrant (data from Table II). Data points cover all isotopes for each metal (Ni: 58, 60; Mo: 92, 94, 95, 96, 97, 98, 100; Pb: 206, 207, 208).

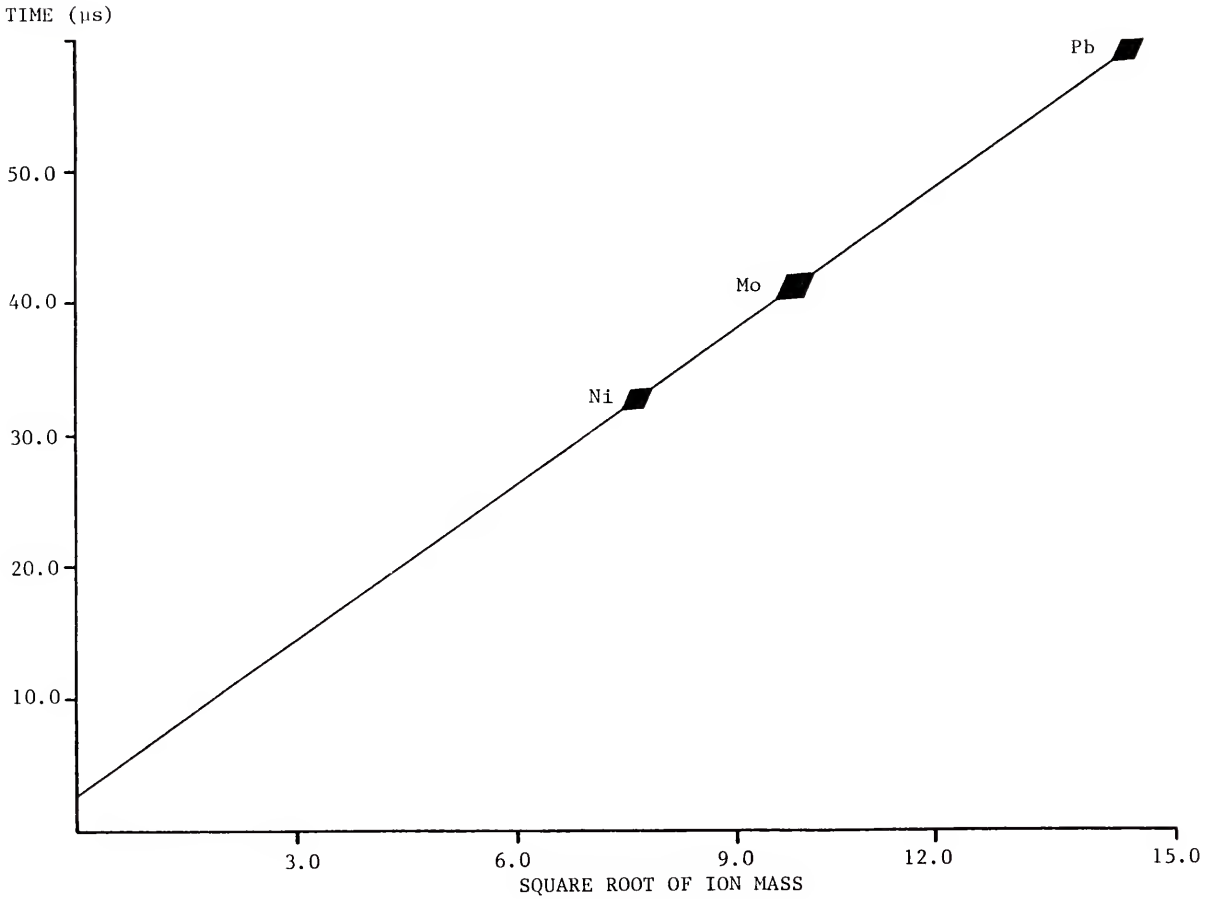
TIME (μs)
50.0
40.0
30.0
20.0
10.0
Pb
Mo
Ni
3.0
6.0
9.0
12.0
15.0
SQUARE ROOT OF ION MASS

Figure 4.2

LAMMA spectra for (A) nickel-molybdenum-lead calibrant, (B) section of rat brain from cobalt lesion site, and (C) section of rat brain from corresponding site in control (unlesioned) animal (m/z 59 designated by *).

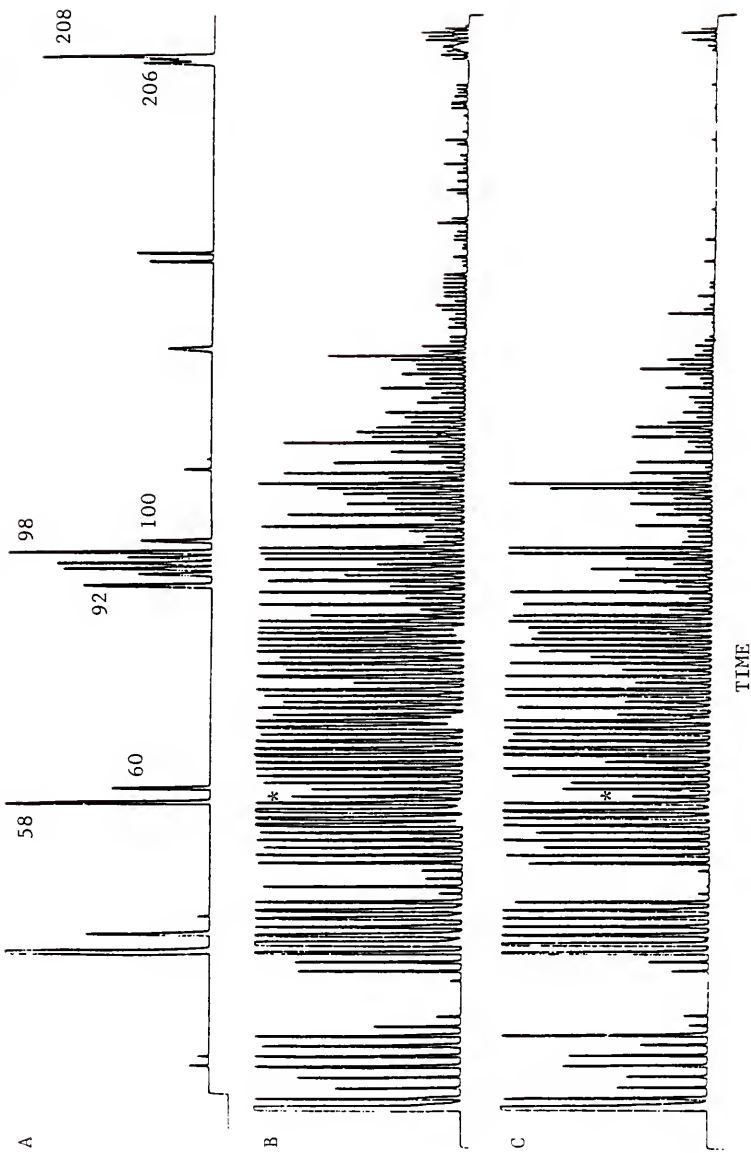
Ni
58
60
Mo
92
98
100
Pb
206
208
A
B
C
ION CURRENT
TIME

precludes any accurate assessment of elemental or molecular composition. These results point out the advantage of having two stages of mass analysis (filtering and selection) for microprobe analysis. By increasing the laser power density, the chemical noise from molecular fragments could be decreased, but it would still be impossible to definitely identify the ion at m/z 59 as cobalt since there is only one naturally occurring isotope. Uncertainty of ion identification becomes greater as mass increases because the number of possible elemental compositions also increases. This deficiency is made obvious in a recent report on LAMMA analysis of coal and shale samples (112). The laser was fired at grazing incidence at 1/8" diameter chips, and ions produced directly by the laser were recorded. Although the authors gave explanations of the spectra and made mass assignments, primarily on the basis of natural isotopic abundances and past literature reports of laser pyrolysis gas chromatography and mass spectrometric studies of homopolymers, a second stage of mass analysis would have added greatly to the certainty of some of the assignments.

Regional Distributions of Phenobarbital and Phenytoin in Rat Brain

At the time this project was started, very little quantitative work on real biological samples had been done by MS/MS. A quantitative study of typical samples amenable to analysis by other methods (i.e., gas-liquid or high performance liquid chromatography) was considered to be a

necessary starting point, to define instrumental conditions, particularly with respect to the CAD behavior of analytes, which would give accurate, reproducible results. Since one of the primary advantages of MS/MS is elimination of the need for pre-MS (chromatographic) separation of mixture components, demonstration of reliable analysis by direct vaporization of samples (extracts) from the solids probe was also considered important.

Rapid vaporization of the entire sample from the solids probe vial with as little temporal separation of analyte and internal standard evaporation profiles as possible was found to be of primary importance. Separation of the analyte and internal standard ion signals (because of differences in their vaporization temperatures) caused the response ratio to be dependent on the number of scans over which the signal was summed. To minimize this effect, a heating rate of about 100°C s^{-1} was employed. This generally resulted in complete sample vaporization within a 30 s period with a near-Gaussian ion current profile. Analyte-internal standard pairs vaporized simultaneously within about 20 s (Fig. 4.3).

Response ratios for drug and internal standard ion currents were also dependent on instrument tuning, so that long-term (day to day) reproducibility of calibration curve slopes was poor; however, linearity was good, with correlation coefficients generally between 0.996 and 0.999. Figure 4.4 shows a histogram of the results for phenobarbital and phenytoin in plasma and various brain regions. The numbers in parentheses beside each bar give the number of samples (before slash)

Figure 4.3

Plots of ion current vs. time for direct solids probe vaporization and selected reaction monitoring of rat brain extract from an animal that received phenobarbital (m/z 233 to m/z 162) and phenytoin (m/z 253 to m/z 182). Other signals are from internal standards, p-methyl phenobarbital (m/z 247 to m/z 191) and p-methyl phenytoin (m/z 267 to m/z 196). RIC is recombined ion current.

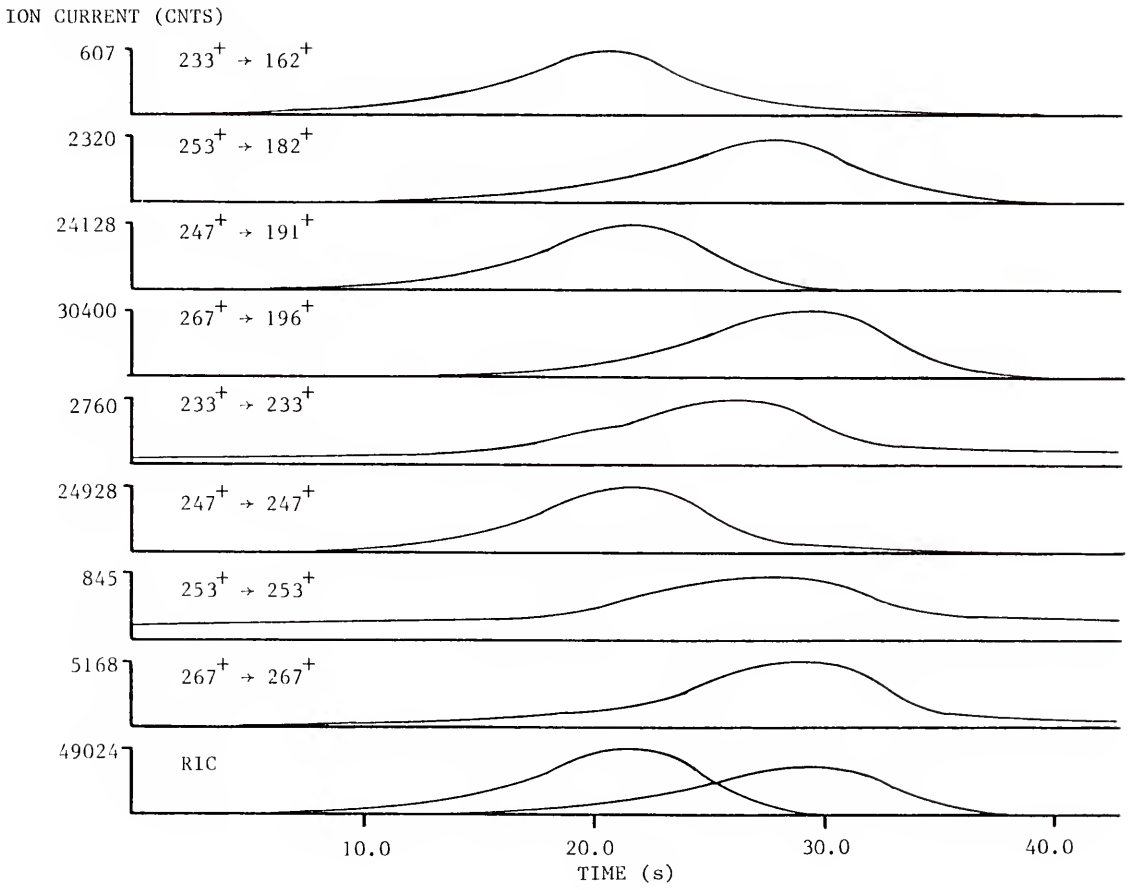
ION CURRENT (CNTS)
607
$233^+ \rightarrow 162^+$
2320
$253^+ \rightarrow 182^+$
24128
$247^+ \rightarrow 191^+$
30400
$267^+ \rightarrow 196^+$
2760
$233^+ \rightarrow 233^+$
24928
$247^+ \rightarrow 247^+$
845
$253^+ \rightarrow 253^+$
5168
$267^+ \rightarrow 267^+$
49024
RIC
10.0
20.0
30.0
40.0
TIME (s)

Figure 4.4

Histogram showing concentrations of phenytoin and phenobarbital in various areas of rat brain (ug/g) and in plasma (ug/mL). Number before slash indicates the number of samples taken and the number after slash shows the number of animals from which those samples were obtained. See caption Fig 4.3 for reactions monitored during analysis.

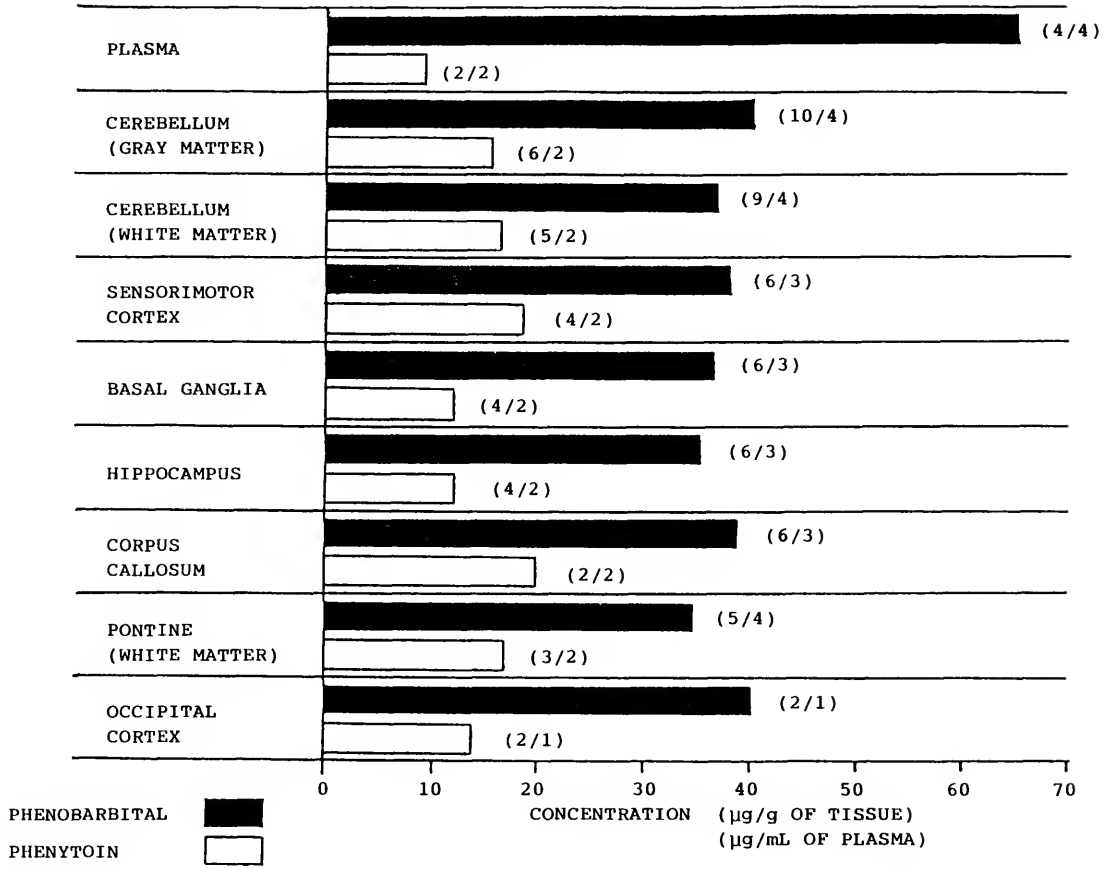
PLASMA
(4/4)
(2/2)
CEREBELLUM
(GRAY MATTER)
(10/4)
(6/2)
CEREBELLUM
(WHITE MATTER)
(9/4)
(5/2)
SENSORIMOTOR
CORTEX
(6/3)
(4/2)
BASAL GANGLIA
(6/3)
(4/2)
HIPPOCAMPUS
(6/3)
(4/2)
CORPUS
CALLOSUM
(6/3)
(2/2)
PONTINE
(WHITE MATTER)
(5/4)
(3/2)
OCCIPITAL
CORTEX
(2/1)
(2/1)
0
10
20
30
40
50
60
70
CONCENTRATION (µg/g OF TISSUE)
(µg/mL OF PLASMA)
PHENOBARBITAL
PHENYTOIN

taken from the number of animals (after slash) sacrificed. Regional distribution of phenobarbital is relatively even. Although phenytoin appears to be slightly more concentrated in white matter and less concentrated in basal ganglia and hippocampus, it also is fairly evenly distributed. Concentrations in structures that are possibly linked with epileptic activity or drug effects (hippocampus, cerebellum, sensorimotor cortex) are not greatly different from those in areas that are not linked with seizures (pontine white matter, occipital cortex). The averages of the histogram values for all structures are $38 \pm 2\ \mu g\ g^{-1}$ and $11 \pm 3\ \mu g\ g^{-1}$ for phenobarbital and phenytoin, respectively; brain to plasma ratios for these averages are 0.568 and 1.73, respectively.

The low relative standard deviations for these samples, 5.6% for 50 phenobarbital determinations, and 20% for 30 phenytoin samples, indicate that monitoring analyte daughter ion intensities for selected reactions with respect to those of suitable internal standards is a valid technique for direct analysis of plasma and brain extracts by triple quadrupole mass spectrometry. The response ratios are made more reproducible by rapid, complete vaporization. This was assured by rapid heating of the solids probe in this experiment. In the instrument under consideration, rapid heating and sample vaporization would be affected by using a pulsed laser as a sampling device.

Laser-Triple Stage Quadrupole Characteristics

Variation of Focal Spot Size with Distance from Focal Point and Laser Cavity Diameter.

The laser beam, which is about 20 mm in diameter when emanating from a totally open cavity, was reflected from a flat mirror 24 inches in front of the output coupler to the 1.5 inch diameter fused silica plano-convex lens used as the laser window in the TSQ. The target was a black piece of cardboard that was placed from 12 mm behind the focal point to 18 mm in front of the focal point. Spot size varied from 3.2 mm at the former to 5.0 mm at the latter and was 1.3 mm at the focal point (Fig. 4.5). Spot size initially increased more slowly with distance in front of the focal point. The cavity diameter was varied by placing an iris diaphragm between the dye cell and the output coupler. The target was located 4 mm in front of the focal point of the lens. Spot size was 1.7 mm, 1.0 mm and 0.5 mm with iris openings of 18 mm, 12 mm and 6 mm, respectively. Below 6 mm the spot size was too small to be measured accurately, but a flash could still be seen at the target with the cavity diameter set to 2 mm. Normal cavity diameters used in this study were 6 mm to 10 mm, depending on the age of the flashlamp and laser dye solution. Focal spot sizes for these settings were 0.5 mm to 1 mm.

Figure 4.5

Variation of focal spot diameter with distance in front of (+, toward) and in back of (-, away from) focal point for 1.5 in. diameter, 12.5 cm focal length fused silica lens used for focusing laser in ion source of TSQ.

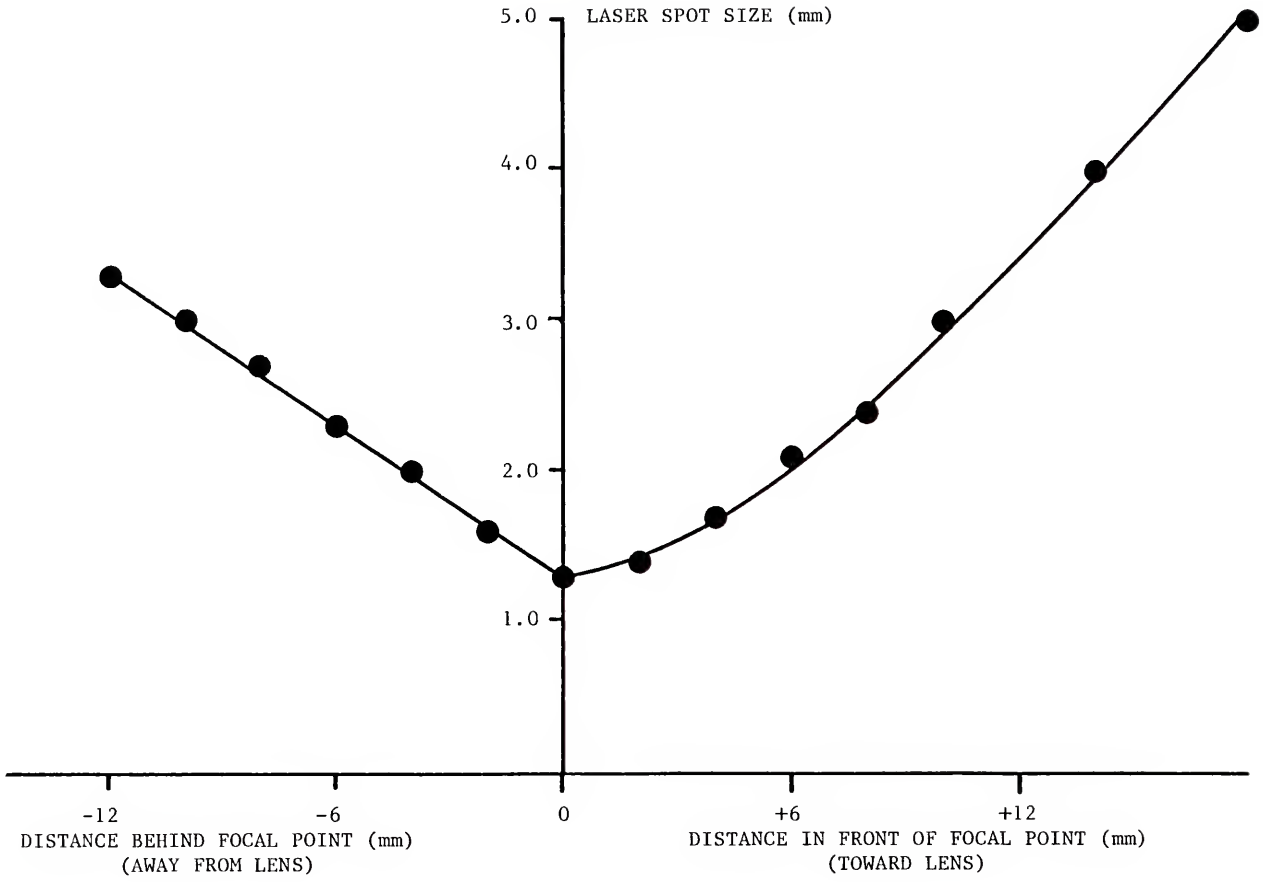
5.0
LASER SPOT SIZE (mm)
4.0
3.0
2.0
1.0
-12
-6
0
+6
+12
DISTANCE BEHIND FOCAL POINT (mm)
(AWAY FROM LENS)
DISTANCE IN FRONT OF FOCAL POINT (mm)
(TOWARD LENS)

Laser Pulse Shape and Duration.

Laser pulse shape and duration were measured using the output from the fast photodiode to drive the storage oscilloscope directly. Figure 4.6 shows the tracings produced by varying the cavity diameter (2 to 12 mm) at 16 kV, 18 kV and 20 kV. In all cases, the light pulse was reflected from two microscope slides to the photodiode so that all pulses remained on the oscilloscope scale (5 V cm^{-1}). Therefore, only about 0.6% of the laser light was incident on the photodiode (8% reflected from each slide). The time base of the scope was set at 2 μs cm^{-1}, indicating a pulse width (full width at half maximum) varying between 1 μs and 3 μs and depending on cavity diameter and driver voltage. At 18 kV and cavity diameters of 6 mm to 10 mm (normal settings), pulse width was 1.5 μs to 2 μs.

Figure 4.6

Laser pulse shapes from photodiode signal as monitored by storage oscilloscope at driver voltage of (A) 16 kV, (B) 18 kV, and (C) 20 kV. Cavity diameter was varied from 2 mm to 12 mm in 2 mm increments giving curves running from low intensity to high intensity in each figure (drawn from photographs of storage oscilloscope screen).

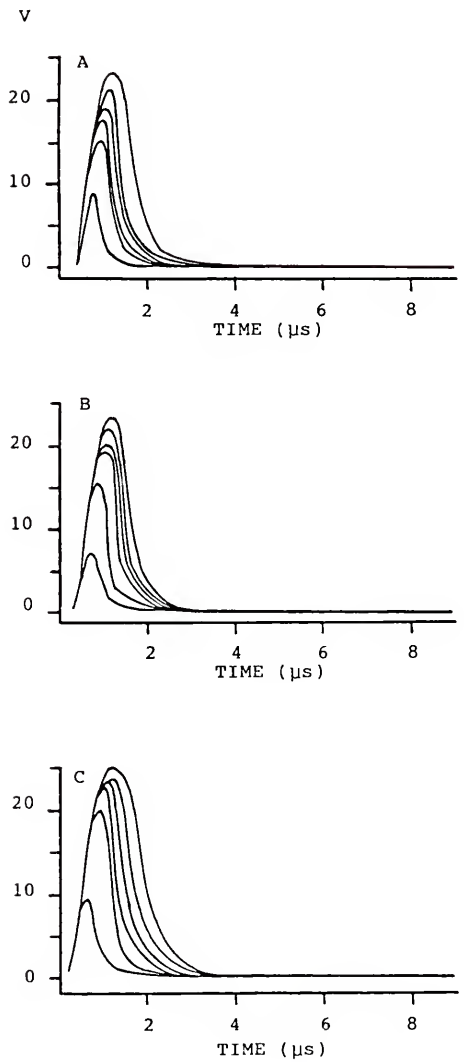
V
A
20
10
0
2
4
6
8
TIME (μs)
B
20
10
0
2
4
6
8
TIME (μs)
C
20
10
0
2
4
6
8
TIME (μs)

CHAPTER V

SHORT-LIVED PROCESSES

Although the quadrupole mass filter scans the fastest of all the scanning mass analyzers, normally covering 1000 to 2000 mass units each second, it is still relatively slow when compared to the ion lifetime of pulsed laser-generated ions. In spite of this incompatibility, an attempt to observe the events immediately following the laser pulse was thought to be desirable for this study for two reasons. First, the laser used in this study was a single shot device (1.5 to 2 μs pulsewidth) and prolonged signals were not expected, and second, observation and verification of normal laser-induced processes such as cationization required mass discrimination and time resolution in the us range. This chapter will present results of experiments conducted using an electron impact ion volume, modified to transmit the laser light, and operated without reagent gas. Under these conditions, ion signals lasted less than 1 ms and were monitored either with a storage oscilloscope or with the TSQ data system. Limited mass discrimination was maintained by selecting the mass of interest with Q1 and, with no collision gas in Q2, selecting a range of masses which may or may not include the mass of interest with Q3 operated in RF-only mode.

Triple Stage Quadrupole Control

The goal in these experiments was to have the TSQ operate as a time-of-flight mass spectrometer for the selected ion, allowing data to be obtained at a single m/z during the course of an experiment. This had been accomplished in a single stage quadrupole instrument by Hardin and Vestal (80), who used a pulsed laser with single ion counting. Setting the analyzer to pass the selected ion mass, and increasing the instrument resolution until only one event was recorded for each laser pulse, they collected data until a statistically significant distribution of ion flight times was acquired for each mass of interest. The TSQ is electronically configured to operate with at least one analyzer quadrupole scanning a range of masses (although that range may be $\leq$1 u wide) in all modes. A system having both quadrupoles set to pass a single mass had not been defined in programmable read only memory (PROM). Since the laser used in this experiment was a single shot device, the instrument had to be set up to provide a continuous signal for the ion selected, with time resolution of a few microseconds. This could have been done either by determining and adding the appropriate instruction or instructions to the PROM to allow each analyzer to be set to pass a single mass without scanning, or by causing the scanned quadrupole to operate in the RF-only mode to allow a range of masses to pass simultaneously rather than sequentially. Since modifying the PROM could have had far-reaching and unforeseen effects on other parts of the TSQ system, elimination of the DC voltage from the scanned quadrupole

was selected as the best way to solve the problem. This was accomplished by changing the rod polarity switch located at the rear of the quadrupole electronics module (QEM) from "+" to "off". This is a three position switch ("+", "off", "-") that allows the operator to change the DC polarity on the quadrupole rods. Under normal conditions, there is no difference in response if the switch is set to "+" or "-". The "off" setting removes the DC component from the rods. The range of masses passed under these conditions can be determined from the stability diagram for the quadrupole. The stability diagram (Figure 5.1) is a plot of the ratio of DC to RF voltages imposed on the quadrupole rods vs. a function including the RF frequency, a dimensional constant for the quadrupole (one-half the diagonal distance between the rods in cm), the RF voltage, and the inverse of the mass-to-charge ratio of the ion. Under normal conditions, the voltage ratio is set so that only the mass ($\pm$0.5 u) under the apex has a stable trajectory through the quadrupole. All other ions have unstable trajectories and are lost by collisions with the rods. If the DC voltage component is removed, all ions that fall under the curve have stable trajectories and will pass. The ratio of the ordinate value under the apex ($1/m_1$) to that at the low-mass abscissa zero ($1/m_2$) is about 7/9. Therefore, if an RF-only quadrupole is set to pass m_1, it will actually pass all masses greater than m_2 which equals 7/9 of m_1.

Table III gives the effects on response for the most pertinent combinations of operation mode (parent and daughter ion experiment), programmed RF function (on/off) and rod polarity switch (+/off). Other

Figure 5.1

Stability diagram for quadrupole mass filter. Plot of DC to RF voltage ratio vs. a function proportional to $(m/z)^{-1}$. Shaded region shows range of ion masses passed through quadrupole set to pass m_1 with both RF and DC voltages imposed (normally, $m_1 \pm 0.5$ u). The RF-only quadrupole will pass all masses higher than m_2 where $m_2 = (7/9)m_1$. Parameters in the ordinate function are: RF voltage, V_{rf}; quadrupole rod spacing (diagonal), r_0; electron charge, e; angular frequency of V_{rf}, ω ; mass-to-charge ratio, m/z.

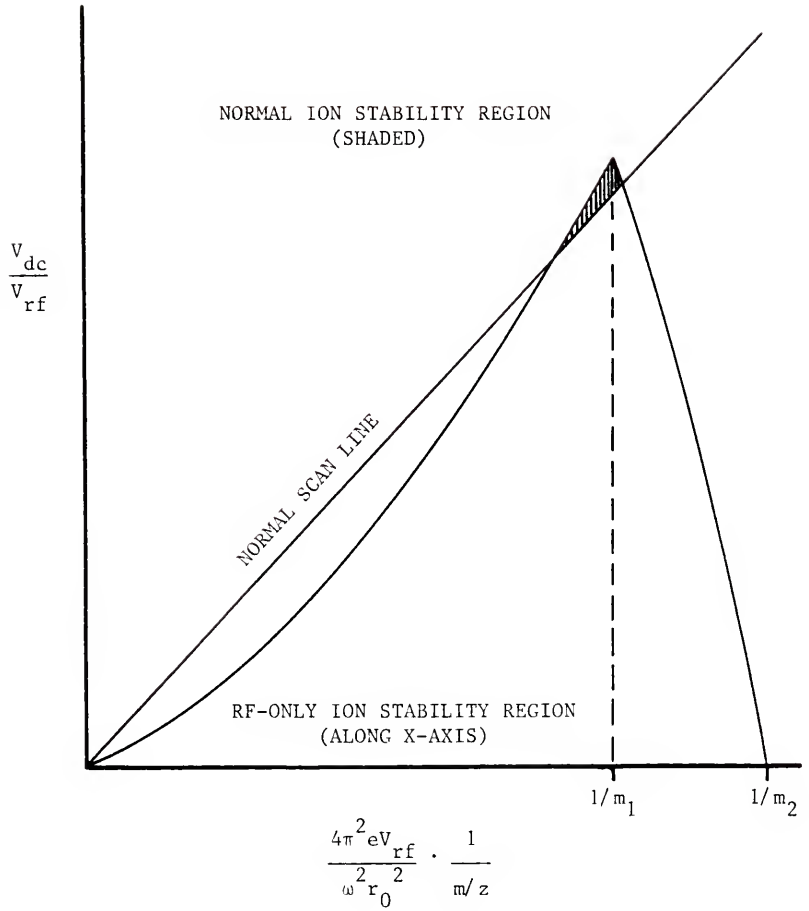
NORMAL ION STABILITY REGION
(SHADED)
$\frac{V_{dc}}{V_{rf}}$
NORMAL SCAN LINE
RF-ONLY ION STABILITY REGION
(ALONG X-AXIS)
$1/m_1$
$1/m_2$
$\frac{4\pi^2 eV_{rf}}{\omega^2 r_0^2} \cdot \frac{1}{m/z}$

Table III. Effects of Programmed RF Function and Rod Polarity Switch Settings During Various TSQ Operational Modes

Condition	Operation Mode	Programmed RF	Rod Polarity Switch Q1	Rod Polarity Switch Q3	Effects
1	Daughter Spectrum	on	+	+	Daughter spectrum. Increasing Q1 first mass removes low m/z (all above 7/9 Q3 first mass passed).
2	Daughter Spectrum	on	+	off	High broad signal. Low m/z and signal intensity controlled by Q1 first mass.
3	Daughter Spectrum	off	+	off	Broad peak displayed only when Q1 first mass set on peak.
4	Parent Spectrum	on	+	+	Parent spectrum. Increasing Q3 first mass removes low m/z (all above 7/9 Q1 first mass passed).
5	Parent Spectrum	on	off	+	Broad signal. Signal intensity 75% of that with Q1 rod polarity +.
6	Parent Spectrum	off	off	+	Broad peak displayed only when Q3 first mass set on peak. Signal intensity less than that in daughter mode.

combinations were not listed because they were unremarkable or had no bearing on the present discussion. The programmed RF function removes the DC component from the unscanned quadrupole. The effects were observed with the instrument under manual control with perfluorotributylamine (FC43) being introduced continuously into the EI source. Effects that include a measurement of relative signal intensity for the rod polarity switch on "+" or "off" were made by observing m/z 69 on the instrument oscilloscope. Loss of mass resolution is expected when the scanned quadrupole is operated in RF-only mode. Condition 3 was selected for most of the work on short-lived processes because Q1 provides mass discrimination and Q3 can be set up to pass or not pass the ion selected by Q1. The advantage to this condition is that a long scan (20 s) can be acquired to eliminate the delay time of a few milliseconds normally required between scans. Further, since Q3 is not resolving masses, this mode will provide an ion intensity vs. time response for the selected ion rather than an ion intensity vs. mass response. In addition, the beginning of the scan can be detected by an oscilloscope attached to the "Y+" input of the TSQ oscilloscope. This is important for monitoring fast processes with the data system because data acquisition begins at the first regular scan after the experiment is initiated at the computer terminal. Data acquisition does not begin immediately because the scan sequence is not interrupted and restarted. Condition 6 is analogous to condition 3 but Q1 is the scanned quadrupole (parent mode). Signal intensities were generally lower for this condition, however, the major

drawback was that the scan signal was not visible at the "Y+" input as it was for the daughter mode.

Comparison of Storage Oscilloscope and Data System

Signal for Ni^+ from Nickel EM Grid

With the TSQ operating in daughter mode with Q3 rod polarity switch off (condition 3), Q1 passing m/z 58 (Ni^+) and Q3 passing all ions above m/z 56 (scanning from m/z 71 to 72 in 20 s with rod polarity switch off), the laser was fired at a clean nickel electron microscope grid inserted into the ion source on the 90° probe tip. The storage scope was attached directly to the electron multiplier through a high-gain differential amplifier module (Type D, Tektronix, Inc.) operated at 1 mv cm^{-1} with a time base of 50 μs cm^{-1}. In Figure 5.2.A, traces 1 and 2 show response with the laser light blocked from the ion source and the light admitted to the source, respectively. Trace 3 was obtained by switching Q1 to pass m/z 90 and Q3 to pass all masses above m/z 140 (scanning m/z 180 to 181 in 20 s), so that Q1 and Q3 would be mutually exclusive and neither quadrupole should pass any ion produced by vaporization of the nickel target. In figure 5.2.B, traces 2 and 3 are analogous to traces 2 and 3, respectively, in part A, except that the response was monitored with the TSQ data system by acquiring in profile mode. Also, Q3 was scanned from m/z 60 to 70 (passing all m/z above 47 to 54) for trace 2 and from m/z 170 to 180 (passing all m/z above 132 to 140) for trace 3. These data show that this method of recording

Figure 5.2

Plots of total ion current vs. time showing (A) storage scope data and (B) profile data for nickel EM grid target. In A, trace 1 is the response with laser light blocked from ion source; trace 2 in A and B is the response with Q1 passing m/z 58 and Q3 passing all m/z above 56 (A) and all m/z above 47 to 54 (B). Trace 3 in A and B is the response with Q1 passing m/z 90 and Q3 passing all m/z above 140 (A) and all m/z above 132 to 140 (B). See text for explanation of differing Q3 scans for storage scope and data system operation. Ion currents are given as counts (CNTS).

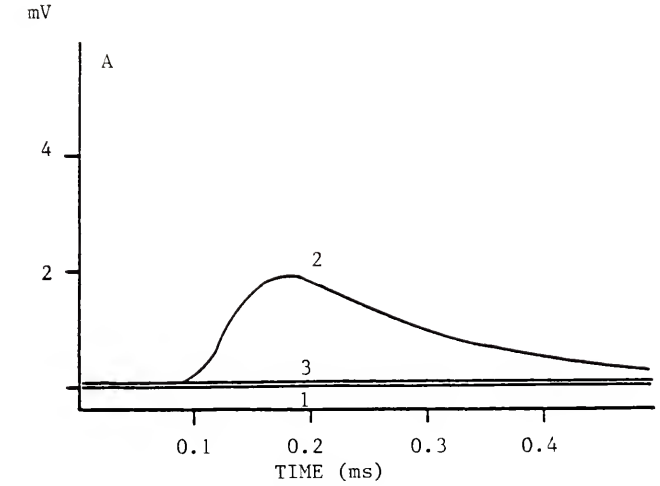
mV
A
4
2
2
3
1
0.1
0.2
0.3
0.4
TIME (ms)

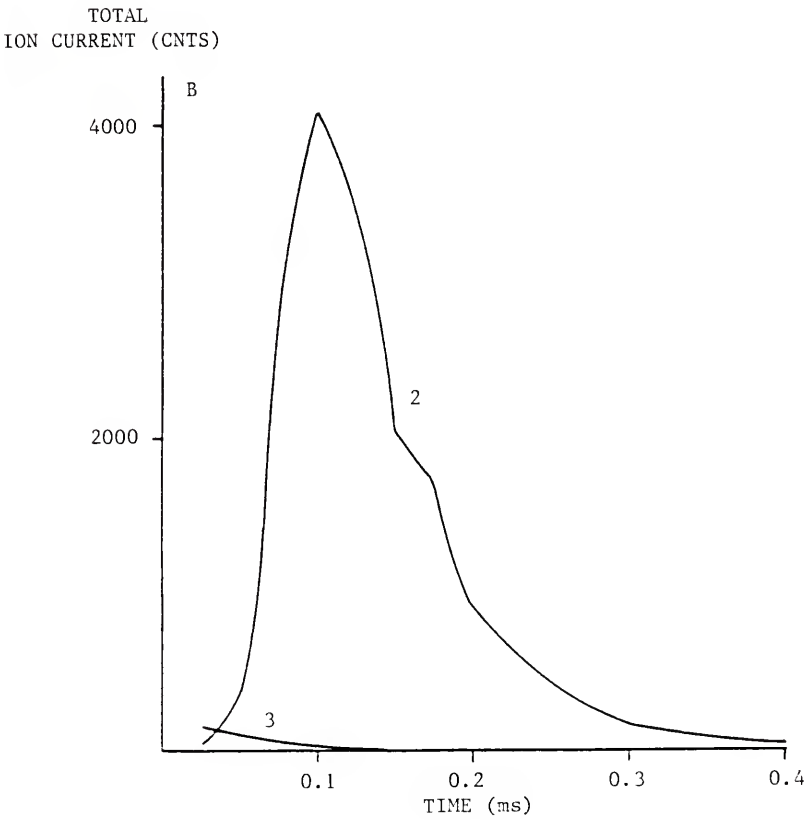
TOTAL
ION CURRENT (CNTS)
B
4000
2000
2
3
0.1
0.2
0.3
0.4
TIME (ms)

intensity vs. time data for fast events may be valid, that quadrupole 1 provides some mass discrimination, even for low mass elemental ions, and that the storage scope and the data system give equivalent data. There is always a minimum signal (rapidly decaying spike) observed by the data system even when no sample is in the ion source, the laser light is blocked before it reaches the source, and the electron multiplier is off. This response is probably due to electrical interference from discharge of the laser storage capacitor when the flashlamp is fired.

Instrumental Acquisition and Display Characteristics

It might be helpful at this point to describe the TSQ scan parameter (SYSTem, System Status, Multiple Ion Detection), calibration (CALIrate), acquisition (ACQUire), and display (PROFile, mass CHROmatogram, and SPECtrum) programs. The above programs will, henceforth, be referred to by the abbreviations used to access them (underlined). Data can be acquired in two modes, centroid and profile. Both are calibrated using the CALI program which establishes a linear relationship between mass and time elapsed since start of a scan. Therefore, even under normal circumstances, the mass of an ion is determined by the appearance time after the scan starts, and the spectrum is displayed as ion intensity vs. mass. Acquisition in profile mode causes storage of all points detected at the maximum sampling rate (25 μs). Storage requirements are maximized, but a relatively continuous plot of ion intensity vs. time is produced, allowing observation of peak shapes. It is this mode that has been used in these experiments on short-lived processes (Chapter V) to obtain a plot of

signal intensity vs. time. A threshold intensity can be chosen (in ADC units), which allows immediate rejection of points having intensities less than the selected threshold. Thresholding is the only decision made by the data system at the full 40 kHz ADC rate. A setting of 1 means all data is recorded (no thresholding). For these experiments, the threshold was routinely set at 2 to eliminate spurious electronic noise. Therefore, a scan 20 s long, during which a signal is produced for a brief instant by a laser shot, would result in a profile lasting only from the time the signal exceeds threshold until it goes below threshold. PROF is the program used to display profile data. Although the program converts time to mass units, it plots essentially a time-dependent, ion intensity curve, and calculates the time the signal is above threshold. The plots of profile data shown in the figures were calculated from these curves. Since time scales were usually different for each profile curve, signal intensities were replotted on a common time scale for comparison. The maximum intensity in a profile plot is 4096 counts, as determined by the 12-bit ADC. Q3 scan parameters were most easily set using the MID program. Q1 mass was set using the SS program. In this way, experiments could be run rapidly by writing the required MID descriptors, and calling them as needed from SS. Q1 mass was changed as required, also from SS.

Acquisition in centroid mode (used for experiments on long-lived processes in Chapter VI) causes calculation and storage of the mass centroid of a peak, minimizing storage requirements and making data manipulation faster. In this mode, the centroid sampling interval is

chosen (using MID) in 25 μs increments between 25 μs and 200 μs to give a reasonable number of data points per mass peak. Therefore, data is acquired at 40 kHz, and 1 to 8 data points are summed to give a single datum point to be used in calculating the peak centroid. If a scan is set up in SS, the highest possible centroid sampling interval (200 μs) will be used. In SYST, a selection is available for centroid samples per peak, however, the number actually used will be determined by the mass range covered in the scan time. The only way to insure use of a particular centroid sampling interval is to set that interval in MID. The CHRO program is used to view the recombined ion current (RIC), or the intensity profiles for each ion with respect to scan number (time). This is analogous to the use of the PROF program for viewing short-lived processes; however, an additional dimension is available (in the SPEC program), which allows display of the mass centroids making up the RIC (mass spectrum). Scan parameters for acquisition in centroid mode (Chapter VI) were again set up using the MID program, both for normal mass spectra and, as required, for parent and daughter ion spectra. The centroid sampling interval was chosen so that scan time could be minimized, and there would be at least 5 points/mass peak for calculation of the peak centroid.

Filtering Characteristics of Quadrupoles 1 and 3

Although the quadrupole is supposed to effectively filter out all ions of unselected mass regardless of ion energy, it is possible for ions of inappropriate mass to pass through the quadrupole field without deflection if their kinetic energy is high enough (109, 113, 114).

Therefore, a series of experiments was performed to determine the filtering capabilities of the system under the conditions used for time profile monitoring.

Figure 5.3.A and B show a comparison of storage scope and profile data, respectively, for phenytoin. Q1 was set to pass m/z 275, $(M+Na)^+$ for phenytoin, and Q3 was scanned from m/z 343 to 353 in 18 s with the rod polarity switch off (passing all m/z above 266 to 274). The phenytoin (4 μL of a solution of 4.35 mg/mL) was layered over a Na_2CO_3 residue (2 μL of a solution of 25 mg/mL) on a 400-mesh copper electron microscope (EM) grid which was inserted into the ion source on the 90° probe tip. Trace 1 shows the first shot. Trace 2 is a second shot at the same site. Although this figure shows an intense signal for cationized phenytoin and significant reduction for a repeat shot (the grid was totally disintegrated at the point of impact of the first shot creating a hole about 0.5 mm in diameter), the signal is not necessarily due to cationized phenytoin alone. Figure 5.4 shows responses for a similar sample for which Q1 was set to pass m/z 150 and Q3 was set to pass all m/z above 202 to 210 (scanning m/z 260 to 270 in 18 s with rod polarity off). In this case Q1 and Q3 are mutually exclusive and Q1 is not passing an ion that should be produced by the sample; however, Q3 is covering a mass range that includes ions that should be present. Trace 1 shows a shot at the center of the grid where the phenytoin concentration, due to uneven evaporation of the methanol, was lowest. Solids were usually concentrated in a ring describing the edge of the sample droplet. Traces 2 through 4 show successive shots at the same

Figure 5.3

Plots of total ion current vs. time showing (A) storage scope data and (B) profile data for phenytoin over Na_2CO_3 on copper EM grid. In A and B Q1 is passing m/z 275 and Q3 is passing all m/z above 267 to 275 (scanning m/z 343 to 353 in 18s with rod polarity switch off). In both A and B, trace 2 is the response from a second laser shot at the same site that gave trace 1.

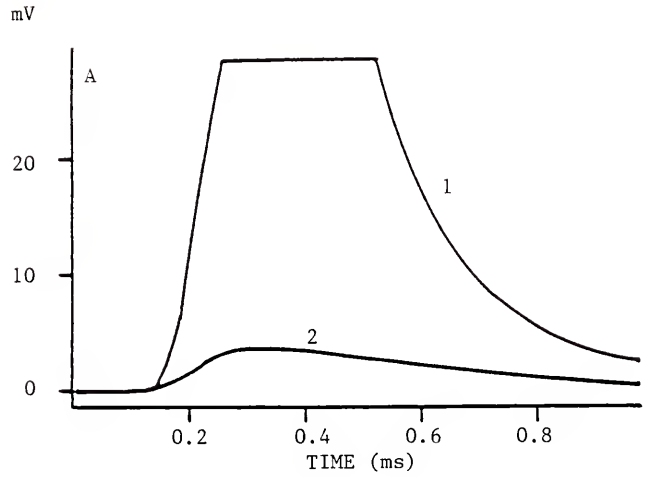
mV
A
20
10
0
1
2
0.2
0.4
0.6
0.8
TIME (ms)

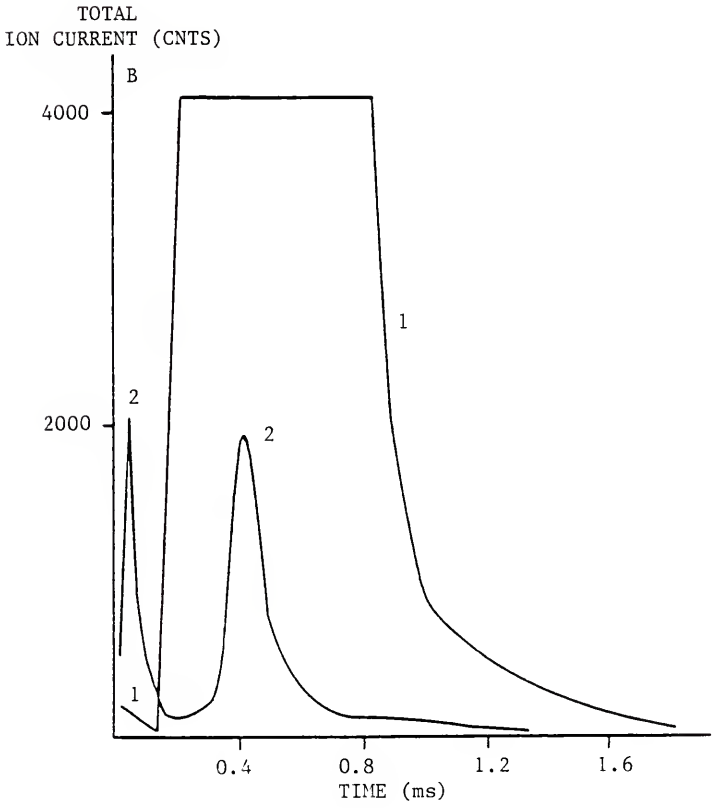
TOTAL
ION CURRENT (CNTS)
B
4000
2000
1
2
2
1
0.4
0.8
1.2
1.6
TIME (ms)

Figure 5.4

Plots of total ion current vs. time showing the efficiency of Q1 and Q3 mass filtering (profile data) for phenytoin over Na_2CO_3 on copper EM grid. In traces 1-4, Q1 is set to filter out all m/z produced by the sample (passing m/z 150) and Q3 is set to pass ions that should be present (passing all m/z above 202 to 210. In trace 5, neither quadrupole is passing ions produced by the sample and they are set to be mutually exclusive (Q1 passing m/z 700 and Q3 scanning normally with rod polarity "+" from m/z 300 to 310. Trace 1 is at grid center where phenytoin concentration is low. Trace 2 is at edge of droplet where concentration is highest. Traces 3 and 4 are successive shots at site 2. Trace 5 is from an identically prepared grid at the edge of sample droplet.

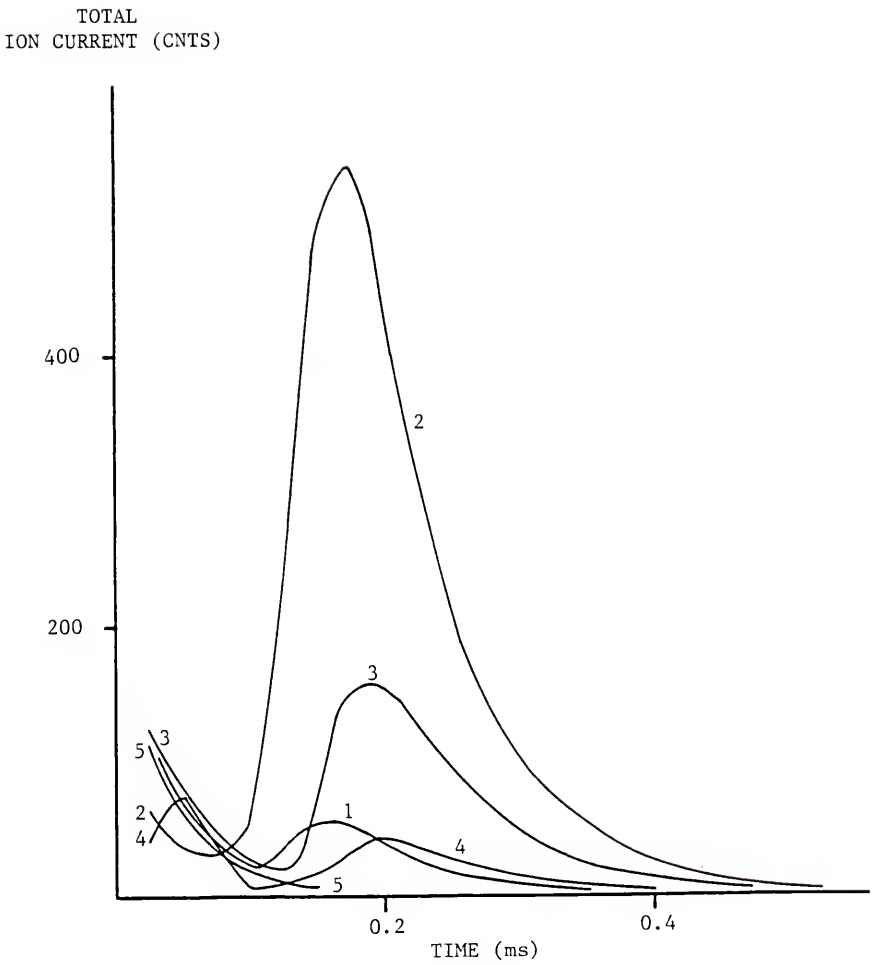
TOTAL
ION CURRENT (CNTS)
400
200
2
3
1
4
5
0.2
0.4
TIME (ms)

site on the edge of this ring where concentration was highest. These traces indicate that Q1 is not totally efficient at filtering ionic species. Trace 5 was recorded with Q1 set to pass m/z 700 and Q3 scanning from m/z 300 to 310 with rod polarity "+" (DC on) so that both quadrupoles were mutually exclusive and neither was passing ions that were produced by the sample. A minimum signal, generally present under any conditions, was produced. This indicated that Q1 and Q3 effectively filtered out sample ions when set to pass masses that differed greatly from the sample ion masses. Another experiment was conducted to determine whether the filtering capabilities of Q1 were lessened when the selected mass was close to the mass of an ion produced by the sample (i.e., is unit mass resolution maintained under the conditions produced by laser desorption in the present ion source). Q1 was set to pass m/z 275 and then, with a new grid, m/z 270 (test point arbitrarily chosen 5 u away from the ion mass), with Q3 passing all m/z above 202 to 210. The signal intensity ratio for the former with respect to the latter was about 5, indicating that unit mass resolution in Q1 is not maintained under these conditions. The particles that are causing these unwanted responses may be fast ions or neutrals which do not "see" the low voltage fields of the lenses and quadrupoles. Discrimination of a selected ion mass from its nearest neighbors is less efficient than from ions that have masses much greater or much less than the selected mass.

This problem was approached from another angle to show the total ion signal with all quadrupoles operated in RF-only mode, and to contrast that with the signal obtained when Q1 was operated as a mass

filter. Q1 was set to pass m/z 275 and Q3 to pass all m/z above 266 to 274 with the sample again phenytoin over Na_2CO_3. Successive shots were fired at the same site (Figure 5.5.A, traces 1-3). Q1 was then set to pass m/z 350 and the programmed RF was turned on so that Q1 would actually pass all m/z above 272. Two shots were fired at the same site (new grid; Figure 5.5.B, traces 1 and 2). Programmed RF was then turned off so that Q1 would then only pass m/z 350 (an ion not produced by the sample) and a single shot was fired at a new grid (Figure 5.5.B, trace 3). These figures show that Q1 does actually filter out a large portion of the total signal that is possible under these conditions. Therefore, the combination of quadrupoles 1 and 3 can be used to obtain limited mass resolution in this rapid acquisition mode to allow monitoring of the fast signal profiles.

Time Resolution of Low-Mass and High-Mass Ions

With these limitations in mind, an attempt was made to observe the resolution of two compounds by time alone by operating the instrument in a time-of-flight mode without mass discrimination in either analyzer quadrupole. Q1 was set to pass m/z 160 with programmed RF on (actually passing all m/z above 124), Q3 was set to pass all m/z above 117 to 124 (scanning m/z 150 to 160 in 18 s with rod polarity off). Data were acquired with the TSQ data system in profile mode. The sample was a mixture of 4-vinyl-4-aminobutyric acid (vinyl gaba, mol. wt. 129) and reserpine (mol. wt. 608) over Na_2CO_3. Expected cationized species were m/z 152 and m/z 631, respectively. All quadrupole offset voltages and lens voltages were set at -20 V. The flight path length from the ion

Figure 5.5

Plots of total ion current vs. time showing efficiency of Q1 mass filtering and effects of programmed RF function in Q1. Part A shows successive laser shots (1-3) at a single site on a copper EM grid with phenytoin over Na_2CO_3 and Q1 passing m/z 275 and Q3 passing all m/z above 267 to 275. Part B shows responses from an identical sample with Q1 passing all m/z above 272 (Q1 set at m/z 350 with programmed RF on); traces 1 and 2 are first and second shots at same site. Trace 3 is from a third identical sample under the latter conditions but with programmed RF off (Q1 passing m/z 350).

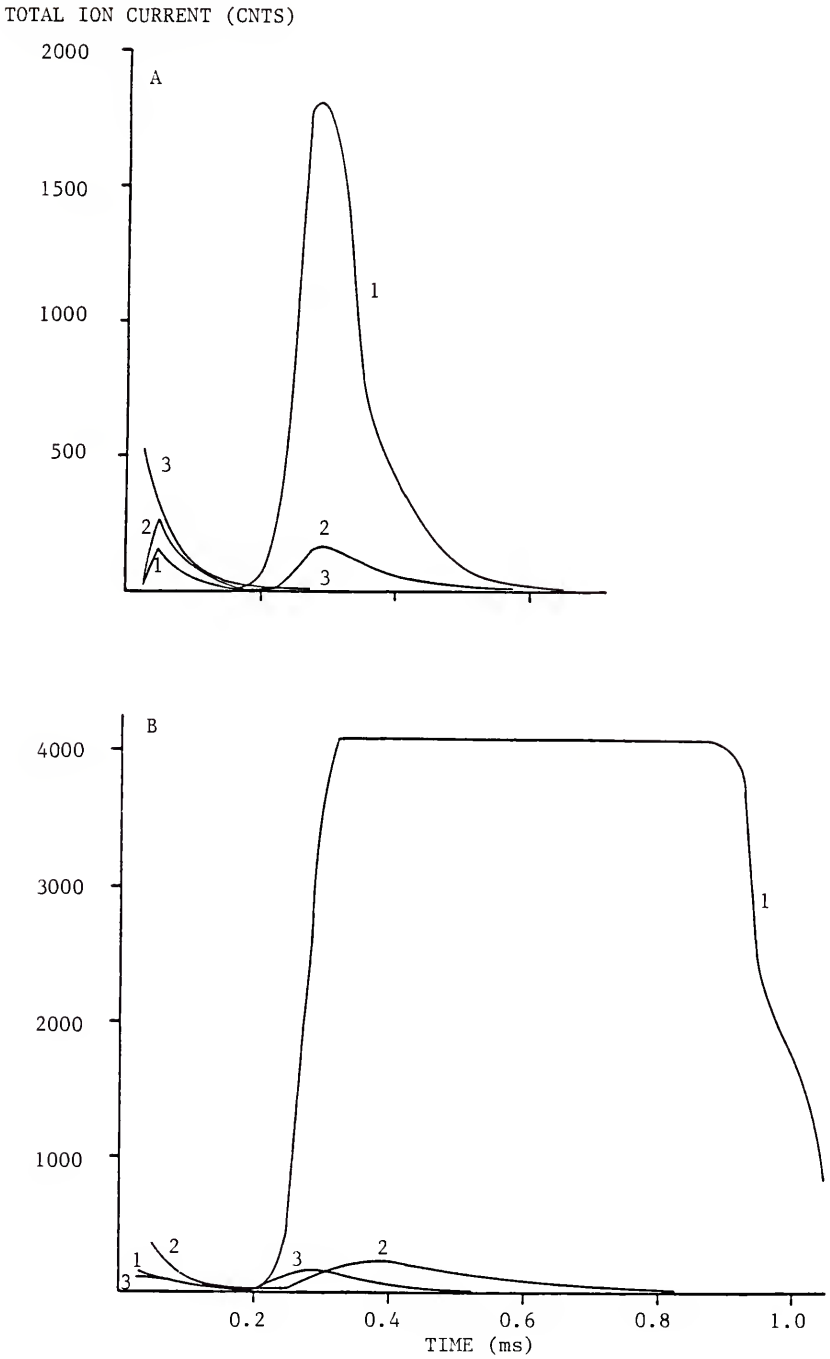
TOTAL ION CURRENT (CNTS)
2000
1500
1000
500
A
1
2
3
4000
3000
2000
1000
B
0.2
0.4
0.6
0.8
1.0
TIME (ms)

source to the detector was measured at 50 cm, making the total expected flight path about 75 cm since the oscillations of ions in the quadrupole fields make the effective length about 1.5 times the actual length (109). Figure 5.6 shows the ion signal from this experiment. The flight times calculated from the peak maxima were 247 μs for vinyl gaba and 372 μs for reserpine. A plot of chart time vs. the square root of ion mass for these two points had a slope of 9.77, and an intercept of 127 μs. This intercept indicates that there is a 127 μs lag between the laser impact and the time when the data system detects the first non-zero signal. The instrumental constant (Eq. 4.4) is 9.77 μs $u^{-1/2}$, and the apparent accelerating voltage seen by the ions is, from Eq. 4.3, 30.5 V. This is not grossly out of line, considering that the drift space is not field free, that the acceleration field imposed by the conversion dynodes at the end of the last quadrupole was not considered, and that no true accelerating pulse was provided at the ion source. There is also a possibility that this doublet does not truly represent time resolution of these two ions. Additional attempts to reproduce this pattern resulted only in peaks with shoulders; however, at no other time during these experiments was a doublet obtained when a single species was vaporized.

Contribution of Reagent Gas and Sample Matrix to Ion Signal

It appeared at this point that monitoring fast processes with the TSQ was interesting from an academic standpoint, but, because of limited mass and time resolution, was not very practical. Further, it did not have the potential for producing accurate numerical data on ion flight

Figure 5.6

Plot of total ion current vs. time for 4-vinyl-4-aminobutyric acid (mol wt 129) and reserpine (mol wt 608) over Na_2CO_3, showing time resolution of respective cationized molecules with m/z 152 (A) and m/z 631 (B).

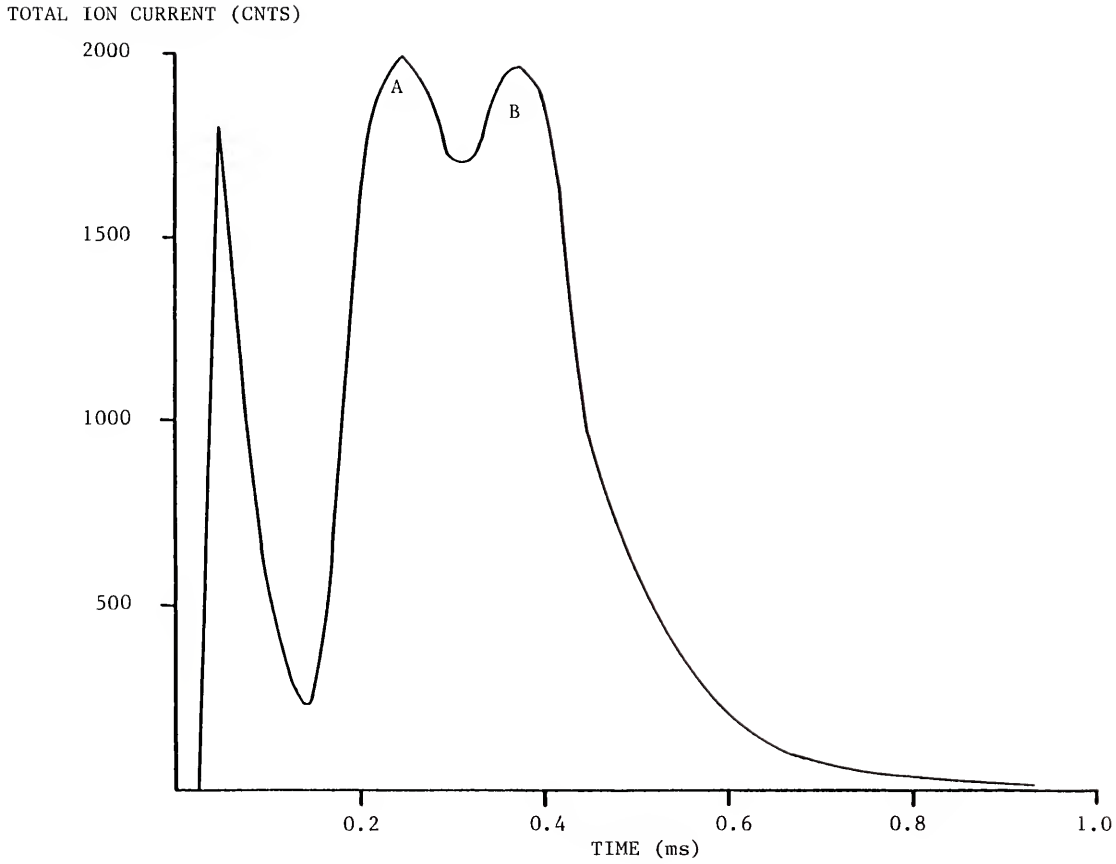
TOTAL ION CURRENT (CNTS)
2000
1500
1000
500
A
B
0.2
0.4
0.6
0.8
1.0
TIME (ms)

times or energy spreads. Time, it was decided, could be better spent observing processes that occurred over longer times, so that the capabilities of the TSQ could be put to better use. Figure 5.7 shows the effects of reagent gas on yield and longevity of signal for cationized phenytoin. Two identical samples of phenytoin over Na_2CO_3 on copper EM grids were vaporized within the electron impact ion volume without reagent gas (trace 1) and with 0.58 torr of methane (trace 2). The filament was off. Q1 was set to pass m/z 275; Q3 all m/z abov 244 to 252. This figure shows that reagent gas does not prolong the signal lifetime of the cationized molecule, and may not contribute to efficient extraction of this ion into the analyzer.

A similar experiment was performed without Na_2CO_3, but with parlodion, a nitrocellulose film material used in electron microscopy, added to the methanolic phenytoin solution (20 mg parlodion/mL). This matrix appeared to cause the phenytoin to be more evenly distributed over the EM grid mesh after droplet evaporation (parlodion alone formed a clear film, but parlodion with solute was white). Q3 was scanning from m/z 170 to 180 with rod polarity off (passing all m/z above 132 to 140) while Q1 was passing m/z 253. The experiment was performed with 0.64 torr of methane in the EI ion volume. Although the maximum ion current was less than that observed for the cationized molecule in Figure 5.7 (most likely because a different ion was being monitored), the lifetime of the signal was significantly increased (Figure 5.8). This is reasonable since the cationization process is directly dependent on thermal effects induced by the laser. The protonation reaction is

Figure 5.7

Plots of total ion current vs. time for phenytoin over Na_2CO_3 showing effects of reagent gas on signal for cationized molecule with Na_2CO_3 present in sample. Traces show signal without reagent gas (1) and with 0.58 torr of methane (2) with filament off, Q1 passing m/z 275, and Q3 passing all m/z above 244 to 252. All experiments done in EI ion volume.

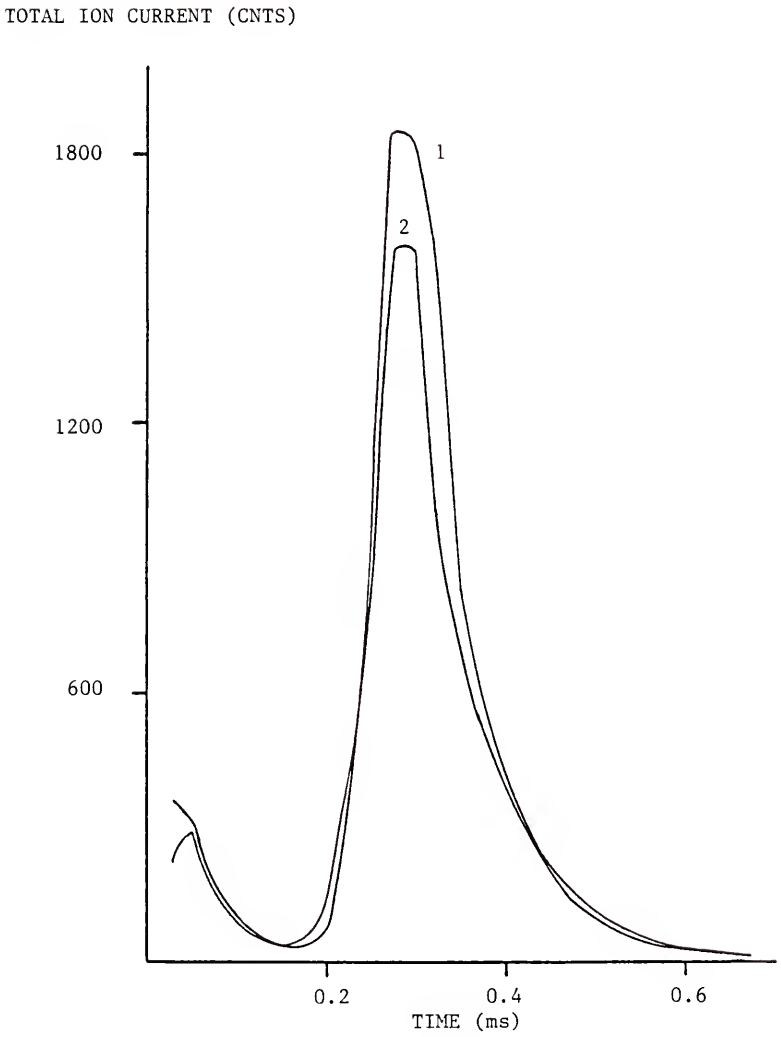
TOTAL ION CURRENT (CNTS)
1800
1200
600
1
2
0.2
0.4
0.6
TIME (ms)

Figure 5.8

Plot of total ion current vs. time for phenytoin in parlodion film (no Na_2CO_3) with auxiliary CI, Q1 passing m/z 253. Reagent gas was methane at 0.64 torr. Experiment run in EI ion volume with filament on.

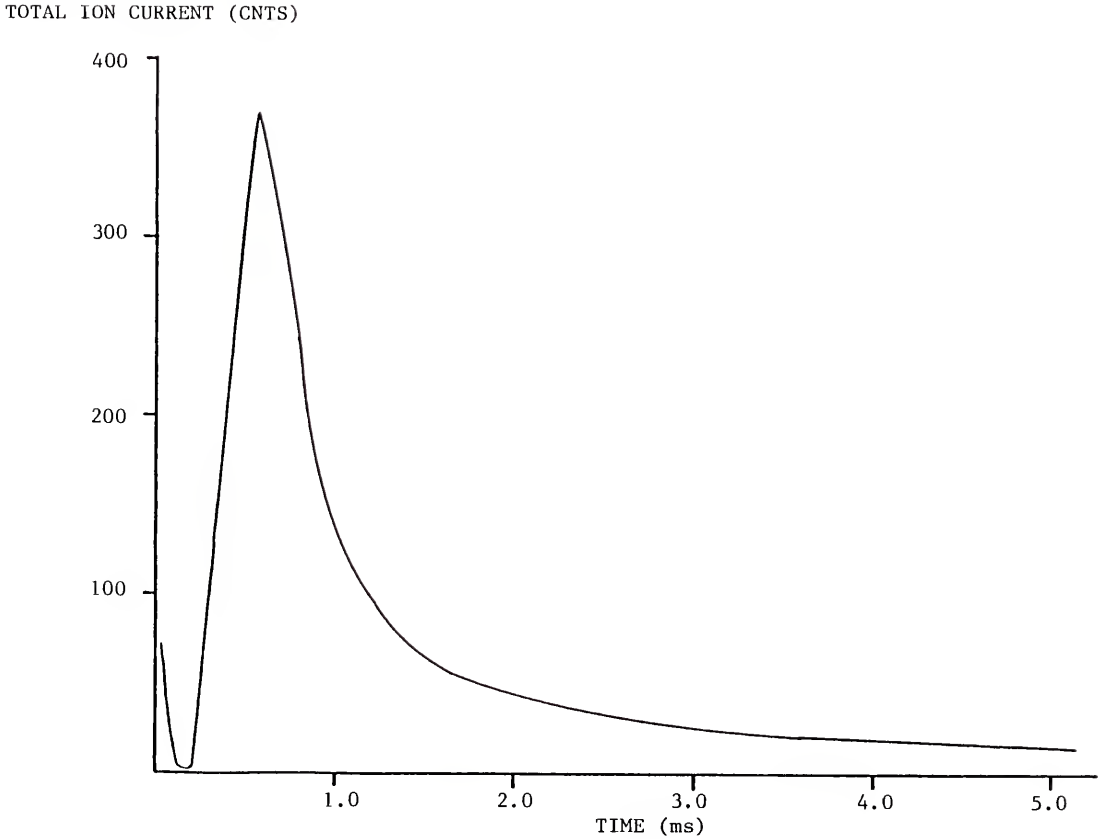
TOTAL ION CURRENT (CNTS)
400
300
200
100
1.0
2.0
3.0
4.0
5.0
TIME (ms)

dependent on conditions existing within the ion source (reagent gas, source pressure, filament on or off, open or closed source). This relatively long-lived signal is indicative of a reaction mechanism that may not be directly linked to the laser pulse. This last result gave renewed hope that signal lifetime could be increased by combining chemical ionization in a closed source with laser vaporization to produce a workable tandem mass spectrometer-based probe-type instrument.

CHAPTER VI

LONG-LIVED PROCESSES

Initial experiments conducted to gain an impression of the possible success of laser microprobe MS/MS produced very encouraging results (115). In contrast to the reports of other workers using single shot lasers, signal lifetimes of seconds, rather than microseconds or, at most, milliseconds, were observed from a number of compounds, irradiated in a CI source pressurized with 0.9 torr of methane. No signals were observed that corresponded to cationized molecules or metal ions, species usually linked directly to the laser event; however, a mixture of nine anticonvulsant drugs was analyzed and each component was detected as a daughter ion which resulted from collisional dissociation of the corresponding molecular ion. This greatly increased the selectivity of the method and indicated that the system had possibilities for probe-type determinations of single components in mixtures.

This chapter presents a more in-depth investigation of these results, with the purpose of explaining the apparent disparity between the preliminary results outlined above and the work of other investigators. A model for the mechanism of ion production is developed and used to show the dependence of the process on source

temperature and pressure, and possible dependence on substrate material. Finally, the laser-induced process and the model are evaluated for their analytical potential.

Long-Lived Signal Profiles

Extending the lifetimes of laser-induced signals is of primary importance if they are to be useful in quantitative analysis. Since the quadrupole mass spectrometer has the capability of scanning at 1 to 5 u ms^{-1}, depending on the centroid sampling interval selected, this requirement can be satisfied if signals can be made to last for one or more seconds. To meet this requirement, the closed CI ion source was substituted for the open EI ion source used for the work reported in Chapter V. Figure 6.1 shows the signals produced by laser evaporation of carbamazepine epoxide (mol wt 252) in parlodion film inserted on a copper EM grid into the CI source heated to 160°C and pressurized to 0.90 torr with methane. The centroid sampling interval was set to 50 μs for this experiment, and Q3 was scanned from m/z 240 to 310 in 29 ms to give a normal mass spectrum of the molecular ion region (2 ms delay between scans). Traces 1-3 in Figure 6.1.A show successive shots at the same site. Trace 4 is from a new site on the same grid. The diameter of the hole produced by the laser was about 0.5 mm for 18 kV laser driver voltage and 8 mm laser cavity diameter. Figure 6.1.B shows trace 4 on an expanded time scale, demonstrating a decay back to zero

Figure 6.1

Plot of reconstructed ion current (RIC) vs. time for laser evaporation of carbamazepine epoxide (mol wt 252) in CI source at 160°C with 0.90 torr of methane. Traces are: (Part A.1-3) successive shots at a single site on copper EM grid; (Part A.4) shot at different site on same grid; and (Part B) trace 4 on an expanded time scale. Ion currents are given as counts (CNTS).

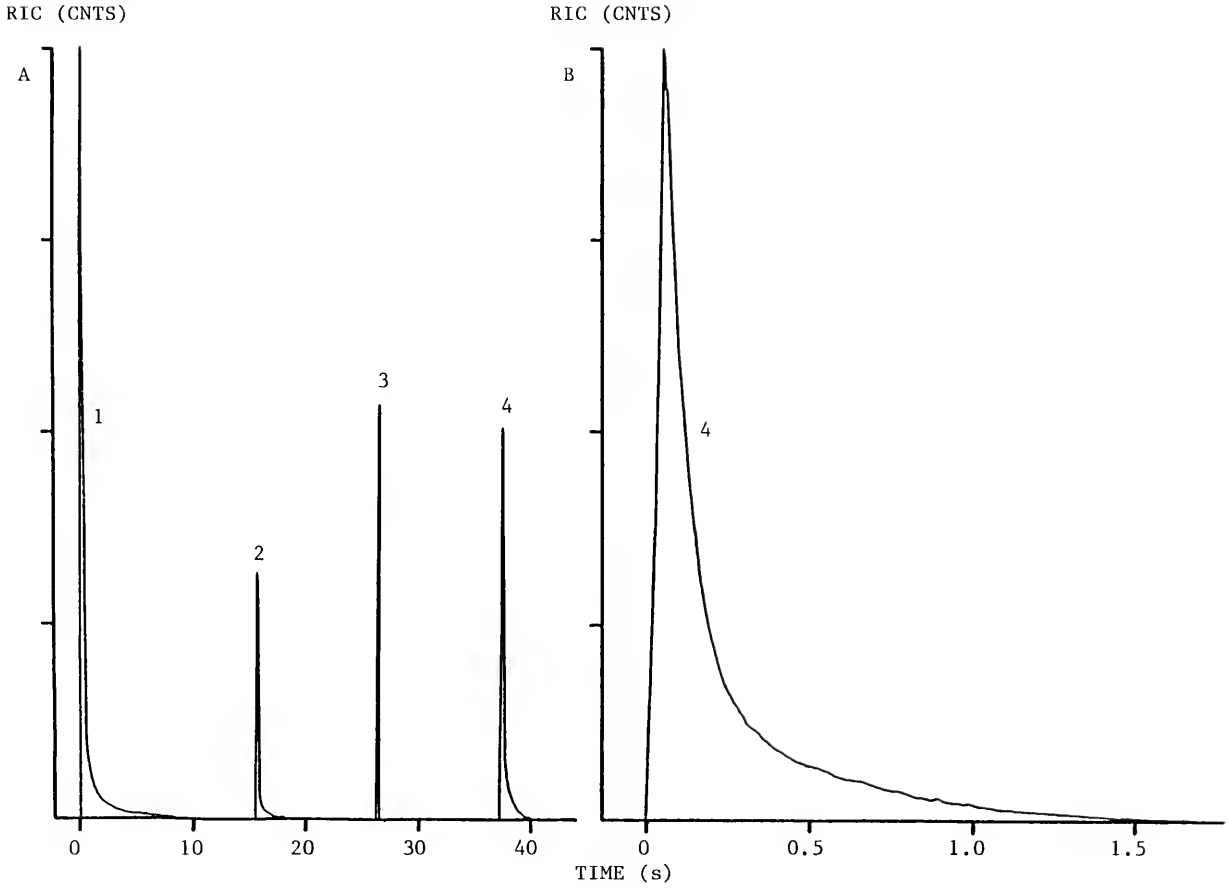
RIC (CNTS)
A
1
2
3
4
0
10
20
30
40
RIC (CNTS)
B
4
0
0.5
1.0
1.5
TIME (s)

intensity after about 1.7 s. This recombined ion current (RIC) consisted of the protonated molecular ion at m/z 253 and normal methane CI adducts, $(M+29)^+$ and $(M+41)^+$, all of which persisted throughout the signal lifetime. Ion signals having this longevity allow scanning over a reasonable mass range during the time the signal is present, and allow use of CAD conditions to provide the selectivity necessary for molecular analysis of mixtures.

Figure 6.2 shows laser-induced ion signals from (A, B) tetrabutylammonium perchlorate, (C) menthol glucuronic acid, (D) adenosine, and (E) acetazolamide, respectively, acquired under the same conditions used for carbamazepine epoxide (normal mass spectrum). The most intense ions are the protonated molecular ions for adenosine (m/z 268) and acetazolamide (m/z 223), and a thermal degradation product for menthol glucuronic acid (m/z 139, M+H-glucuronic acid). These ions were present throughout the signal lifetime. The most intense ions from tetrabutylammonium perchlorate initially were the degradation products, m/z 184, 185, 186 (M-butyl fragments). These made up the initial spike, however, there was a considerable contribution (A) from the tetrabutylammonium ion (m/z 242) to signal B, which rapidly became the predominant ion, indicating that degradative processes were not totally responsible for the signal. All laser-induced RIC signals had similar profiles showing an intense initial spike that lasted for one to several scans before decreasing rapidly to a more slowly decaying signal, which sometimes began with an obvious secondary wave (D and E). Specific ion

Figure 6.2

Plots of ion current vs. time for laser vaporization of (B) tetrabutylammonium perchlorate, (C) menthol glucuronic acid, (D) adenosine, and (E) acetazolamide with Q3 scanned over the appropriate 70 u mass range in 29 ms with a 2 ms delay between scans. Base peaks are (B) m/z 184, (C) m/z 139, (D) m/z 268, and (E) 223. The upper trace (A) shows the profile of the tetrabutylammonium ion from tetrabutylammonium perchlorate. B-D are reconstructed ion currents. Profile A is single ion current.

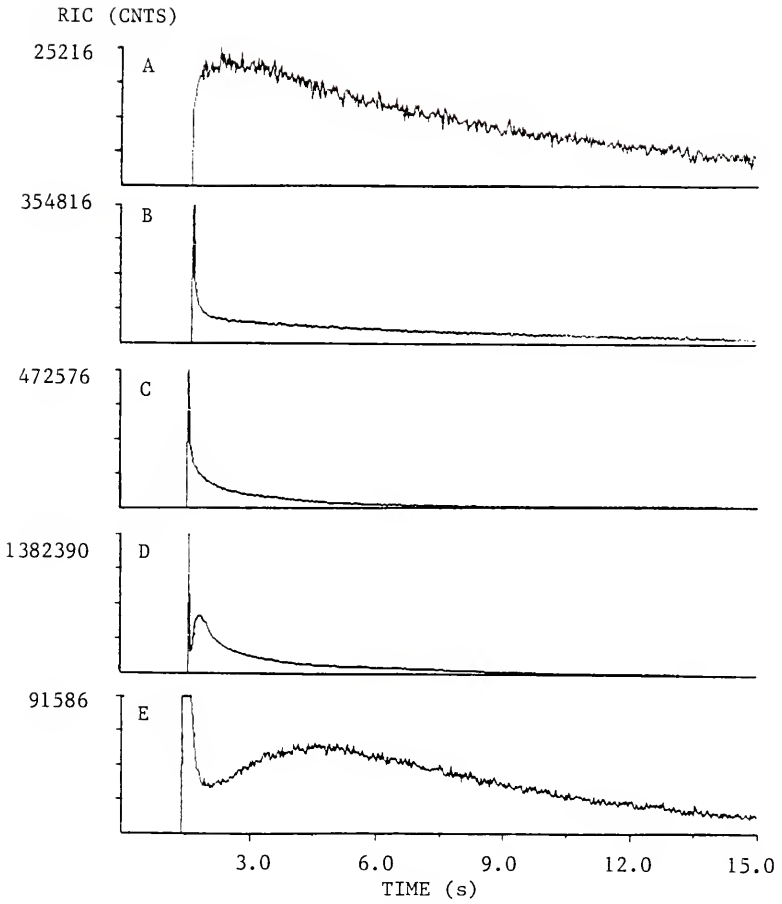
RIC (CNTS)
25216
A
354816
B
472576
C
1382390
D
91586
E
3.0
6.0
9.0
12.0
15.0
TIME (s)

signals, primarily the protonated molecular ion and typical adduct ions (e.g., $(M+C_2H_5)^+$ and $(M+C_3H_5)^+$ for methane reagent gas) generally, but not always, persisted (within the limits of sensitivity) throughout both spike and wave sections. The scan being acquired at the time the laser was fired always contained an intense ion signal, due to electronic interference, that corresponded to the mass being passed at that instant. All scans after the first contained only ion signals resulting from ionization (protonation), adduct formation, and fragmentation of the sample. The secondary wave (more noticeable in D and E than in B and C) indicates that a second mechanism, which may be laser-induced but continues to operate after the thermal effects of the laser should have subsided, is responsible for part of the signal. The appearance of an obvious second wave is not linked to specific compounds or functional groups, but occurs randomly with all compounds that exhibit intense, long-lived ion signals. Characteristics of laser induced ion signals for other test compounds are given in the appendix and show signal lifetimes (time for signal to reach 10% of maximum) which varied from about 0.1 s to 70 s.

Desorption Chemical Ionization

As is often the case in research, several serendipitous occurrences provided clues to the origin of the signals. The first of these occurrences was the replacement of an ailing electron multiplier in the TSQ, and the second was the modification of the 45° probe tip to allow samples to float in the ion source without the stainless steel backing that the 90° probe tip provided. The new electron multiplier was

extremely sensitive, and could be operated at 30-40% of the voltage required with the old multiplier. It was only after this multiplier was installed that spontaneous ion signals were obtained prior to firing the laser when an EM grid with sample was inserted into the CI ion source on the 90° probe tip. Modification of the 45° probe tip (henceforth called the DCI probe tip) enhanced this process (apparently by more efficiently exposing the sample to the reagent gas plasma) so that it was observed whenever a sample was introduced and not just occasionally as with the 90° probe tip. This phenomenon occurred with all compounds that could be vaporized from the solids probe by direct heating, and required no stimulus other than being placed in a heated source with reagent gas (filament on). This process is not new and was reported by Baldwin and McLafferty (116) in 1973 and called Direct Chemical Ionization. Since then it has been investigated by a number of other workers (91, 110, 117-120) and is now commonly referred to as Desorption Chemical Ionization (DCI).

The process (not laser-induced) is shown in Figure 6.3 for phenytoin, a relatively nonvolatile compound with a melting point of 294-298°C. The RIC is shown along with the solids probe temperature for CAD of m/z 253 with 2 mtorr of nitrogen in Q2 and a collision energy of 18 eV. Q3 was scanned from m/z 100 to 300 in 2 s. Source temperature was 160°C and the methane reagent pressure was 0.90 torr. The probe was cooled to 10°C using freon and allowed to reheat by conduction from the source block. After the ion signal had risen to a plateau, the probe was cooled to -7°C. For this experiment, about 9 ug

Figure 6.3

Plots of RIC vs. time and solids probe temperature (°C) vs. time for desorption chemical ionization of phenytoin from copper grid floating in CI source at the electron entrance aperture.

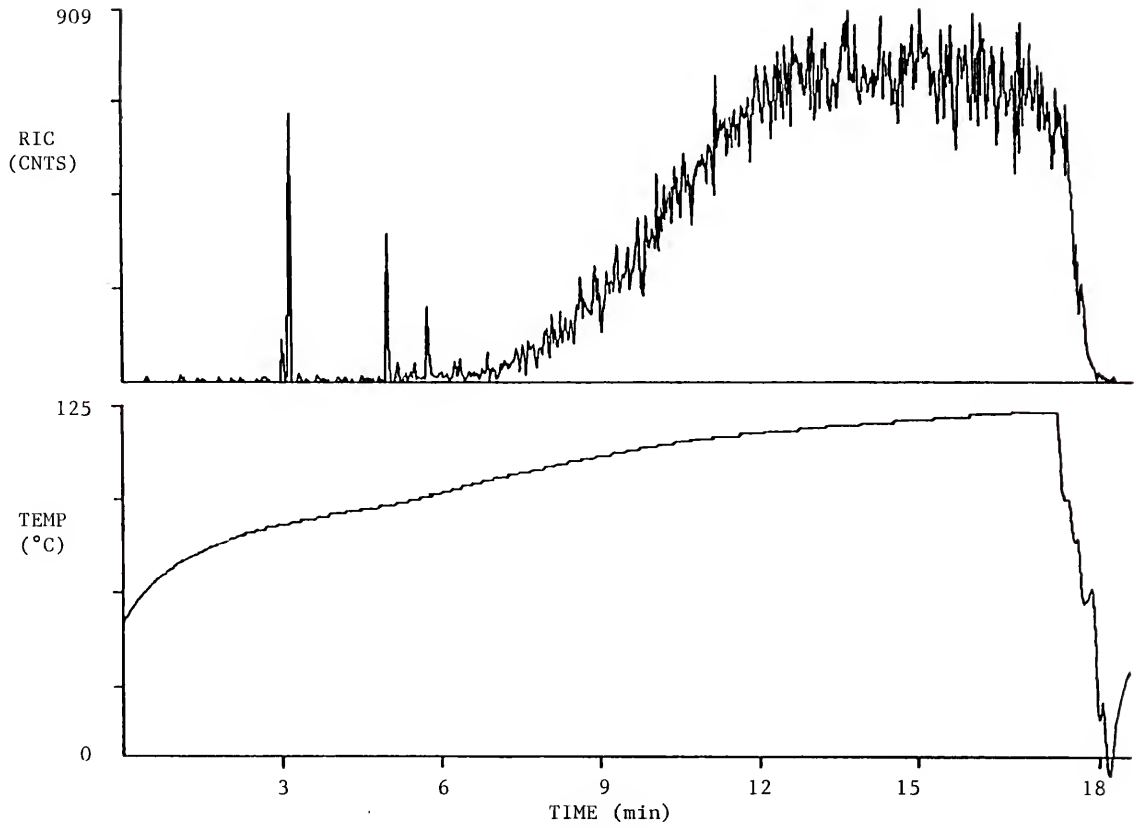
909
RIC
(CNTS)
125
TEMP
(°C)
0
3
6
9
12
15
18
TIME (min)

of phenytoin was evaporated onto a copper grid from a methanol solution containing parlodion. The grid was placed in the source directly in front of the electron entrance aperture. All daughter ions followed this profile.

Figure 6.4 shows negative ion CI/CAD summed ion current profiles and solids probe temperature profiles for direct probe evaporation (evaporation from a glass solids probe vial by resistive heating of the solids probe) and DCI of 7.2 ng of Hydergine (ergotoxine methanesulfonate). The reagent gas was methane:nitrous oxide (100:11) at a combined pressure of 1.11 torr. A collision energy of 25 eV was used with nitrogen collision gas at a pressure of 2 mtorr. Source temperature was 160°C. The sample was evaporated from methanol solution in the tip of a glass solids probe vial for the direct probe CI experiment, and on a 400 mesh nickel EM grid for the DCI experiment. Ergotoxine is a 1:1:1 mixture of three hydrogenated ergot alkaloids, dihydroergocristine (mol wt 611), dihydroergocryptine (mol wt 577), and dihydroergocornine (mol wt 563), each made up of dihydrolysergic acid (mol wt 270) and a cyclized tripeptide. The lysergic acid portion (as dihydrolysergamide, mol wt 269) is lost in the CI ion source to give, almost exclusively, ions characteristic of the polypeptide portion of each molecule. These ions undergo neutral loss of mass 99, again almost exclusively, to give representative daughter ions for each alkaloid (122). Therefore, Q1 was set to pass the $(M-269)^-$ ions for each component, m/z 294, 308, and 342. Q3 was scanned from m/z 180 to 350 to detect the selected parent ions as well as the respective daughter ions

Figure 6.4

Plots of RIC vs. time and solids probe temperature vs. time for (A) direct probe evaporation from a glass solids probe vial, and (B) desorption chemical ionization from a 400 mesh nickel EM grid of hydergine (dihydroergotoxine methane-sulfonate). Negative ion CI/CAD with methane:nitrous oxide (100:11) with Q1 passing successively m/z 294, 308, and 342 and Q3 scanning from m/z 180 to 350 in 0.145 s. Nitrogen collision gas pressure: 2 mtorr; collision energy: 25 eV.

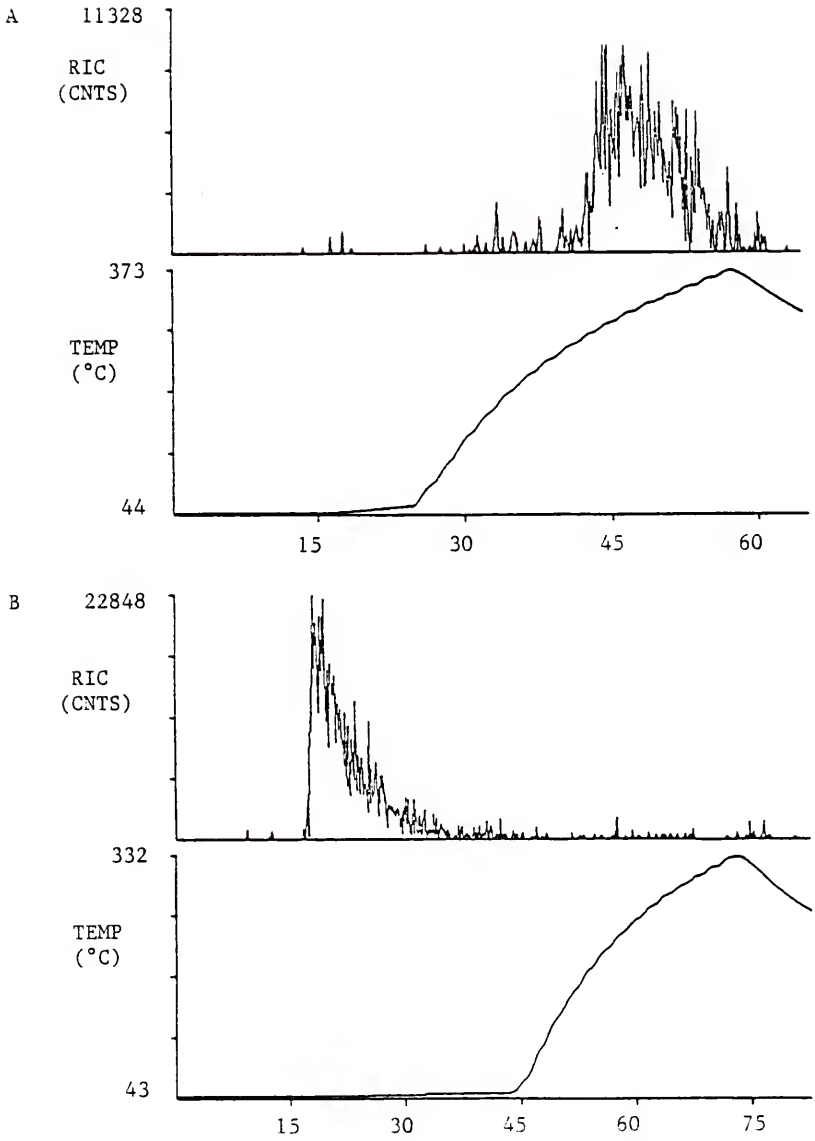
A
11328
RIC
(CNTS)
373
TEMP
(°C)
44
15
30
45
60
B
22848
RIC
(CNTS)
332
TEMP
(°C)
43
15
30
45
60
75

arising from loss of 99, m/z 195, 209, and 243. All ions gave similar ion current profiles. As can be seen from the probe heating cycle (B) initiated after the DCI signal had decayed to baseline, essentially all of the sample vaporized while the probe remained at ambient temperature (43°C). In contrast, significant vaporization from the probe vial did not begin until the heating cycle (A) was almost completed (247°C). This is consistent with the findings of other investigators (116, 120) who reported vaporization of compounds by DCI at temperatures about 150°C lower than those required for direct probe evaporation.

Effect of sample position in source. Figure 6.5 shows the effect of the position of the EM grid in the source on the ion current during DCI (normal mass spectrum, Q3 scanning from m/z 100 to 300 in 2 s). The inset shows the relative positions within the ion source. The sample (phenytoin in parlodion film on copper grid) was inserted into the source, suspended from the end of the DCI probe tip, so that the grid would initially be in front of the electron entrance (A). The solids probe was then rotated to position the grid successively in front of the reagent gas inlet (B), the collector (C), the laser aperture (D), the electron entrance (A), the reagent gas entrance (B), and the collector (C). Relative ion intensities were similar throughout the experiment. The data show that the sample was most readily desorbed or vaporized when it was directly in front of the reagent gas inlet. If the grid were inserted on the 90° probe extension which prevented the reagent gas from directly hitting the grid, DCI was delayed or prevented, and, if it occurred, was less intense.

Figure 6.5

Plot of RIC with respect to position of sample in CI ion source for phenytoin on copper grid. Sample inserted into source with grid (A) positioned in front of electron entrance. Probe rotated to position grid in front of reagent gas inlet (B), in front of collector (C), in front of laser aperture (D), in front of electron entrance (A), in front of reagent gas inlet (B), and in front of collector (C). Diagram shows relative positions in ion source.

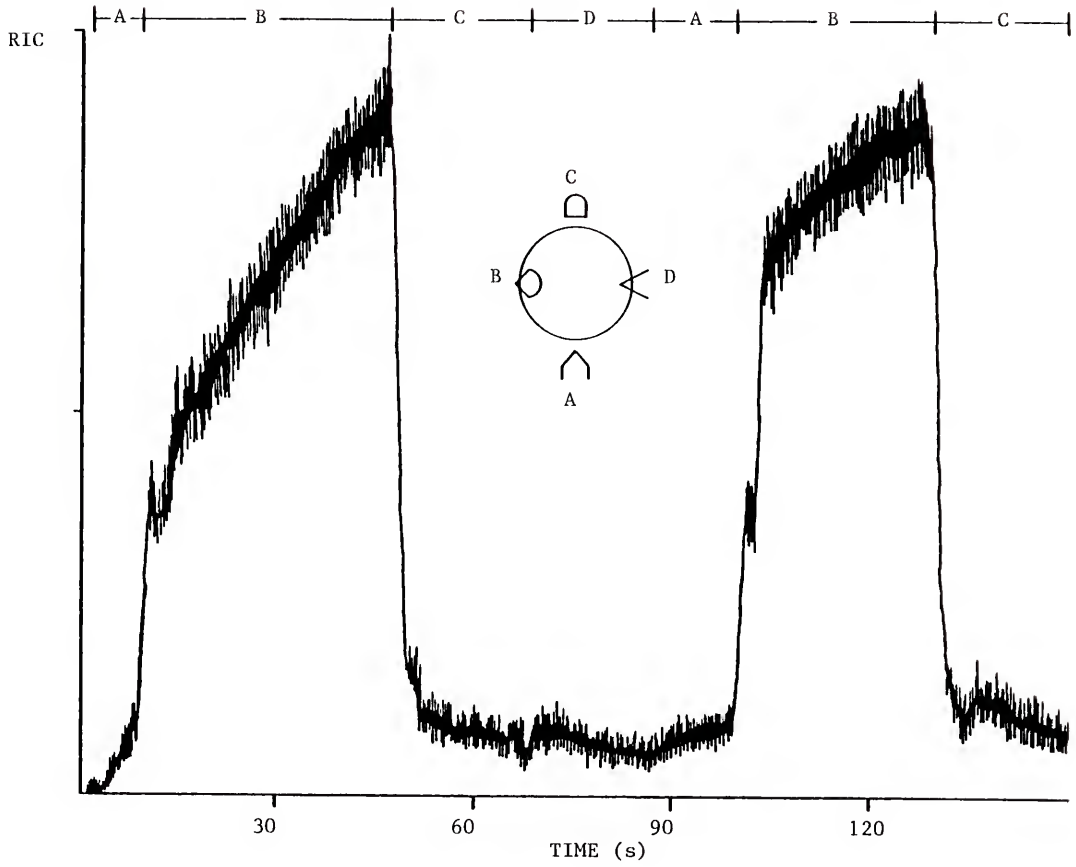
A
B
C
D
A
B
C
RIC
C
B
D
A
30
60
90
120
TIME (s)

The above experiment, and the fact that sample was not vaporized from a grid placed in the CI source under the same conditions but without reagent gas, pointed to the action of the reagent gas molecules on the sample surface as the primary mechanism of sample vaporization. Since the optimum sample position was directly in front of the reagent gas inlet, this mechanism may even involve a sample bombardment by reagent gas entering the source. This was further proved by turning the filament on at different times after inserting a series of identical samples (sodium phenytoin) into the CI source with reagent gas present (helium at 0.90 torr). Helium was selected as the reagent gas for this experiment because it caused desorption of molecules, but allowed ionization and fragmentation primarily by electron impact (121). The positive He-CI spectra of phenytoin free acid and sodium phenytoin were similar and showed extensive fragmentation of the molecular ion. The major ions were m/z 165 (100%) and m/z 180 (80%). The molecular ion for both forms of phenytoin was m/z 252 (M^+, 8%). The sodium salt of phenytoin was used in this experiment for several reasons. First, no signal could be obtained when 800 ng of the salt was placed in a probe vial and heated to 353°C. Second, while no signal was obtained for 800 ng of salt placed on a copper grid and subjected to DCI conditions, a substantial signal was obtained when a nickel grid was used. Third, the presence of a preformed ion (PHT^-) in the sample might provide a signal if ablation occurred when the filament was off. Figure 6.6 shows the results of this experiment (normal positive mass spectrum), in which the sample was inserted into the source (160°C) on the DCI probe extension

Figure 6.6

Plots of RIC vs. time for DCI of sodium phenytoin inserted into source at 160°C with 0.90 torr of methane. Filament turned on (A) before insertion, (B) 12 s after insertion, and (C) 34 s after insertion. Points 1 and 2 show the points at which filament came on in B and C, respectively.

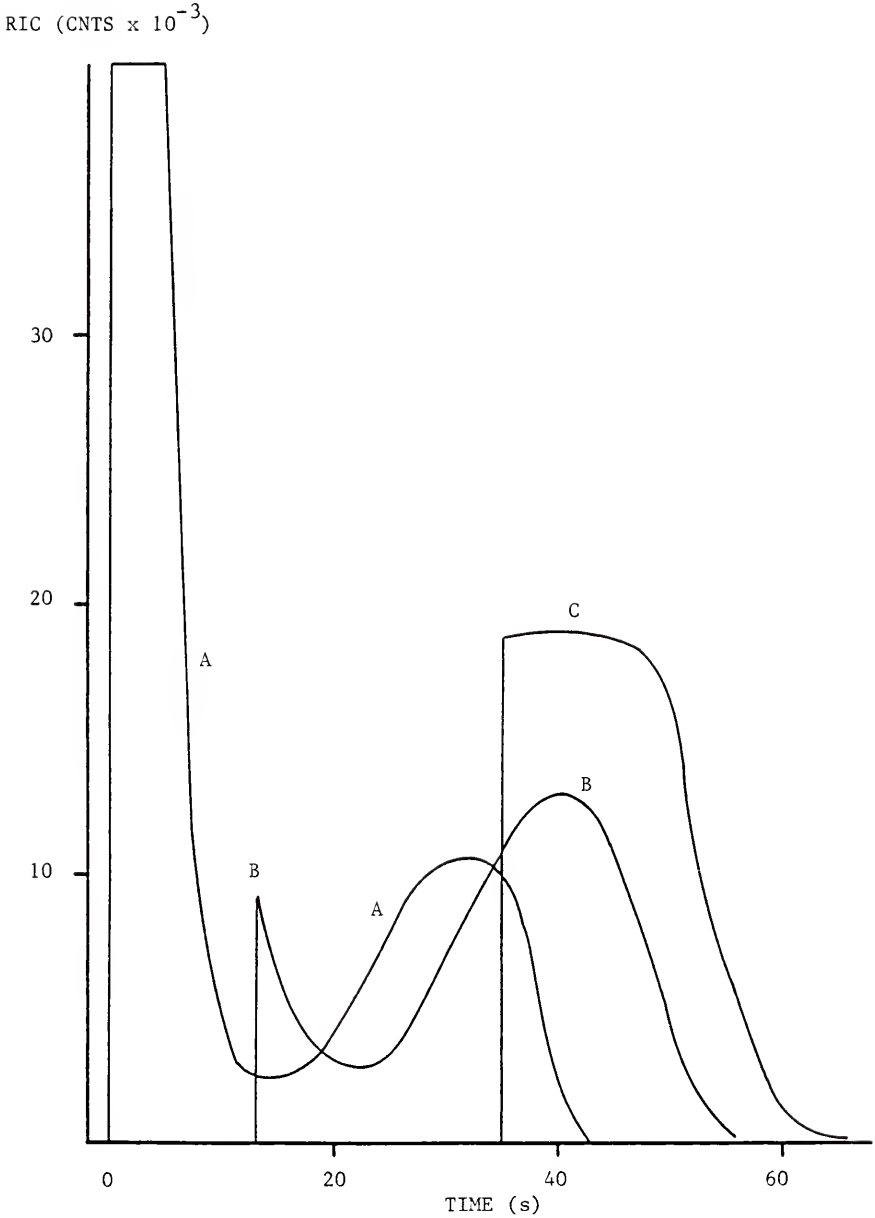
RIC (CNTS x 10^{-3})
30
20
10
A
B
A
B
C
0
20
40
60
TIME (s)

(A) with the filament on, (B) with the filament off initially but turned on after 12 s, and (C) with the filament off initially but turned on after 34 s. Apparently, ablation occurs as long as reagent gas is impinging on the sample, whether or not the filament is on. Signals B and C begin when the filament is turned on, but appear to pick up the profile of signal A at that point that corresponds to the time the sample has been in the source. There is no signal, however, when the filament is off, so the molecules that vaporize or desorb during that time, do so as neutral species and are not observed. The molecular ion was evident in A only for the first 5 to 6 s. Thereafter, the m/z 165 and 180 fragments made up the total ion current in A, B, and C. The intensities of these two ions summed over the time of each curve were 5.49×10^6, 1.32×10^6, and 1.32×10^6 counts for A, B, and C, respectively. These values appear to indicate that there is a relatively loosely bound (possibly by inter-molecular forces) group of molecules, which can be easily vaporized. There is, however, another group of more tightly bound molecules (possibly by molecule-surface binding forces), which requires input of more energy to be vaporized. Otherwise, the summed ion intensity for curve C would be less than that for curve B, since the sample was in the source about 3 times longer before the filament was turned on. Therefore, the ionized reagent gas must impart more energy to the sample surface than the neutral gas molecules.

Laser-Induced (Enhanced) Desorption Chemical Ionization

Since the process of DCI could be stopped by cooling the grid indirectly through the solids probe, the question remained as to the effect of cooling on the laser-induced process. As it turned out, cooling the grid to -20°C had no effect on the response elicited when the laser was fired. Figure 6.7 shows this for phenobarbital deposited on a copper grid with parlodion (normal positive methane CI spectrum, Q3 scanned from m/z 160 to 300 in 33 ms, 75 μs centroid sampling interval). The plot of RIC vs. time and the corresponding plot of solids probe temperature vs. time show the presence of the DCI signal (1) and the decrease in DCI with probe cooling. The effect of probe cooling is not so immediate as with phenytoin because the melting point (174-178°C) of phenobarbital and, presumably, the heat of vaporization are much lower than those for phenytoin. The laser was fired (2) when the ion current had decreased to a low level, and the signal that resulted contained the initial high spike and long tail, typical of the process. This process can therefore be called Laser-Induced or Laser-Enhanced Desorption Chemical Ionization (LIDCI or LEDCI), depending on whether the DCI signal is absent or present when the laser is fired. Ions present during the DCI phase and after the laser was fired included the protonated molecular ion, $(M+29)^+$, and $(M+41)^+$. Point 3 on the RIC curve indicates the point at which the laser was fired again at the same point on the sample. The ion current dropped rapidly to zero, evidently because the input of additional energy hastened the clearing of the ion source, and no additional sample was available at the point of focus.

Figure 6.7

Plots of RIC vs. time and solids probe temperature (°C) vs. time showing Laser-Enhanced Desorption Chemical Ionization of phenobarbital. DCI signal (1) appears before the laser is fired (2) and decreases almost to baseline because of solids probe cooling to -20°C. Laser was fired a second time at point 3.

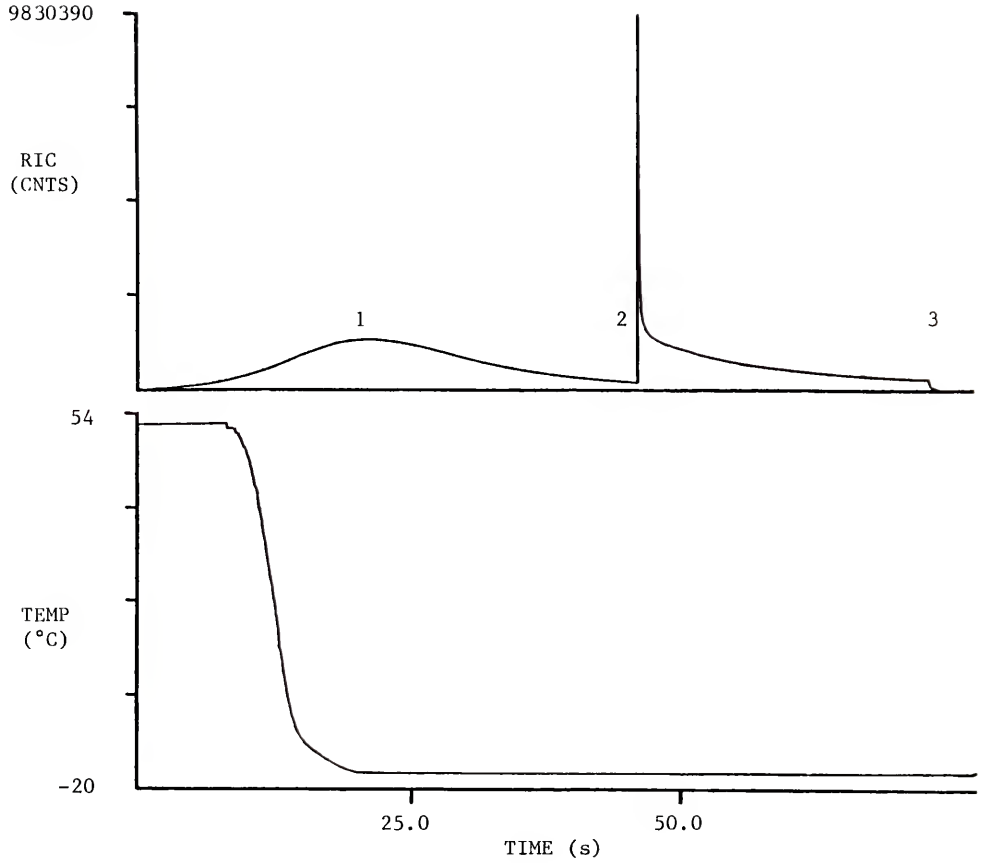
9830390
RIC
(CNTS)
1
2
3
54
TEMP
(°C)
-20
25.0
50.0
TIME (s)

Cotter (60) reported an effect on reagent gas peak intensities, (transient 2- to 10-fold increase in m/z 56, 57, and 58 from isobutane) which occurred over about 5 ms after the laser was fired. Therefore, it is not unreasonable to think that species already vaporized in the source could be affected by acquiring an additional kinetic energy, which either decreased the efficiency of ion extraction, or caused extensive fragmentation to species outside the mass scan range.

Model for Laser-Induced Desorption Chemical Ionization

There is some question as to whether the term, desorption, is applicable in this context, since the process appears to be a thermally-induced vaporization, which involves input of energy sufficient to overcome intermolecular interactions. There is still some question as to whether the process involves the input of energy sufficient to overcome a molecule-to-surface binding energy (desorption). Actually, both processes appear to be at work, the latter predominating when concentrations of analyte are low (a low surface density of sample). The following discussion gives a physical description of the laser effects, and also gives evidence showing that the substrate contributes to sample ablation. Dependence of response on ion source temperature and pressure is determined using DCI as a model for LIDCI.

Pattern of sample removal by a single laser shot. Incidence of focused laser radiation on the EM grid containing a solute residue in a parlodion film results in a specific pattern of sample removal. Each 400 mesh grid (copper, nickel, or silver) is 3 mm in diameter, about

13 μm thick, having a regular square mesh with holes 37 μm square defined by 25 μm thick "wires" (the grid is acually of one-piece construction). The grid is totally vaporized at the point of focus of the laser. In that area of the target, therefore, it would be difficult to propose a mechanism based on transfer of energy from the substrate to the sample. There is, however, a circular area around the hole, having about 2 times the hole diameter, that appears to be cleared of sample with the grid still intact. Examination of the grids under a microscope (100X) revealed that the tips of the wires showed signs of melting (they were bent or of smaller diameter than the rest of the wire. This is to be expected and indicates a gradation of heat emanating from the point of laser focus. Therefore, it is reasonable to propose more than one mechanism of sample ablation to correspond to the different temperature zones present.

Amount of sample removed by a single laser shot. Ion current profiles obtained for identical samples were variable with respect to RIC and, therefore, the amount of sample removed from a grid by a single laser shot was determined by high performance liquid chromatography. To eliminate effects from DCI, the reagent gas was turned off and 5 of 10 identically prepared copper grids (2 μL of a mixture of 0.40 mL of methanol plus 0.20 mL of parlodion solution containing 20 mg/mL of methanol:ether (1:3)) were placed sequentially in a 160° CI source on the 90° probe extension. Each grid contained 1.11 μg of phenytoin in a residue about 1.7 mm in diameter (48 μg phenytoin cm^{-2}). The laser was fired once at each grid, and the residue left on each grid (as well as

the residue on each of the other 5 control grids) was extracted and analyzed by high performance reversed-phase liquid chromatography with p-methylphenobarbital (MPB) as the internal standard. The results of the analysis including visual (microscopy at 100X magnification) determination of the hole areas and areas from which the film was vaporized around the hole are shown in Table IV. From the average amounts of PHT recovered from the test (0.92±0.04 μg) and control (1.05±0.03 μg) grids, it appears that an average of 13% of the PHT was removed by the laser shot. The average area of the residue noticeably affected (hole plus de-filmed area) is 18%. These values indicate that the distribution of solute in the film may not be as even as it appears, with solute still being concentrated near the edge of the residue (laser was focused in the center of the grid). Even so, the residue is noticeably more evenly distributed than it is without the parlodion film.

Reproducibility of ion current profiles and relative ion intensities. Figure 6.8 shows plots of RIC vs. time for LIDCI (normal Q3 mass spectrum) of a mixture of PHT and 1,3-^{15}N-2-^{13}C-phenytoin (PHT*) (2 μL of a mixture of 0.40 mL of a solution of 9.60 mg/mL of PHT and 8.94 mg/mL of PHT* in methanol plus 0.40 mL of a solution of 20 mg/mL of parlodion in methanol:ether (1:3)). This solution was evaporated on 5 copper grids, and each grid was inserted into the ion source on the 90° probe tip. Two shots were fired at each grid on opposite edges (but within the boundaries) of the residue. Plot A shows all first shots, and plot B shows all second shots. All traces decayed to baseline

Table IV. Weight of Phenytoin[a] Removed from Copper Grid by a Single Laser Shot

Sample[b]	Ratio[c]	Weight Phenytoin (μg) Loaded	Recovered[d]	Removed[e]	Area ($cm^2 x 10^3$) Hole	De-filmed)
T1	1.13	1.11	0.904	0.21 (0.15)	0.66	4.5
T2	1.23	1.11	0.984	0.13 (0.07)	0.96	4.0
T3	1.16	1.11	0.929	0.18 (0.12)	0.50	4.2
T4	1.09	1.11	0.873	0.24 (0.18)	0.61	4.8
T5	1.14	1.11	0.913	0.20 (0.14)	0.48	3.5
C1	1.27	1.11	1.02	-	-	-
C2	1.29	1.11	1.03	-	-	-
C3	1.34	1.11	1.07	-	-	-
C4	1.34	1.11	1.07	-	-	-
CAL1	0.615	0.50	correlation coefficient	:	0.9996	
CAL2	1.27	1.00	slope	:	1.26	
CAL3	1.84	1.50	intercept	:	0.010	
CAL4	2.52	2.00				

a) 1.11 μg PHT deposited as a solution containing parlodion.
b) T = test sample; C = control sample; CAL = calibration sample.
c) From HPLC: ratio of peak heights, PHT/MPHT.
d) From HPLC.
e) Calculated from weight actually loaded, or (in parenthesis) from the average weight recovered from control samples.

Figure 6.8

Plots of RIC vs. time for a mixture of phenytoin and 1,3-^{15}N-2-^{13}C-phenytoin with parlodion evaporated on copper grids. Traces are for 2 shots fired at each of 5 grids. All first shots (A) are compared with all second shots (B).

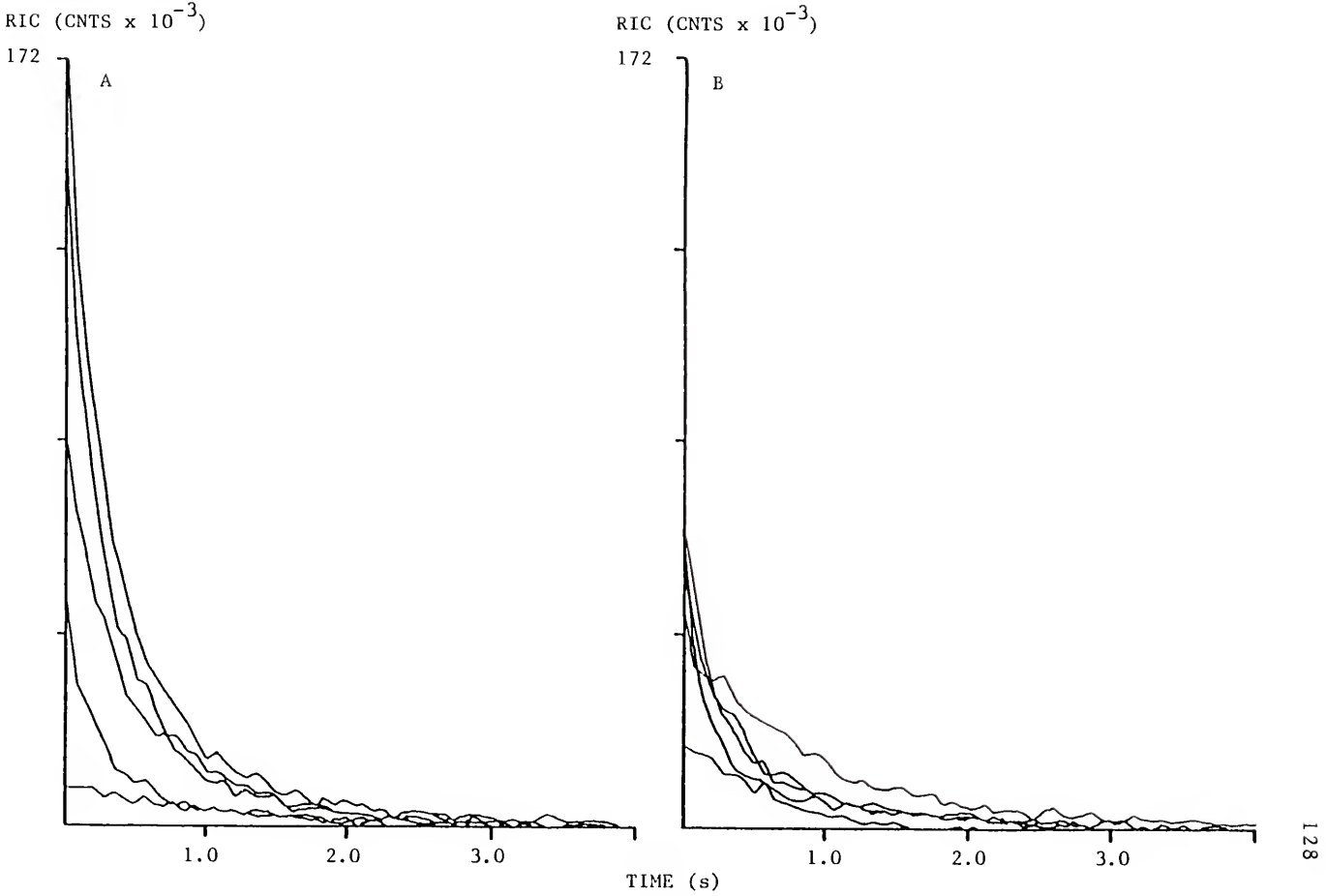
RIC (CNTS x 10^{-3})
172
A
1.0
2.0
3.0
RIC (CNTS x 10^{-3})
172
B
1.0
2.0
3.0
TIME (s)

within 4 s. Table V gives the ratios of the integrated $(M+H)^+$ ion intensities for PHT (m/z 253) to those of PHT* (m/z 256), calculated by summing the scans from the first scan after the laser shot to the scan whose RIC was 25% of that of the first scan. The scan being acquired at the time the laser was fired was always eliminated from calculations, because this scan contained an intense artifact peak which appeared at the mass being passed at the instant of laser firing. Although the RIC curves were variable in intensity, relative ion intensities were reproducible for the protonated molecular ions. These ions accounted for between 82% and 99% of the total RIC. The only other ions present were the normal methane CI adduct ions. Maximum RIC at the scan after the laser shot varied between 8448 and 172288 counts. This variability in RIC is not unexpected, because laser ablation and laser desorption mass spectrometry have been plagued from the outset by a pronounced irreproducibility of relative and absolute ion intensities (32). The relatively stable ion intensity ratios, however, provide hope that, if ion lifetimes can be extended to allow signal averaging, the precision required for quantitation may be obtained.

Effect of substrate on DCI signals. The uncertainty over whether there is a desorption process occurring in addition to a vaporization process was resolved by comparing signals obtained with different sample substrates. An analyte stock solution (graded melting point standard) was made up which contained a series of compounds having melting points spanning the range from 76°C to greater than 300°C (Table VI). A working solution was made by adding 1 µL of stock to 100 µL of methanol,

Table V. $(M+H)^+$ Ion Intensity Ratios for LIDCI of PHT and PHT* Deposited with Parlodion on Copper Grids. Comparison of 2 Shots at Different Sites on Each of 5 Grids

	Ion Intensity Ratio[a]	
Grid	First Shot	Second Shot
1	0.912	0.940
2	0.967	0.947
3	0.992	0.866
4	0.907	0.961
5	0.950	0.951
ave. ± SD	0.945 ± 0.033	0.93 ± 0.04
ave ± SD for all shots:	0.94 ± 0.04	

a) Ratio of m/z 253 to m/z 256.

Table VI. Graded Melting Point Standard Solution Containing Compounds Having Melting Points from 76°C to Above 300°C

Compound (Abbrev.)	Melting Point (°C)	Mol Wt (g/mol)	Conc[a] (mg/ml)	Characteristic Ions	
				Parent[b]	Daughter[c]
2-methyl-2-propylsuccinimide (MPS)	76-77	155	4.11	156	86
mephenytoin (MES)	136-137	218	3.76	219	134
phenobarbital (PB)	174-178	232	4.75	233	162
p-methylphenytoin (MPHT)[d]	225-226	266	6.73	267	196
phenytoin (PHT)	295-398	252	4.45	253	182
p-hydroxyphenytoin (HPHT)	above 300	268	4.10	269	175

a) Dissolved in methanol.
b) Positive Ion Methane CI.
c) Most intense daughter ion (for Figures 6.10, 6.15, 6.16).
d) Dissolved in a separate solution for use as an internal standard.

and 1 μL was spotted on 400 mesh copper, nickel, and silver EM grids. Each was inserted into the CI source on the DCI probe tip. The source was maintained at 180°C and was pressurized with 0.90 torr of methane. Q3 was scanned in the normal mass spectrum mode from m/z 100 to 320 in 0.1 s. Figure 6.9 shows the ion current vs. time curves for the protonated molecular ions for the copper grid (A), the nickel grid (B), and the silver grid (C). The copper grid does not give a continuous signal for the highest-melting compound, HPHT. Vaporization (desorption) envelopes begin at later times as compound melting point increases. This is more easily seen for the copper grid since compounds appear to be more strongly held to that material than to the nickel or silver. It is possible that there is some complex formation between the sample components and the copper (123, 124), rather than a simple physisorption of the sample on the less reactive metals, nickel and silver (124). It is doubtful that these effects can be correlated with thermal conductivities of the metals, since those of copper and silver are about equal (3.98 and 4.27 W cm^{-1} $°C^{-1}$, respectively), and that of nickel is much lower (0.899 W cm^{-1} $°C^{-1}$). The only species for which the maximum ion current for copper is higher than that for nickel and silver is MPS, the compound having the lowest melting point (Table VII). Summed ion currents are greater in all cases for nickel than for silver, but greater for the lower melting point components on copper than on nickel. Also, while maximum and summed ion currents decrease as melting points increase for sample components on copper, these values appear less dependent on component melting point for nickel and silver. These

Figure 6.9

Plots of ion current vs. time for protonated molecular ions from graded melting point stock 1:100 dilution (Table 6.3). DCI at 180°C from (A) copper, (B) nickel, and (C) silver 400 mesh EM grids with 0.90 torr of methane. Ions are for MPS (156), MES (219), PB (233), PHT (253), and HPHT (269).

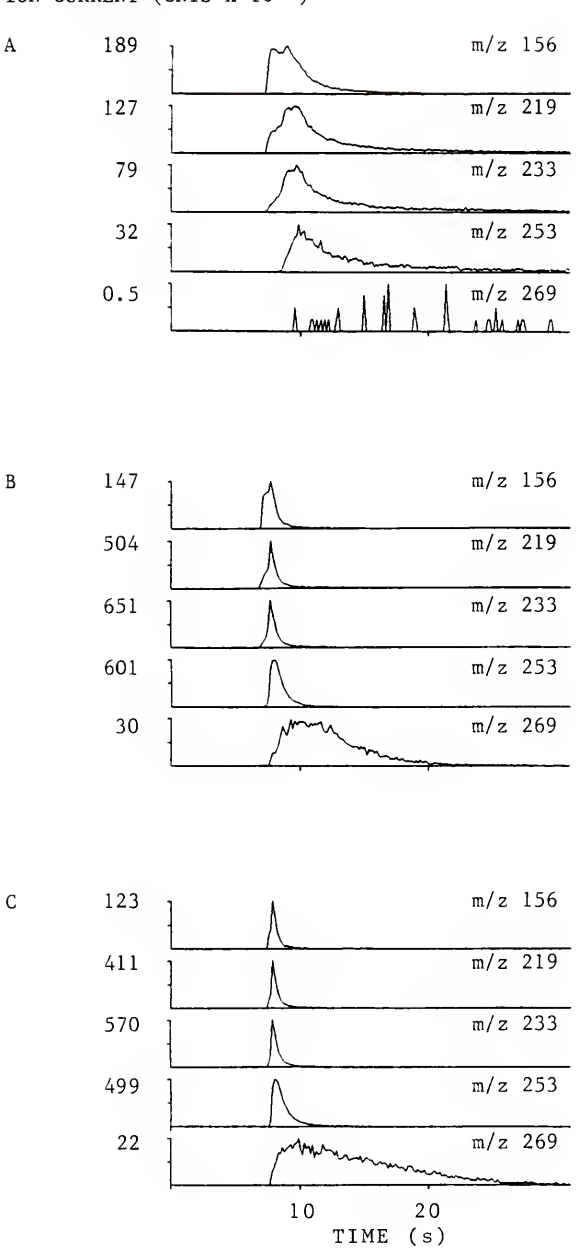
ION CURRENT (CNTS x 10^{-3})
A
189
m/z 156
127
m/z 219
79
m/z 233
32
m/z 253
0.5
m/z 269
B
147
m/z 156
504
m/z 219
651
m/z 233
601
m/z 253
30
m/z 269
C
123
m/z 156
411
m/z 219
570
m/z 233
499
m/z 253
22
m/z 269
10
20
TIME (s)

Table VII. Comparison of Maximum and Summed Ion Currents for DCI of Graded Melting Point Stock 1:100 Dilution[a] from Copper, Nickel and Silver EM Grids

	Ion Current (Counts)				
Grid	MPS	MES	PB	PHT	HPPH
Maximum (Counts x 10^{-3})					
Cu	189	127	79	32	0.5[b]
Ni	147	504	651	601	30
Ag	123	411	570	499	21
Summed (Counts x 10^{-4})					
Cu	413	390	231	97	0.8
Ni	103	272	333	470	175
Ag	44	146	223	393	112

a) See also Figure 6.9.
b) Discontinuous; spikes only.

results indicate that there is a substrate effect, and that, of the three metals used here, nickel and silver are preferable to copper because there appears to be less of an interaction between the substrate and the sorbed species. This, in turn, gives an evaporation profile that is less dependent on melting point or heat of vaporization of the analyte. The substrate effect is an indication that true desorption (molecules in contact with surface) may be occurring in addition to vaporization (molecules in contact with other molecules).

Investigators who have studied DCI have shown an enhancement of the process when nonreactive substrates such as Teflon (118) and Vespel (111) are used. Therefore, desorption profiles for DCI of the graded melting point standard on nickel and Teflon were examined by evaporating identical 1 μL samples onto nickel grids and a Teflon "paddle" made by flattening the end of a short piece of 1.5 mm o.d. capillary tubing. The length of the Teflon probe extension was adjusted so that the paddle would be directly in front of the reagent gas inlet when the probe was inserted into the source (sample side facing inlet). Dilutions of the graded melting point standard (Table VI) were made to give concentrations ranging from about 30 to 300 ng/μL of each drug. The mass spectrometer was set up to acquire in parent spectrum mode sequentially monitoring the daughter ions from the corresponding parent ions as given in Table VI. Figure 6.10 shows the difference in the desorption profiles for a sample containing about 60 to 76 ng of each drug evaporated on nickel and Teflon. Vaporization according to melting point is more noticeable for the sample on Teflon; each ion profile is

Figure 6.10

Plots of ion current vs. time for desorption of graded melting point standard (60-76 ng of each drug) from (A) nickel EM grid, and (B) Teflon probe extension. Selected reaction monitoring parent spectrum. See Table VI for standard composition and parent ion-daughter ion designations. Discontinuous profiles are due to scan characteristics of TSQ operating in MS/MS mode.

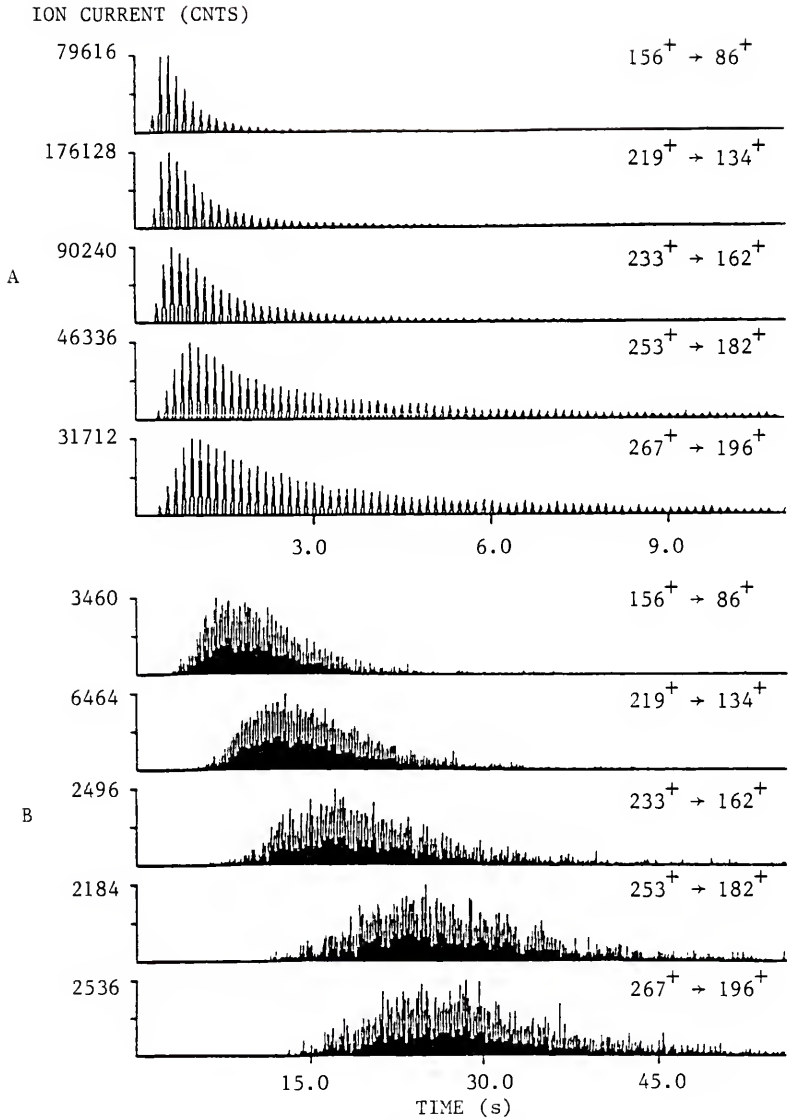
ION CURRENT (CNTS)
79616
156+ → 86+
176128
219+ → 134+
90240
233+ → 162+
A
46336
253+ → 182+
31712
267+ → 196+
3.0
6.0
9.0
3460
156+ → 86+
6464
219+ → 134+
2496
233+ → 162+
B
2184
253+ → 182+
2536
267+ → 196+
15.0
30.0
45.0
TIME (s)

nearly Gaussian, and lasts 7 to 10 times longer than that for the same sample on nickel. The maximum ion current for the sample on nickel, however, is 13 to 36 times greater, and the area under the curve is 2.5 to 5.6 times greater (depending on the compound, but not correlating with melting point) for the sample on nickel. The profile more closely resembles a Poisson distribution. These results are indicative of a primarily thermal process occurring on Teflon, which is impeded by the low thermal conductivity of the substrate. The sample seems to be efficiently desorbed from the nickel, and the metallic surface does not hinder, but enhances the process, because its higher thermal conductivity increases the rate of heat transfer to the sample. The nickel may, in fact, be better for this reason than the inert but less conductive materials. In contrast to copper and stainless steel, nickel has been shown to be nonreactive with respect to labile compounds when used as a column material in gas chromatography (123). Another reason for the faster desorption from the nickel grid could be simply that the area available for contact with the reagent gas is greater with the 400 mesh grid than with the solid Teflon paddle.

Effect of source temperature and pressure. The influence of source temperature and pressure on DCI and LIDCI were examined in view of the results given above which indicate a thermal process, dependent upon close contact between the sample and the reagent gas. Sodium phenytoin (411 ng) was evaporated from methanol solution on nickel EM grids and inserted on the DCI probe tip into the ion source. The mass spectrometer was set up to acquire normal positive ion/negative ion mass

spectra, scanning from m/z 160 to 300. For the temperature experiments, the source pressure (methane) was maintained at 0.70 torr, and the source temperature was varied from 90°C to 180°C. For the pressure experiments, the source temperature was maintained at 160°C, and the pressure was varied from 0.25 torr to 0.98 torr. Figures 6.11 and 6.12 show the RIC vs. time profiles for the temperature and pressure experiments, respectively. As would be expected, ion signal decreases in intensity and longevity as temperature or pressure is decreased. Extent of fragmentation for both negative and positive molecular ions decreased with decreasing temperature and pressure. Negative ions predominated over positive ions as temperature and pressure decreased; however, both negative and positive ion spectra showed the same trends. Figure 6.11 shows the negative ion RIC because there was no positive ion current at the lowest source temperature. Figure 6.12 shows the positive ion RIC. Temperature and pressure conditions are also interdependent, in that a higher temperature will compensate somewhat for a lower pressure. In another experiment with phenytoin free acid, the threshold pressure for desorption was 0.18 torr at a source temperature of 160°C and 0.35 torr at 130°C. These temperature and pressure requirements were also observed for LIDCI; however, it was possible to obtain signals upon firing the laser when temperature and pressure conditions were not sufficient for DCI. Figure 6.13 shows the results of an experiment (normal mass spectrum with selected ion monitoring) in which the graded melting point standard on a nickel grid was inserted on the 90° probe tip into a 160°C source pressurized with

Figure 6.11

Plot of negative ion RIC vs. time for DCI of sodium phenytoin at various source temperatures. Source temperatures are (1) 180°C, (2) 140°C, (3) 120°C, (4) 100°C, (5) 90°C. Source pressure: 0.70 torr.

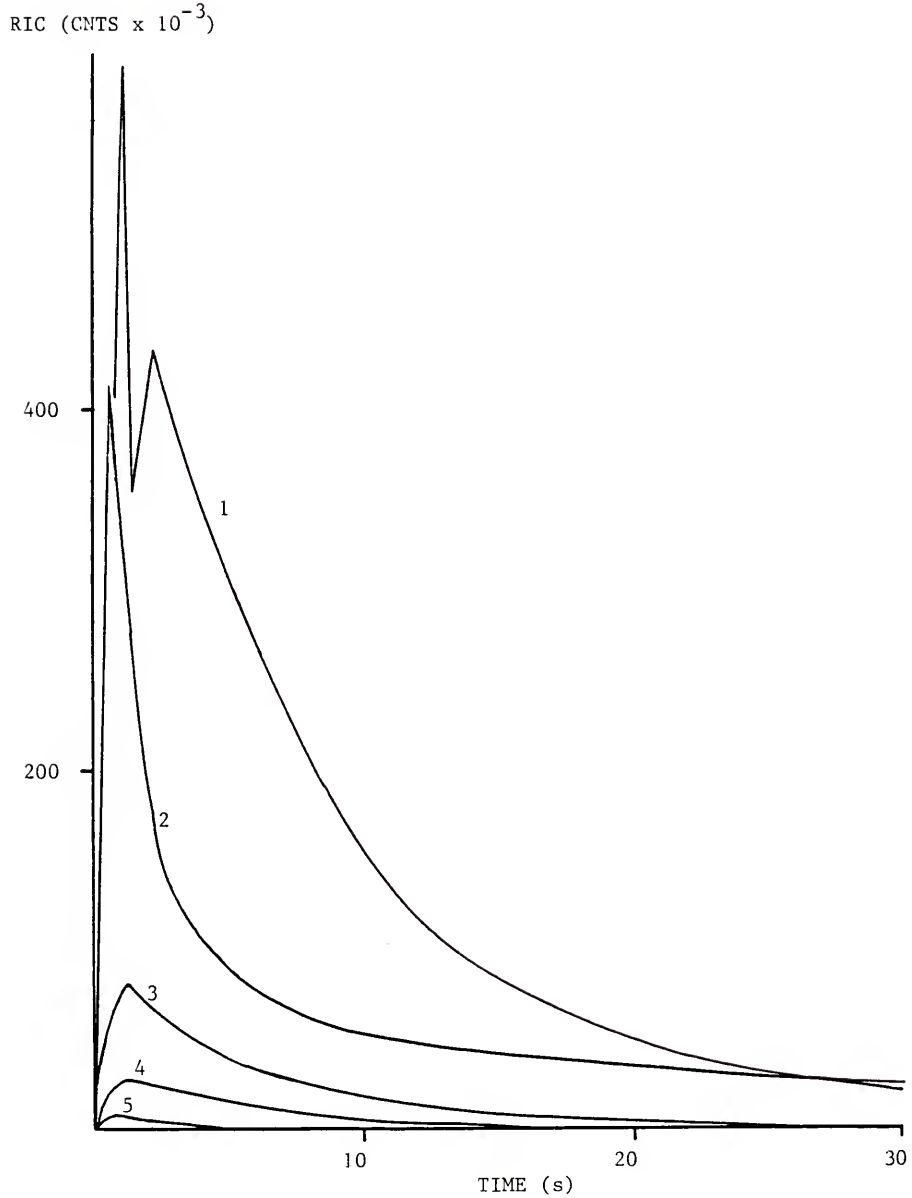
RIC (CNTS x 10^{-3})
400
200
1
2
3
4
5
10
20
30
TIME (s)

Figure 6.12

Plot of positive ion RIC vs. time for DCI of sodium phenytoin at various source pressures. Source pressures are (1) 0.98 torr, (2) 0.71 torr, (3) 0.52 torr, (4) 0.34 torr, (5) 0.25 torr. Source temperature 160°C.

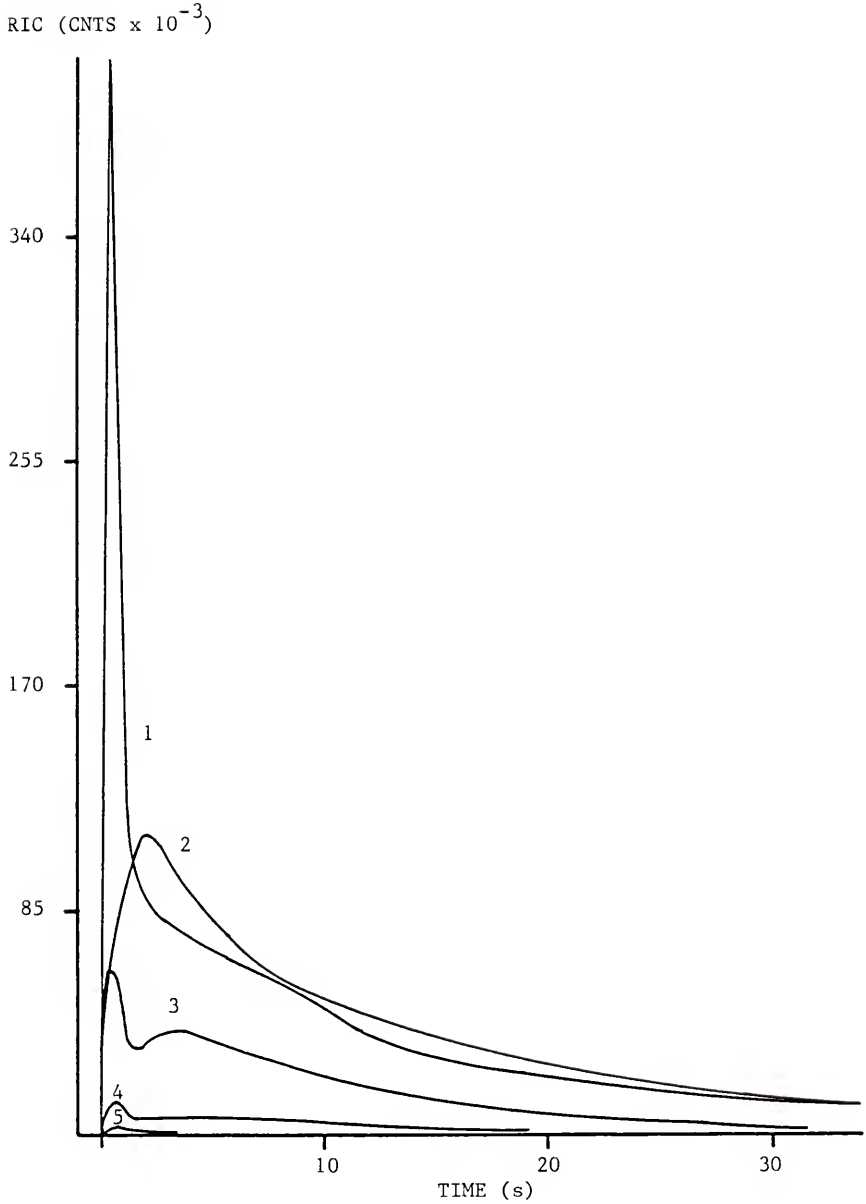
RIC (CNTS x 10^{-3})
340
255
170
85
1
2
3
4
5
10
20
30
TIME (s)

Figure 6.13

Plot of ion current vs. time for LIDCI of components of graded melting point standard. Source temperature was 160°C; pressure of methane was 0.90 torr. Q3 mass spectrum, selected ion monitoring. Signals are for MPS, m/z 156, MES, m/z 219, PB, m/z 233, PHT, m/z 253, MPHT, m/z 267, and HPHT, m/z 269. Profiles plotted to show signal at 1% of maximum for each ion. Laser fired at points 1 and 2.

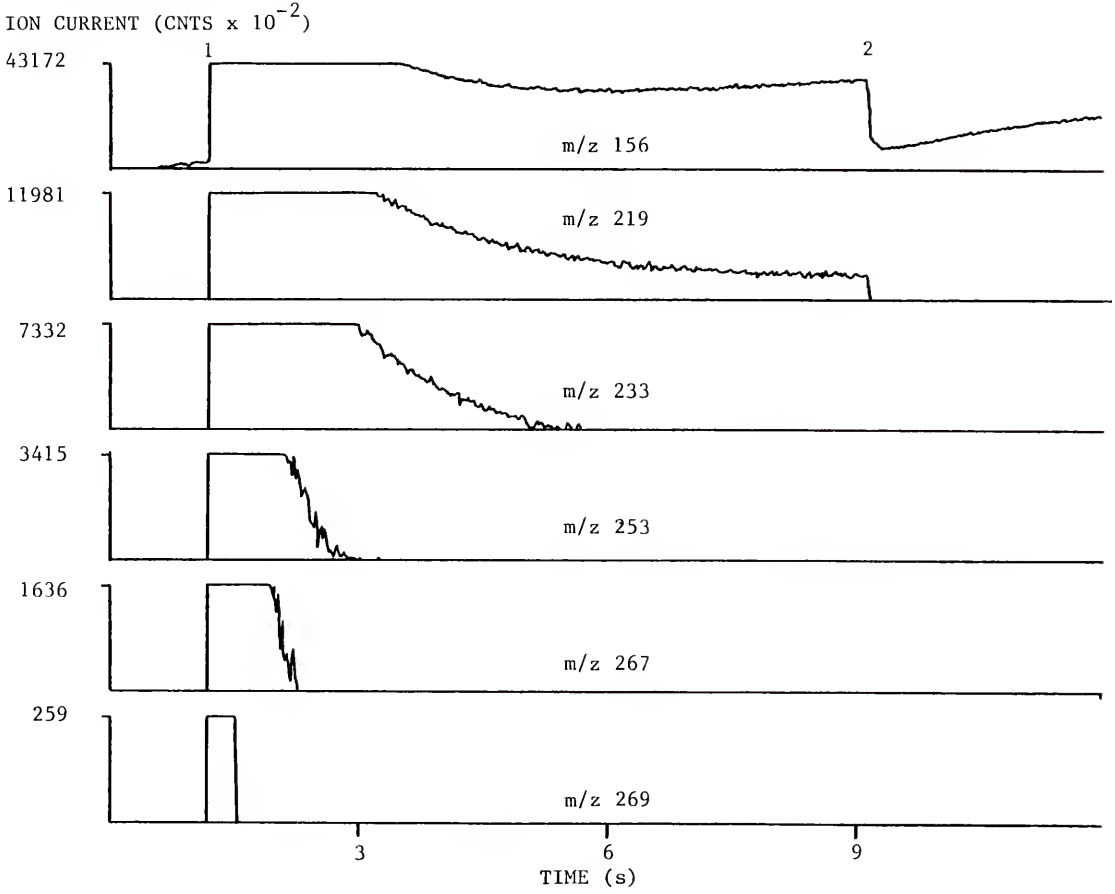
ION CURRENT (CNTS x 10^{-2})
43172
1
2
m/z 156
11981
m/z 219
7332
m/z 233
3415
m/z 253
1636
m/z 267
259
m/z 269
3
6
9
TIME (s)

0.90 torr of methane. The component having the lowest melting point (MPS, 76-77°C) began to vaporize before the laser was fired (1), and DCI resumed after the ion source was cleared by a second laser shot (2) at the same target site. This is an example of LEDCI. The signal for the second most volatile component, PB, terminated at the second laser shot, again due to a rapid clearing of the source by the input of additional energy, but did not resume because conditions were not conducive to DCI. None of the other components desorbed prior to the laser shot and they exhibited LIDCI signals having lifetimes and intensities which were dependent upon the melting point (heat of vaporization). This is a definite disadvantage and portends difficulties in use of LIDCI for quantitative analysis for two reasons. First, the versatility of the method will be limited because compounds having high melting points will give short-lived signals. Second, sensitivity will decrease with increasing melting point of the analyte resulting in selective detection of low melting species and discrimination against high melting species.

Quantitative Analysis and Application of LIDCI

In view of the above findings, numerous attempts were made to obtain analytical curves for mixtures of antiepileptic drugs using DCI and LIDCI. The LIDCI experiment in which reproducible ratios of PHT:PHT* were obtained (Figure 6.8, Table V) were very promising; however, this experiment was run with the TSQ in the normal Q3 mass mode. Since the forte of tandem mass spectrometry is the analysis of

mixtures without prior chromatographic separation, but with a mass separation followed by CAD and mass analysis of component fragments, calibration experiments were performed with the instrument operated as a true tandem mass spectrometer.

Lower Limit of Detection for DCI

The lower limit of detection was checked for hydergine by DCI from a nickel grid in a 160°C source pressurized with methane:nitrous oxide (1.00:0.11) at 1.11 torr to give a mixture of acidic ($C_2H_5^+$) and basic (OH^-) reagent ions (125). Figure 6.14 shows the RIC plots for the negative parent ions obtained in a selected reaction monitoring experiment with Q3 successively selecting m/z 195, 209, and 243, and Q1 passing each corresponding parent ion, m/z 294, 308, and 342, respectively. Ion current profiles for all three compounds were similar. Plot A shows the desorption envelope for 0.558 ng of hydergine, and plot B, for 5.42 ng. A blank run under the same conditions had a peak signal level of 294 counts, as compared with signal maxima of 1160 counts (3 times blank level) for the low standard and 4640 counts (15 times blank level) for the high standard. If the lower limit of detection is taken to be the amount of sample giving a signal 5 times the blank level, the limit of detection is 1.42 ng. A lower limit was not determined for LIDCI because of experimental difficulties in working with small sample weights in the present instrument system, however, the DCI limit gives an idea of the possible LIDCI limit for an optimized system. Another observation that can be made from this figure is that the signal life-time is dependent on

Figure 6.14

Plots of RIC vs. time for DCI/CAD of (A) 0.558 ng and (B) 5.42 ng of Hydergine on nickel grid showing dependence of signal lifetime on sample size. Negative parent ion experiment with selected reaction monitoring. See text for reactions.

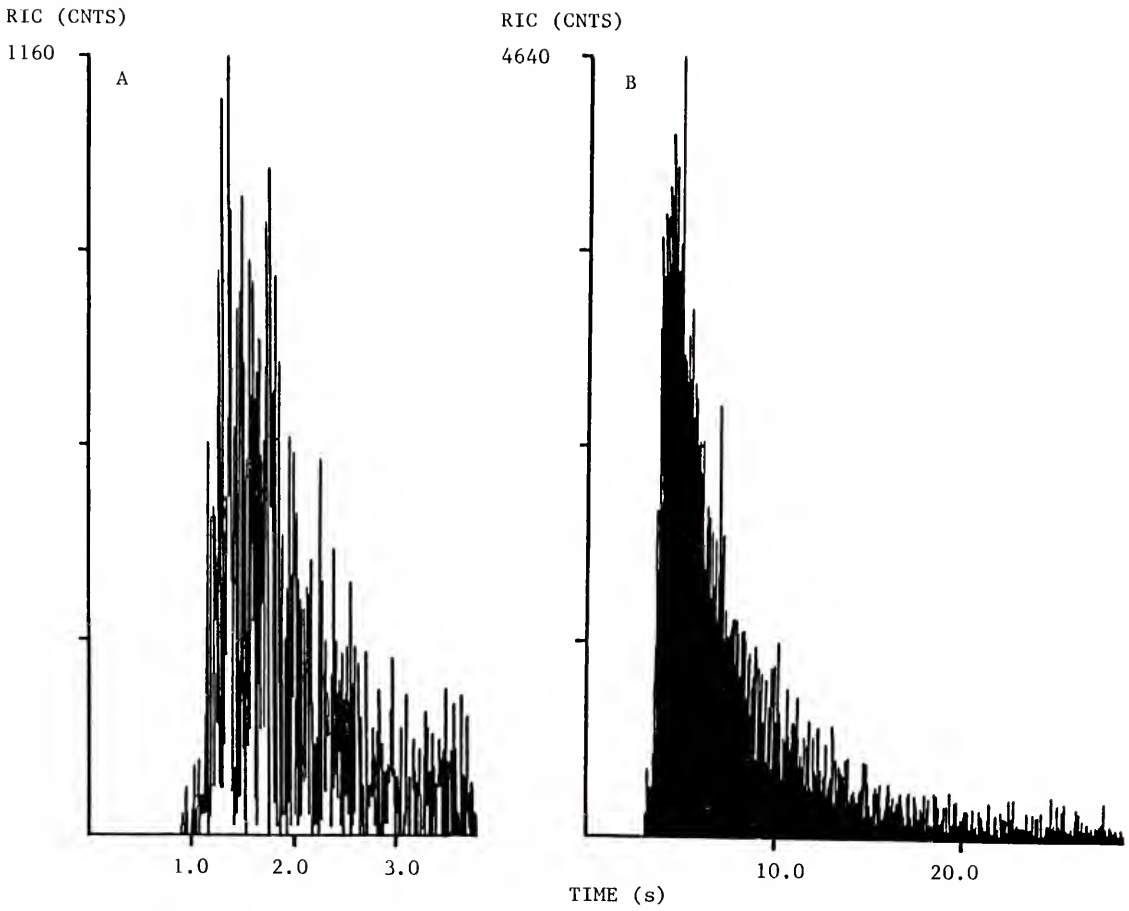
RIC (CNTS)
1160
A
1.0
2.0
3.0
RIC (CNTS)
4640
B
10.0
20.0
TIME (s)

sample size. Signals for the 0.558 ng sample and the 5.42 ng sample decayed to 25% of maximum in 1.4 s and 3.7 s, respectively. This could be a problem and must be considered if any further work is done in this area. When detection is time-limited, the signal lifetime must be independent of concentration if the optimum limit of detection is to be realized.

Calibration Curves for DCI and LIDCI

DCI calibration for graded melting point standard on nickel grids and Teflon paddle. These calibrations were done using a dilution of the graded melting point standard which provided standard solutions containing from 30 to 380 ng/μL of each analyte. Table VIII gives the make-up of the calibrant solutions. Figures 6.15 and 6.16, respectively, show the curves of analyte-to-internal standard response ratio (parent ion experiment, selected reaction monitoring according to Table VI) obtained for each drug upon DCI from a nickel grid and a Teflon paddle. Lines shown for 2-methyl-2-propylsuccinimide (MPS), and phenobarbital (PB) were calculated by using all but the highest calibrant. The line for mephenytoin (MES) was calculated using only the data for the three low calibrants. PHT gave the best curves with coefficients of determination (r^2) of 0.955 for nickel and 0.988 for Teflon (all calibrants included). The other three drugs showed a change in slope to negative values at high calibrant concentration. These results indicate the importance of choosing the correct internal standard for an analysis. The dependence of signal lifetime on sample concentration and signal intensity on sample heat of vaporization causes

Table VIII. Calibrant Solutions Made from Graded Melting Point Standard[a] for DCI/CAD from Nickel and Teflon Substrates[b]

Calibrant	µL Standard	µL Int. Std.[c]	µL Parlodion	µL methanol
1	0	5	20	100
2	1	5	20	99
3	2	5	20	98
4	4	5	20	96
5	7	5	20	93
6[d]	10	5	20	90

a) See Table VI.
b) See Figures 6.15 and 6.16.
c) All samples contain 0.269 µg/µL MPHT internal standard.
d) Concentrations are: MPS, 0.329 µg/µL; MES, 0.301 µg/µL; PB, 0.380 µg/µL; PHT, 0.356 µg/µL.

Figure 6.15

Plot of response ratio (analyte/internal standard) vs. amount of analyte on grid for DCI/CAD of 1 µL of graded melting point calibrant solutions (Table VIII) on nickel grids. Parent ion experiment with selected reaction monitoring (Table VI). Symbols: ● , MPS; ■ , PB; ▲ , PHT; ⬢ , MES; ✚ , MPS+PB+PHT (3 points overlap).

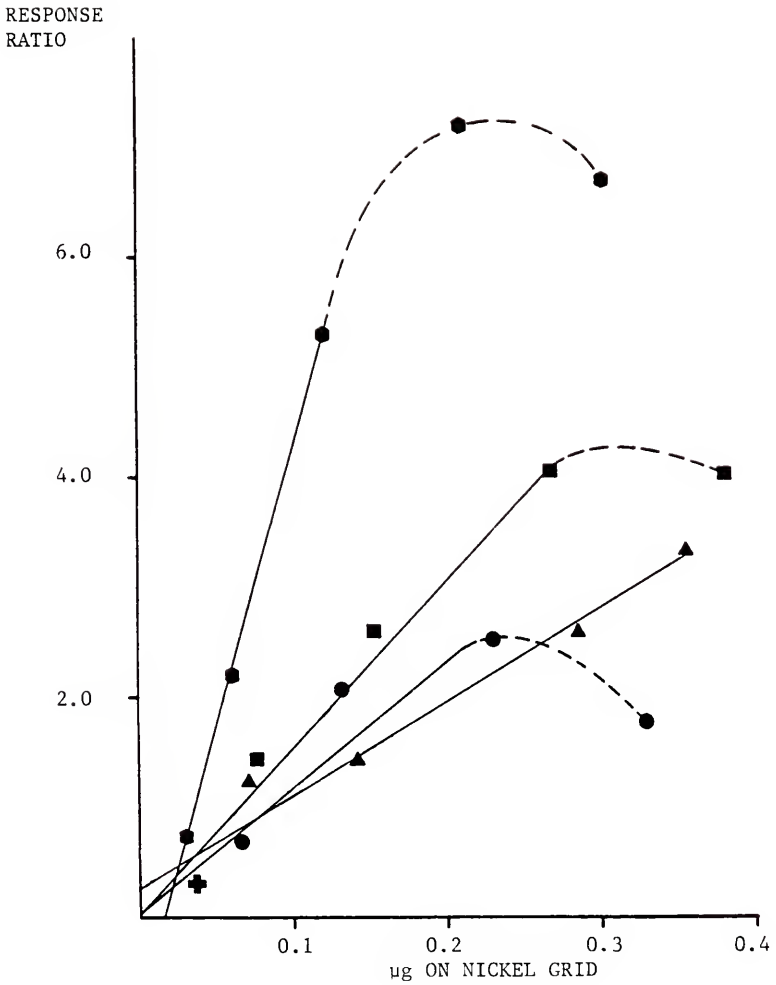
RESPONSE
RATIO
6.0
4.0
2.0
0.1
0.2
0.3
0.4
µg ON NICKEL GRID

Figure 6.16

Plot of response ratio (analyte/internal standard) vs. amount of analyte on grid for DCI/CAD of 1 μL of graded melting point calibrant solutions (Table VIII) on Teflon paddle. Parent ion experiment with selected reaction monitoring (Table VI). Symbols: ● , MPS; ■ , PB; ▲ , PHT: ⬢ , MES; ✚ , MPS+PB+PHT (3 points overlap).

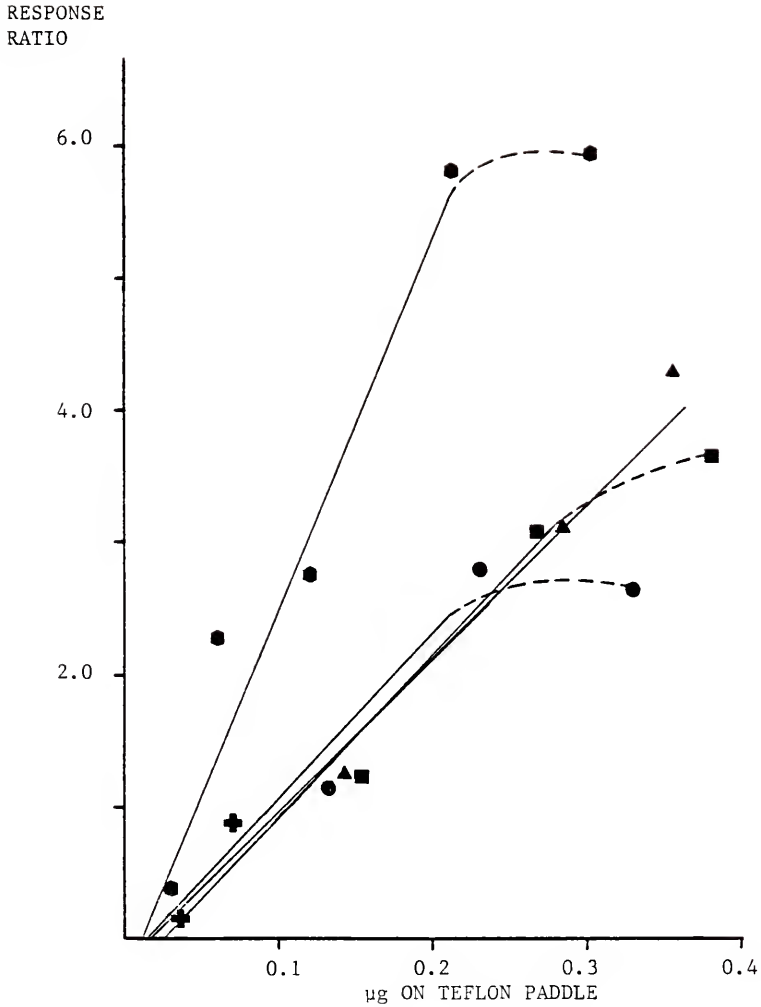
RESPONSE
RATIO
6.0
4.0
2.0
0.1
0.2
0.3
0.4
µg ON TEFLON PADDLE

the DCI technique to be less tolerant of differences between the analyte and internal standard than direct solids probe evaporation (glass probe vial) with rapid heating.

LIDCI calibration for PHT on nickel grid. The difficulty experienced in obtaining an adequate calibration for a multicomponent sample in DCI prompted the decision to try calibration for a single analyte by LIDCI. Table IX gives the contents of each calibrant for PHT with PHT* used as the internal standard. A 1 μL sample was spotted on each grid and 2-3 shots were made at different sites on a grid. Data were acquired in the parent ion mode with Q3 sequentially selecting m/z 182 (PHT) and m/z 183 (PHT*) and Q1 scanning from m/z 250 to 260 in 9 ms with a 2 ms delay between scans to detect the respective parent ions, m/z 253 and m/z 256. Figure 6.17 shows a plot of ratio of selected reaction response for PHT to that for PHT* vs. amount of PHT on the grid (line 1). Again, the coefficient of determination was low (r^2=0.910) indicating poor correlation between response ratios and weight of drug. Elimination of the high results and the high and low results for one of the calibrants which gave 3 widely spaced ratios (marked by *) left 10 results spanning the range from 0.098 μg to 1.37 μg PHT on a grid. The best straight line calculated for this group of points is line 2 in Figure 6.17. Table X gives the coefficients of determination for the three sets of calibrations (DCI-nickel, DCI-Teflon, LIDCI) and also the coefficients obtained after eliminating obviously deviant data points, which improved correlation significantly in almost all cases. The only data sets for which data did not have to be eliminated (no points

Table IX. Phenytoin (PHT) Calibrant Solutions for LIDCI from Nickel Grids.

Calibrant	µL PHT Standard[a]	µL PHT* Int. Std[b]	µL Parlodion	µl Methanol
1	0	100	10	100
2	5	100	10	95
3	10	100	10	90
4	20	100	10	80
5	40	100	10	60
6	70	100	10	30
7[c]	100	100	10	0

a) Concentrations phenytoin: 4.10 mg/mL.
b) Concentration 1,3-^{15}N-2-^{13}C-phenytoin: 4.90 mg/mL.
c) Maximum PHT concentration: 1.95 µg/µL.

Figure 6.17

Plot of response ratio (PHT/PHT*) vs. amount of PHT on nickel grid for LIDCI/CAD of PHT calibrant solutions (Table IX). Parent ion experiment with selected reaction monitoring of m/z 253 going to m/z 182 (PHT) and m/z 256 going to m/z 183 (PHT*). All points used for least squares calculation (1); Indicated points (*) excluded for least squares calculation (2).
Symbols: ● , single datum point; ✚ , two data points.

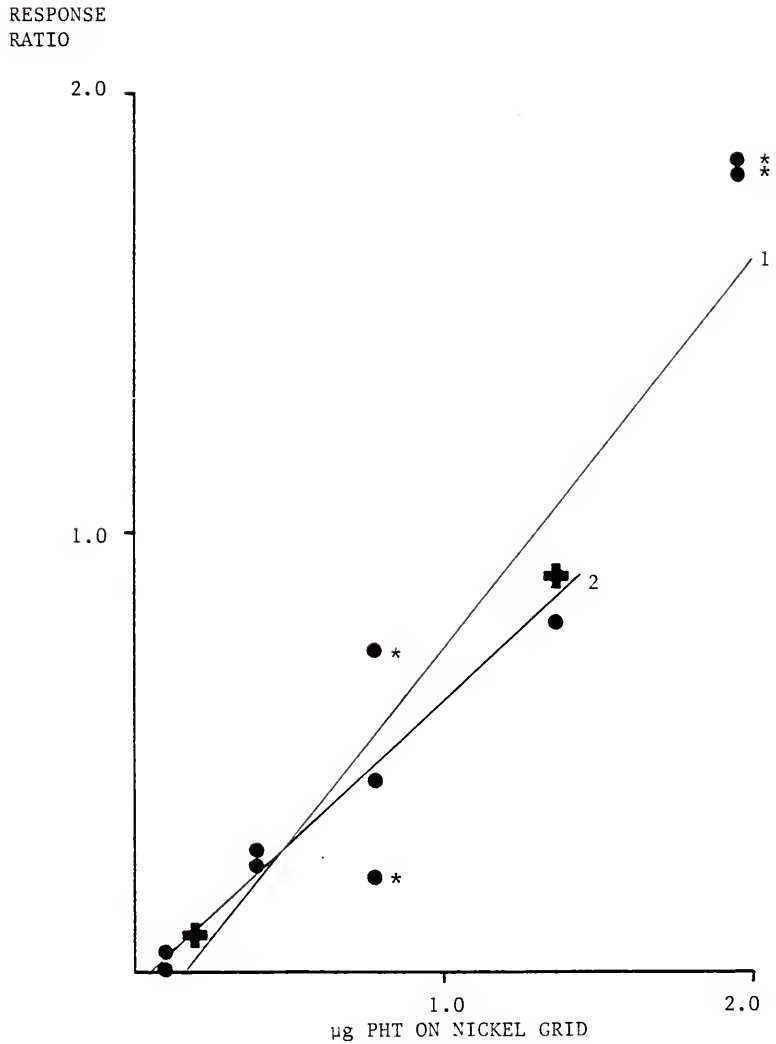
RESPONSE
RATIO
2.0
1.0
1
2
1.0
2.0
µg PHT ON NICKEL GRID

Table X. Coefficients of Determination (r^2) for DCI Calibration[a] with Nickel Grids and Teflon Paddle, and for LIDCI Calibration[b] with Nickel Grids (See Figures 6.15, 6.16, 6.17).

Data	MPS[c]	MESC	Pb[c]	PHT[c]
DCI-Ni-All	0.524	0.797	0.874	0.955
DCI-Ni-High Calibrant Omitted	0.909	0.952	0.978	-
DCI-Teflon-All	0.868	0.908	0.962	0.988
DCI-Teflon-high calibrant omitted	0.945	0.950	0.962	-
LIDCI-Ni-all	-	-	-	0.910
LIDCI-Ni-high calibrant and widely variant results (*) omitted				0.988

a) Concentrations in high calibrant: MPS, 0.329 μg/μL; MES, 0.301 μg/μL; PB, 0.380 μg/μL; PHT, 0.356 μg/μL; MPHT (int. std.), 0.269 μg/μL. Other calibrants contain 0.7, 0.4, 0.2, and 0.1 times high-calibrant concentration. Sample size: 1 μL.

b) Concentration in high calibrant: PHT, 1.95 μg/μL, PHT* (int. std.), 2.33 μg/μL. Other calibrants contain 0.7, 0.4, 0.2, 0.1, and 0.05 times high calibrant concentration. Sample size: 1 μL.

c) MPS (2-methyl-2-propylsuccinimide); MES (mephenytoin); PB (phenobarbital); PHT (phenytoin); PHT* (stable isotope label).

obviously out of line) were those for PHT DCI. Of these, the samples evaporated from Teflon gave the best results, indicating that the process which occurred in that case was more controlled, probably because of decreased or non-existent substrate effect. It is also probable that methylphenytoin is a more suitable internal standard for phenytoin than for the other analytes. The end result of these attempts at calibration is that the process, with this instrumentation, is too uncontrolled at this point to be used for quantitative analysis; however, it can be used for qualitative analysis.

Qualitative Analysis of Rat Brain by LIDCI

This experiment was performed to attempt to answer the question posed at the end of Chapter I. Again, that is:

> Although a molecule may be present in tissue, is it in a form that is recoverable by direct vaporization or is it incorporated into membranes, proteins and anatomical structures in such a way as to make it unrecognizable?

The procedure used to prepare samples for this part of the study was described at the end of Chapter III. Table XI gives the sample descriptions and phenytoin concentrations found in the frozen and fixed brain and liver samples taken from the rats that had been loaded with phenytoin (150 mg/kg). The total amounts of phenytoin found in the fixative solutions are also given. The two frozen liver samples (1 and 2) were homogenized by sonication. Since liver is relatively difficult to homogenize, it is possible that the concentration difference in these two samples is due to incomplete homogenization. There are also

Table XI. Phenytoin Concentrations in Rat Brain and Liver Samples and in Fixative Solutions

Sample	Description	Concentration
Brain (1)	frozen	47.4 µg/g
Brain (2)	frozen	46.6 µg/g
Brain (3)	Fixed 72 hr	25.7 µg/g
Liver (1)	frozen	211 µg/g
Liver (2)	frozen	130 µg/g
Liver (3)	fixed 72 hr	82.4 µg/g
fixative-Brain	(0.50 mL analyzed	2.66 µg/10 mL
fixative-Liver	out of 10 mL)	8.32 µg/10 mL

discrepancies between the concentrations in frozen and fixed brain and in frozen and fixed liver. The amount of phenytoin found in the fixative is not enough to account for the differences. The fixed samples, however, were homogenized in a ground glass grinder with a ground glass pestle, which is very efficient. Therefore, the reason for the differences between the frozen and fixed samples cannot be explained by the present data. Since the phenytoin deficits in the fixed tissues are unaccounted for, it is possible that the fixed tissues used for LIDCI MS may have concentrations as high as those in the frozen samples, or as low as those in BRAIN 3 and LIVER 3. Therefore, the brain sample used for LIDCI probably had a phenytoin concentration between 26 and 47 µg/g wet weight; the liver sample may have contained from 82 to 211 µg/g wet weight.

Sections of fixed brain and liver were trimmed to be about 0.5 mm thick and 2 mm square with a small tab on one corner. The TSQ was set up to acquire in daughter ion mode with Q1 passing m/z 253 and Q3 scanning from m/z 170 to 260 in 19 ms with a 1 ms delay between scans. Centroid sampling interval was set at 75 µs. Source pressure (methane) was 0.90 torr and the source temperature was 160°C. Collision energy was 18 eV and collision gas pressure (nitrogen) was 2.6 mtorr. Fresh rhodamine 6G dye was put into the laser and the driver voltage was set at 18 kV. Cavity diameter was 10 mm. Figure 6.18 shows the ion current profiles for the major PHT ions (parent and daughter) which resulted from a single laser shot fired at the liver section. The hole produced

Figure 6.18

Plots of ion current vs. time for parent ion, major daughter ions and ion recorded at laser firing for LIDCI/CAD of rat liver tissue section taken from animal loaded with 150 mg/kg of phenytoin. Daughter ion experiment: Q1 passing m/z 253; Q3 scanning from m/z 170 to 260 in 19 ms.

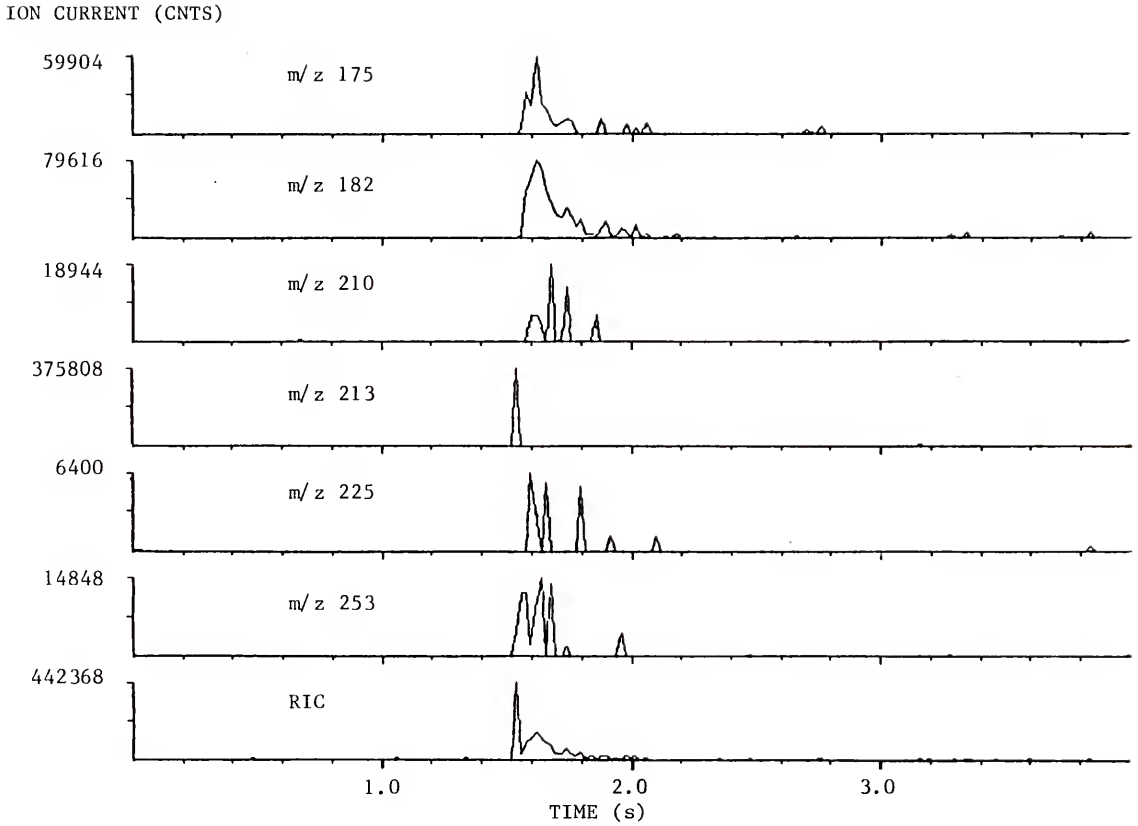
ION CURRENT (CNTS)
59904
m/z 175
79616
m/z 182
18944
m/z 210
375808
m/z 213
6400
m/z 225
14848
m/z 253
442368
RIC
1.0
2.0
3.0
TIME (s)

in the tissue sample was about 0.7 mm in diameter (2×10^{-4} cm^3 vaporized.). The large spike at m/z 213 is from the laser firing. Several other shots at different sites on the tissue produced ions representative of PHT, but this one gave the best profile. PHT was not detected in the brain sample. Figure 6.19 shows spectra from the liver sample (12 scans after the laser shot summed), and from a sample of pure PHT placed on a grid and vaporized with the laser immediately after the tissue samples were run.

These results, although inconclusive because they were not repeated, are promising in that PHT, introduced into a sample in vivo, was detected by direct vaporization of the tissue in the ion source. It is also possible that there is "free" PHT which is accessible and "bound" PHT which is not. There is some hope that, if a microprobe tandem mass spectrometer can be developed by overcoming the time limitations of the present system, it will be possible to detect molecular species directly in intact tissue samples.

Figure 6.19

Daughter spectra of m/z 253 from summation of 12 scans after laser shot for (A) rat liver tissue section from Figure 6.18, and sample of pure PHT on nickel grid. Pure sample analyzed after liver sample.

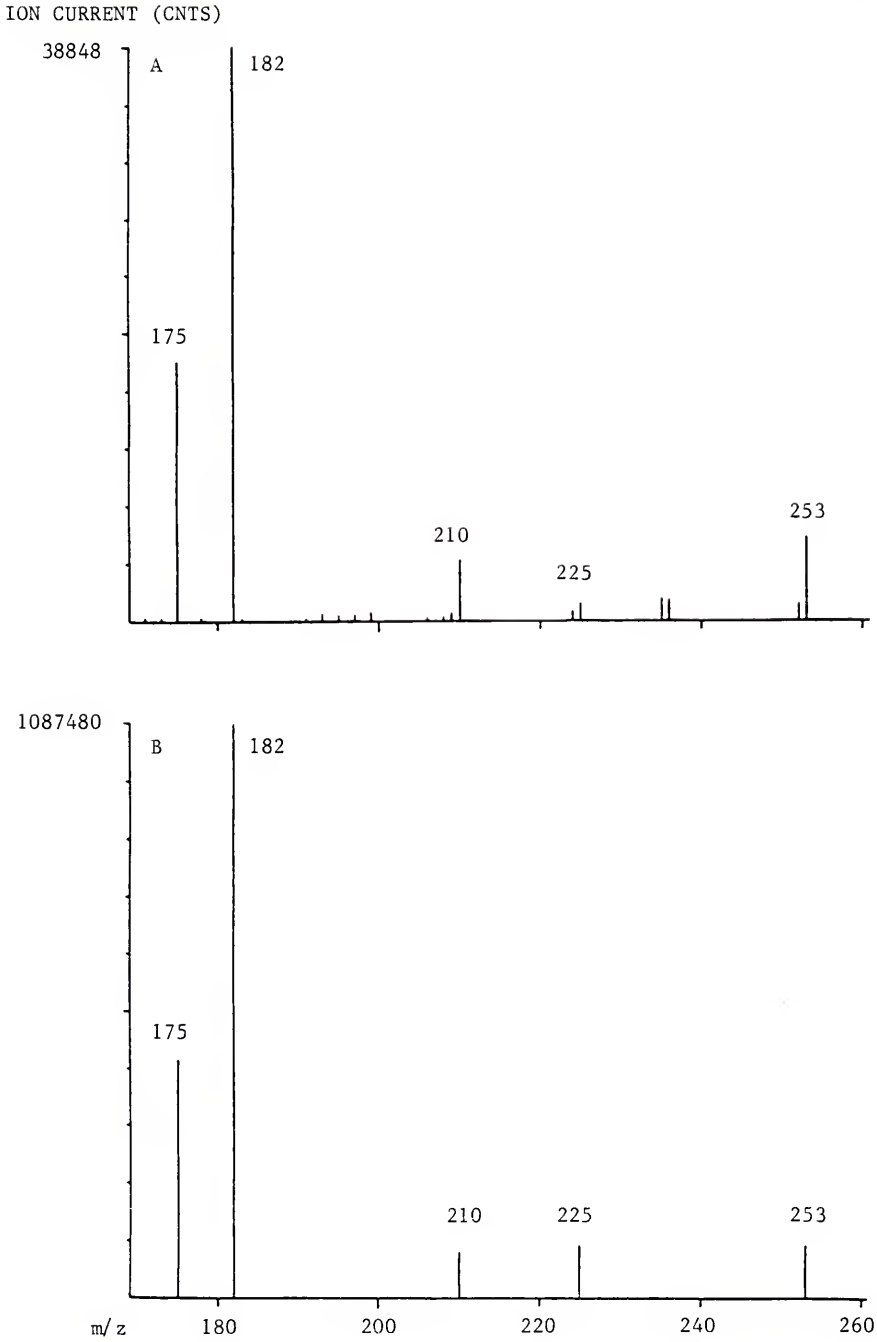
ION CURRENT (CNTS)
38848
A
182
175
210
225
253
1087480
B
182
175
210
225
253
m/z
180
200
220
240
260

CHAPTER VII

CONCLUSIONS AND FUTURE WORK

The original purpose of this work was to introduce the concept of using tandem mass spectrometry as a means of obtaining the selectivity required for molecular analysis under probe-type sampling conditions. To achieve this end, a single-shot laser was interfaced to a triple quadrupole mass spectrometer, and the system was evaluated with respect to short-lived and long-lived processes which were induced by the incidence of the laser radiation on molecular samples. This chapter is a summary of the conclusions based upon this work, and a prospective view of future research which may contribute to the development of a microprobe capable of providing a molecular image of intact, heterogeneous and compartmentalized samples.

Conclusions Based on the Present Work

Direct Analysis of Mixtures by MS/MS

Initially, tandem mass spectrometry, implemented with a triple quadrupole analyzer, was shown to be a valid technique for quantitation of drugs in small sections of rat brain. The internal standard technique was used and crude extracts were vaporized into the ion source from a rapidly heated solids probe while the molecular ions of interest

were selected with Q1, fragmented in Q2, and the corresponding daughter ions were observed after selection by Q3 (selected reaction monitoring). The same samples, analyzed with the mass spectrometer operating in the normal mass spectrum mode, gave little or no evidence of the presence of the analytes or internal standards. In addition, the chemical background was intense with significant signal at all masses in the range of interest. This condition was similar to that obtained with a currently available laser mass spectrometer microprobe (LAMMA 500), which proved unsuitable for detection of cobalt in sections of a cobalt-induced lesion in rat brain. These studies pointed out the deficiency of the single stage mass analyzer in direct analysis of mixtures, both in the bulk analysis and in the microprobe modes, and showed the advantage that could be gained by introduction of a second stage of mass analysis.

Laser Studies

Short-lived processes. Although the triple quadrupole mass spectrometer is not specifically designed for monitoring brief signals, a system having limited mass resolution for ions generated by the laser was developed in which the ion of interest was selected by Q1, and Q3 was configured to allow a range of masses to pass simultaneously. In this way, a time-dependent signal of the selected ion intensity was produced. Time resolution was limited to 25 μs by the ADC rate. All signals monitored in this mode had lifetimes of less than 1 ms. Mass filtering was not totally efficient (i.e., less than unit mass resolution), and some signal was observed if a mass close to that of an ion present in the source were selected by Q1. If Q1 and Q3 were configured to pass

ions widely separated in mass, a minimal signal, which was always present when the data system was used, was obtained. This signal was due to electrical interference which resulted from discharge of the storage capacitor used to fire the laser flashlamp. When the storage oscilloscope, triggered by the output of a fast photodiode which received a portion of the laser light, was used to monitor the signal directly from the electron multiplier under the same conditions, a baseline signal was obtained. This indicated that the storage scope was less sensitive to electrical interference than the data system, and that the interference was probably due to an antenna effect of the mass spectrometer cables. When both quadrupoles were operated in RF-only mode (passing all ions having masses greater than 7/9 of the selected mass), a two partially resolved peaks were obtained when a sample containing two compounds differing in mass by about 500 u was vaporized by the laser. From this time-of-flight experiment, an instrumental constant of 9.77 $\mu s\ u^{-1/2}$ was calculated. The intercept of the time vs. square root of mass curve for these two data points indicated a delay of 127 μs between the time the ions were formed, ideally at the time the laser was fired, and the first detection of a signal above threshold. This set of experiments gave some information about how the quadrupoles functioned as filters for laser generated ions. The available mass and time resolution of the instrument was insufficient to allow positive identification of ions detected, or to allow operation of the instrument as a true tandem mass spectrometer. Experiments with reagent gas

present in the ion source indicated that long-lived signals could be obtained, which would allow more effective use of the mass selection capabilities of the TSQ.

Long-lived processes. When reagent gas was present in a closed chemical ionization source, ion signals which lasted for hundreds of milliseconds to several seconds could be obtained for a number of compounds (Appendix). Initially, it appeared that these signals were initiated by the laser and that their longevity was due to conditions in the source which prolonged the lifetime of the ions vaporized by the laser. Subsequent experiments showed that the signal was actually a convolution of two signals; one the result of ions produced by chemical ionization of the laser produced molecules, and the second longer lasting signal the result of desorption chemical ionization (DCI) of sample vaporized by the action of reagent gas molecules on the sample surface. Use of the laser as a means of introducing thermal energy into the sample initiated these processes when conditions unfavorable to DCI existed (when the sample was blocked from direct contact with reagent gas entering the source) to give a phenomenon called Laser-Induced Desorption Chemical Ionization (LIDCI). If conditions were favorable for DCI, the laser was used to enhance the signal in a process called Laser-Enhanced Desorption Chemical Ionization (LEDCI). Compounds that could be vaporized from the solids probe by normal resistive heating could be vaporized without the addition of probe heat, but with the heat provided only by the ion source. In one case, a compound that could not be vaporized from a glass probe vial gave a signal under DCI conditions. The DCI signal was influenced by sample substrate, and exhibited

threshold pressure and temperature requirements. Threshold levels of ion source pressure and temperature were also required for production of laser-initiated signals; and signal lifetime was dependent on compound melting point and sample size.

Analytical application of laser-initiated processes. The dependence of the laser-initiated processes on compound melting point and sample concentration limits the analytical potential of these techniques. Although limits of detection for DCI of a higher molecular weight alkaloid were in the very low nanogram range, attempts at calibration with a mixture of commonly used antiepileptic drugs were relatively unsuccessful, and gave low coefficients of determination (r^2). For 3 out of 4 of the compounds studied, suppression of the signal at the highest concentration was observed. The compound that did not show this effect was the most similar to the internal standard. When identical samples containing a mixture of phenytoin (PHT) and a stable isotope-labeled analog (PHT*) were subjected to LIDCI with the instrument operated in the normal mass spectrum mode, ion response ratios for the protonated molecular ions were reproducible with a relative standard deviation of 5%. When samples having equal weights of PHT* (internal standard) and weights of PHT varying from 0.098 μg to 1.95 μg were subjected to LIDCI (selected reaction monitoring), most analyte/internal standard response ratios showed a linear increase with concentration. Elimination of 4 outlying points out of 14 points gave a reasonable coefficient of determination of 0.988. These results indicate that, with proper internal standardization (126, 127), it may be possible to use this technique for quantitation. Practical lower

limits of quantitation are high, however, compared to results obtained by more conventional methods (128). In addition, versatility is limited because of the dependence of signal lifetime on analyte melting point (heat of vaporization). This will introduce an undesired selectivity because mixtures containing components having a range of vaporization temperatures will exhibit signals favoring the components having the lower heats of vaporization.

Detection of phenytoin in rat liver. The most promising result obtained in this study was the detection of phenytoin, which was introduced in vivo, in a section of rat liver by direct laser vaporization of the tissue inside the CI ion source. The protonated molecular ion was selected in Q1, fragmented in Q2, and daughter ions were detected for about 400 ms after the laser shot by scanning Q3 over a 90 unit mass range. The spectrum obtained in this way from the liver sample matched that of a sample of pure phenytoin vaporized under the same conditions. This result indicates that molecular species can be recognized by direct vaporization from tissue, and that their identity may not be obscured by binding to macromolecules and tissue membranes. This is not so important when elemental analysis is performed by a microprobe method because the elements will be recognizable by their isotopic patterns even if all surrounding tissue is destroyed. A primary concern, however, at the start of this project, was that the lack of a working microprobe for molecular analysis many years after the development of ion microprobes and microscopes was due to the difficulties of in situ detection of molecules after they had been incorporated into biological systems. This result gives hope that

molecular analysis by direct vaporization of tissue is possible, and gives, in this preliminary stage of investigation, a positive answer to the question posed at the end of Chapter I.

Previous work with laser desorption and laser ablation MS, which has been cited earlier in this report, indicated that auxiliary ionization techniques coupled with laser sampling could give extended lifetimes to ion signals. The current work has extended the lifetimes of laser-initiated signals from a few milliseconds to several seconds for a single 1 to 2 μs laser pulse. This prolonging of signal is important because of the statistical nature of the detection process. To produce an analytically useful response, several conditions must be satisfied. These include: (1) the sampling and response times of the detection system must be significantly shorter than the potential lifetime of the signal; (2) the potential lifetime of the signal must not be dependent upon analyte concentration; (3) the mechanism of signal generation must not discriminate between analyte response and internal standard response; and (4) analyte and internal standard responses must be distinguishable within the constraints of signal lifetime and detector response time. In addition, several conditions should be inherent in the design of a versatile molecular microprobe, including: (1) it should be possible to maintain the sample at or below room temperature to maintain the integrity of fragile samples such as biological tissues; (2) the system should be capable of generating ions from molecules that are normally amenable to MS and also

those that are thermally unstable or nonvolatile; and (3) the system should be able to take advantage of processes such as cationization and anionization.

The present system, while showing that combination of a spatially controllable desorption ionization technique (laser) with tandem mass spectrometry may be a valid approach to building a molecular microscope, lacks the versatility that would be demanded of such an instrument. The triple quadrupole mass spectrometer is not fast enough to adequately characterize molecules ionized by cationization or anionization after desorption by a single shot laser. The laser-induced desorption CI process, demonstrated on this instrument, does not satisfy the need for a vaporization/ionization technique applicable to a wide variety of molecules (polar, nonvolatile, thermally unstable). Lastly, the discrimination among molecules according to heat of vaporization, as evidenced by widely different sensitivities for compounds having different melting points, makes quantitation difficult, and places more stringent requirements on internal standard selection. A fast-pulsed laser system could have contributed greatly to the characterization of the present instrument system and the processes observed by allowing continuous monitoring of ion signals while instrumental and sample conditions were varied.

Future Work

Proposed Instrument Designs

The primary considerations at this time are the choices of sampling device and mass analyzer. Although this report has dealt with the laser as a sampling device, an ion beam should also be considered. The mass analyzer or combination of analyzers must provide mass selection, secondary fragmentation, and mass analysis of the resulting fragments, within the lifetimes of the primary molecular ions desorbed or vaporized from the sample. This system must have a high transmission, and the ion source and fragmentation stage must be very efficient to optimize detection limits.

Sampling devices. Both laser (34) and ion beams (18) have been used with success for sampling on a microscopic scale for elemental analysis. As has been mentioned previously, speculative comments have been made during the past 5 years (47-51) concerning an instrument for molecular microscopy. More recently, mass spectrometric systems have been described which are capable of molecular imaging. Stoll et al. (129) have recently described an instrument, based on SIMS (secondary ion mass spectrometry), with a high resolution, double-focusing mass spectrometer. The primary cesium ion beam was focused to a 0.3 μm diameter spot with a current density of 1 A cm^{-2} and a power density of 10^4 W cm^{-2}. Molecular maps of a low mass (m/z 131) and a high mass (m/z 1281) ion were produced from a perfluoropolyether, deposited on a 500 mesh EM grid. This instrument provided more selectivity for molecular analysis than one having nominal mass resolution; however, an instrument

having a second, confirmatory stage of fragmentation and mass analysis is more desirable. Kelner et al. (130) have recently introduced a system which they call a "molecular microprobe". They considered all of the requirements listed above, and designed an instrument, based on SIMS, which incorporates a high transmission, triple quadrupole analyzer. The system had not been tested at the time of the report.

Sampling with a primary ion beam has several advantages, including: (1) fineness of focus (20 nm for a cesium ion gun); (2) ease of beam translation by electronic rastering under computer control; and (3) accurate control over and measurement of beam current and primary ion kinetic energy. Sensitivity and signal lifetime, however, are highly dependent upon the sample matrix (50). Since a microprobe is primarily designed to detect species in their natural state, this is a definite disadvantage. In fact, much of the success of molecular SIMS is due to pretreatment of the sample, or dispersing it in a nonvolatile liquid matrix, to form polar or pre-ionized species, and to provide a continuously renewable surface (131, 132). The liquid matrix also allows use of a high current density primary ion beam, which increases sensitivity. The wide-ranging molecular reordering which occurs through collision cascades resulting from primary particle impact, limits the beam current that can be used on static surfaces (133). Another disadvantage of basing a microprobe system on SIMS is the small sampling depth (molecular monolayer). This factor limits sensitivity, increases analysis time, and limits the versatility of the technique, particularly with biological samples. In this case, an instrument with an instantaneous sampling depth of at least 0.5 μm, and capability for

penetration to 0.5 mm would be more desirable, since cell dimensions usually span tens of micrometers.

The primary disadvantages of the laser as a sampling device are its expense, lack of reproducibility of beam characteristics (energy/pulse), and poor functional reliability. These drawbacks, however, are diminishing with advances in laser technology (134). The advantage of the laser lies in its capability of sampling at depths which are more reasonable for biological systems. In addition, the sampling depth can be determined by the power density of the laser emission at the sample surface. The power density also determines the extent of fragmentation of molecular ions or ion adducts (32, 135). Therefore, this parameter can be adjusted for optimum sensitivity (lower power density produces only molecular ions) or for maximum structural information (higher power density produces fragmentation). Actually, since the cost of the sampling device would be a relatively small fraction of the total cost of an instrument having the proposed capabilities, and since laser and ion beam sampling are complementary, it would be most reasonable to incorporate both sampling systems.

Mass analyzers. At this time, multi-stage mass spectrometry has seemingly been performed with every available type and combination of mass analyzer. From the original magnetic-electric sector (B-E) reversed geometry MS/MS instrument (136), progress has seen the introduction of triple quadrupole (QQQ) (54), multiple sector (137, 138), and hybrid multiple sector-multiple quadrupole instruments (139). In addition, MS/MS experiments have been performed on Fourier transform (FT) mass spectrometers (56, 140), and by monitoring ion flight times

through a magnetic sector after CAD (141, 142). Recently, Glish and Goeringer (143) have described a tandem quadrupole time-of-flight (Q-TOF) instrument, which could be operated as a Q-TOF, or as a TOF-TOF MS/MS. It may be a design similar to this that provides the key to linking desorption ionization with tandem mass spectrometry to produce a workable molecular microprobe.

The dependence of signal lifetime upon sample size and heat of vaporization seriously limits the applicability of the long-lived LIDCI and LEDCI processes to the development of a molecular microprobe. Therefore, the performance of the triple quadrupole mass spectrometer in this application is also limited, because the required scan time is still too long to take advantage of true laser desorption processes. These processes produce intense, brief pulses of ions and neutral molecules having energy spreads from tens of electron volts, initially, to a fraction of an electron volt after several microseconds (83). Decay of the energy spread is beneficial because increased resolution can be obtained in a TOF mass spectrometer by delaying the ion acceleration pulse (77). Sensitivity, however, is decreased because the particle abundance is also decreasing rapidly. Therefore, to take full analytical advantage of the ions and neutral molecules generated by the laser pulse, the first stage of the instrument should be an ion source and storage device, in which laser-desorbed ions and ions created from neutral molecules could be contained. This storage device could be an ion cyclotron resonance (ICR) cell, such as is used in FTMS. Laser desorption has been used successfully with FTMS (104,144). The only drawback to such a system is the need for a high field magnet, which

surrounds the ICR cell. This would complicate and perhaps preclude the design of the specimen viewing system for the microprobe. One possible solution to this problem might be to use a quadrupole to inject the ions into the ICR cell (145); however, this does not accomplish the initial goal of fully using both ions and neutrals desorbed by a laser. A 3-dimensional quadrupole ion trap (146, 147) could provide an alternative solution, although the mass range of current designs is limited to about 650 u. The sample could be located within or outside of the trap, which would be operated in the total storage mode. Neutrals could be ionized by electron impact. After a variable delay, a high voltage ion drawout pulse could sample the contents of the source-trap, accelerating the ions through a short field-free region into a deceleration region, and, finally, into a Q-TOF system. After the TOF analysis of daughter ions from the selected ion, the source could be pulsed again, and the same or a different parent ion could be selected. The system could be operated as a single stage TOF, as a Q-TOF, or as a TOF-TOF mass spectrometer, as described by Glish and Goeringer (143).

It is clear from the literature that a number of investigators are now convinced that it is possible to construct an instrument having the capabilities described in this work. There is even a hint that the instrument will combine desorption ionization and tandem mass spectrometry (148). At this point, it may only require the correct combination of technologies that currently exist.

APPENDIX

CHARACTERISTICS OF DIRECT PROBE CHEMICAL IONIZATION (PCI), DESORPTION CHEMICAL IONIZATION (DCI), AND LASER-INDUCED DESORPTION CHEMICAL IONIZATION (LIDCI) BEHAVIOR OF TEST COMPOUNDS

Compound	Mol Wt[a]	PCI[b] (Temp)[c]	DCI[b]	LIDCI[b]	LIDCI Decay Time (s)[d]	Major Ions[e]
acetazolamide	222	N (132)	N	N	0.465	223
adenosine	267	N (320)	N	N	4.05	268
4-aminobutyric acid	103	N (230)	N	N	18.8	104
carbamazepine	252	N (170)	N	N	0.403	253
chlordiazepoxide	299, 301[f]	N (250)	N	N	2.85	300, 302[f]
cytidine	243	N (320)	N	N	0.440	244
folic acid[g]	441	-	-	-	-	-
glutamic acid	147	N (308)	N	N	2.21	148
glutamine	146	M (315)	N	N	0.310	147
homocysteine	135	N (230)	N	N	18.5	136
hydergine mesylate	-	ND (300)	ND	ND	0.232	-
(dihydroergocornine)	564					295[h]
(dihydroergocristine)	612					343[h]
(dihydroergocryptine)	578					309[h]
menthol glucuronide	332	ND (208)	ND	ND	3.10	139[i], 159[j], 177[k]
methylumbelliferyl glucuronide	352	ND (267)	ND	ND	71.4	159[j], 177[l]
p-nitrophenol glucuronide	315	ND (210)	ND	ND	4.03	140[m], 159[j], 177[k]
phenytoin acid	252	N (320)	N	N	1.18	153
phenytoin, sodium salt	252	-	N	-	-	253
pyridoxal	167	N (240)	N	N	17.0	168
reserpine	608	M (360)	N	N	0.754	609

Compound	Mol Wt[a]	PCI[b] (Temp)[c]	DCI[b]	LIDCI[b]	LIDCI Decay Time (s) [d]	Major Ions[e]
spermine	202	M (317)	N	N	22.4	203
sucrose	342	ND (311)	ND	ND	0.166	127, 145, 163[n]
Tetrabutylammonium perchlorate	242	ND (366)	ND	N	10.5	184, 185, 186, 242

a) Molecular weight of free acid or base of salts (g/mol).
b) N = normal spectrum of reasonable intensity with $(M=1)^+$ and typical adducts, $(M+41)^+$. RIC during direct probe evaporation had Gaussian or near-Gaussian profile. M = marginal spectrum with some $(M+H)^+$ but without typical adducts or reasonable intensity. RIC profile during direct probew evaporation was irregular, discontinuous, or skewed. ND = decomposition spectrum with no $(M+H)^+$ but with representative fragments of reasonable intensity, typical adducts, and Gaussian RIC profile during direct probe evaporation.
c) Probe temperature at first increase of ion current for RCI.
d) Time for signal to drop to 10% of peak (measured at scan after laser spike).
e) Present in all spectra.
f) ^{35}Cl, ^{37}Cl.
g) No signal under test conditions.
h) $(M + H - 270)^+$.
i) $(M + H -$ glucuronic acid$)^+$.
j) $(\text{Glucuronic acid} - 2H_2O)^+$.
k) $(\text{Glucuronic acid} - H_2O)^+$.
l) Methylumbelliferone + $H)^+$ with $(\text{glucuronic acid} - H_2O)^+$.
m) $(p\text{-Nitrophenol} + H)^+$.
n) $(M + H - 180 - 2H_2O)^+$; glucose, fructose (mol wt 180).
o) Tetrabutylammonium ion.

LITERATURE CITED

1. Rochow, T.G.; Rochow, E.G. "An Introduction to Microscopy by Means of Light, Electrons, X-Rays or Ultrasound"; Plenum Press: New York, 1978.

2. Siegel, B.M.; Beaman, D.R. "Physical Aspects of Electron Microscopy and Microbeam Analysis"; John Wiley and Sons, Inc.: New York, 1975.

3. Kelley, J.S.; Simmonds, M.A.; Straughan, D.W. In "Methods in Brain Research"; Bradley, P.B., Ed.; John Wiley and Sons, Inc.: London, 1975. Chapter 7.

4. Berman, H.J.; Hebert, N.C., Eds.; "Ion Selective Microelectrodes"; Adv. Exp. Med. Biol. 50; Plenum Press: New York, 1974.

5. Adams, R.N. Anal. Chem (1976) 48, 1126A-1137A.

6. Costa, E.; Iversen, L.L.; Paoletti, R., Eds.; "Studies of Neurotransmitters at the Synaptic Level"; Adv. Biochem. Psychopharm. 6; Raven Press: New York, 1972.

7. Nairn, R.C., Ed.; "Fluorescent Protein Tracing", 4th ed.; Churchill Livingstone: Edinburgh, 1976.

8. Lojda, Z.; Gossran, R.; Schiebler, T.H. "Enzyme Histochemistry - A Laboratory Manual"; Springer-Verlag: Berlin, 1979.

9. Bullock, G.R.; Petrusz, P., Eds.; "Techniques in Immunohistochemistry"; Academic Press: London, 1982 (Vol. 1), 1983 (Vol. 2).

10. Meek, G.A.; Elder, H.Y., Eds.; "Analytical and Quantitative Methods in Microscopy"; Cambridge University Press: Cambridge, 1977.

11. Williams, M.A. "Autoradiography and Immunocytochemistry"; North-Holland Publishing Co.: Amsterdam, 1977.

12. Cuello, A.C., Ed.; "Brain Microdissection Techniques"; John Wiley and Sons, Inc.: New York, 1983.

13. Otsuka, M.; Miyata, Y. In "Studies of Neurotransmitters at the Synaptic Level"; Costa, E.; Iversen, L.L.; Paoletti, R., Eds.; Adv. Biochem Psychopharm. 6; Raven Press: New York, 1972. Pp. 61-74.

14. Lowry, O.H.; Passoneau, J.V. "A Flexible System of Enzymatic Analysis"; Academic Press: New York, 1972.

15. Birks, L.S. "Electron Probe Micronanalysis"; Interscience Publishers: New York, 1963.

16. Evans, C.A. Anal. Chem. (1975) 47, 818A-829A.

17. Evans, C.A. Anal. Chem. (1975) 47, 855A-866A.

18. Morrison, G.H.; Slodzian, G. Anal. Chem. (1975) 47, 932A-943A.

19. O'Shea, D.C.; Callen, W.R.; Rhodes, W.T. "Introduction to Lasers and Their Applications"; Addison Wesley Publishing Co.: Menlo Park, 1978.

20. Brech, F.; Cross, L. Appl. Spectrosc. (1962) 16, 59.

21. Honig, R.E.; Woolston, J.R. Appl. Phys. Lett. (1963) 2, 138-139.

22. Harding-Barlow, I.; Snetsinger, K.G.; Keil, K. In "Microprobe Analysis"; Anderson, C.A., Ed.; John Wiley and Sons, Inc.: New York, 1973. Pp. 423-455.

23. Harding-Barlow, I. Laser Appl. Med. Biol. (1974) 2, 133-149.

24. Laqua, K. In "Analytical Laser Spectroscopy"; Omenetto, N., Ed.; John Wiley and Sons, Inc.: New York, 1979. Pp. 47-118.

25. Dhamelincourt, P.; Wallert, F.; Leclerg, M.; N'Guyen, A.T.; Landon, D.O. Anal. Chem. (1979) 51, 414A-421A.

26. Delhaye, M.; Bridoux, M.; Dhamelincourt, P.; Barbillat, J.; DaSilva, E.; Roussel, B. Microbeam Anal. (1982) 17, 275-278.

27. Kwong, H.S.; Measures, R.M. Anal. Chem. (1979) 51, 428-432.

28. Conzemius, R.J.; Capellan, J.M. Int. J. Mass Spectrom. Ion Phys. (1980) 34, 197-271.

29. Conzemius, R.J.; Simons, D.S.; Shankai, Z.; Byrd, G.D. In "Microbeam Analysis--1983"; Gooley, R., Ed.; San Francisco Press: San Francisco, 1983. Pp. 301-328.

30. Hillenkamp, F.; Unsold, E.; Kaufmann, R.; Nitsche, R. Nature (1975) 256, 119-120.

31. Vogt, H.; Heinen, H.J.; Meier, S.; Wechsung, R. Fresenius' Z. Anal. Chem. (1981) 308, 195-200.

32. Denoyer, R.J.; VanGrieken, R.; Adams, F.; Natusch, D.F.S. Anal. Chem (1982) 54, 26A-41A.

33. Hercules, D.M.; Day, R.J.; Balasanmugam, K.; Dang, T.A.; Li, C.P. Anal. Chem (1982) 54, 280A-305A.

34. Sessions of LAMMA Symposium, Dusseldorf, West Germany, October 8-10, 1980. Fresenius' Z. Anal. Chem. (1981) 308, 193-320.

35. Schiller, C.; Kupka, K.D.; Hillenkamp, F. Fresenius' Z. Anal. Chem. (1981) 308, 304-308.

36. Muller, J.F.; Berthe, C.; Magar, J.M. Fresenius' Z. Anal. Chem. (1981) 308, 312-320.

37. Kupka, K.D.; Schropp, W.W.; Schiller, C.; Hillenkamp, F. Fresenius' Z. Anal. Chem (1981) 308, 229-233.

38. Hirche, H.; Heinrichs, J.; Schaefer, H.E.; Schramm, M. Fresenius' Z. Anal. Chem. (1981) 308, 224-228.

39. Mathey, A. Fresenius' Z. Anal. Chem. (1981) 308, 249-252.

40. Schroder, W.H. Fresenius' Z. Anal. Chem. (1981) 308, 202-217.

41. Seydel, U.; Lindner, B. Fresenius' Z. Anal. Chem. (1981) 308, 253-257.

42. Heinen, H.J.; Meier, S.; Vogt, H.; Wechsung, R. Int. J. Mass Spectrom. Ion Phys. (1983) 47, 19-22.

43. Heinen, H.J.; Meier, S.; Vogt, H. Spr. Ser. Chem. Phys. (1983) 25, 229-234.

44. Feigle, P.; Schueler, B.; Hillenkamp, F. Int. J. Mass Spectrom. Ion Phys. (1983) 47, 15-18.

45. Dhamelincourt, P. In "Microbeam Analysis"; Newbury, D.E., Ed.; San Francisco Press: San Francisco, 1979. Pp. 155-164.

46. Seydel, U.; Lindner, B. Spr. Ser. Chem. Phys. (1983) 25 240-244.

47. Day, R.J.; Unger, S.E.; Cooks, R.G. Anal. Chem. (1980) 52, 557A-572A.

48. Unger, S.E.; Vincze, A.; Cooks, R.G.; Chrisman, R.; Rothman, L.D. Anal. Chem. (1981) 53, 976-981.

49. Cooks, R.G.; Busch, K.L. J. Chem. Educ. (1982) 59, 926-933.

50. Busch, K.L.; Hsu, B.H.; Xie, Y.; Cooks, R.G. Anal. Chem (1983) 55, 1157-1160.

51. Cooks, R.G.; Busch, K.L.; Glish, G.L. Science (1983) 222, 273-291.

52. Kondrat, R.W.; Cooks, R.G. Anal. Chem. (1978) 50, 81A-92A.

53. McLafferty, F.W.; Bockoff, F.M. Anal. Chem. (1978) 50, 69-76.

54. Yost, R.A.; Enke, C.G. Anal. Chem. (1979) 51, 1251A-1264A.

55. McLafferty, F.W., Ed.; "Tandem Mass Spectrometry"; John Wiley and Sons, Inc.: New York, 1983.

56. White, R.L.; Wilkens, C.L. Anal. Chem. (1982) 54, 2211-2215.

57. Perchalski, R.J.; Yost, R.A.; Wilder, B.J. Anal. Chem. (1982) 54, 1466-1471.

58. Zackett, D.; Schoen, A.E.; Cooks, R.G.; Hemberger, P.H. J. Am. Chem. Soc. (1981) 103, 1295-1297.

59. Davis, D.V.; Cooks, R.G.; Meyer, B.N.; McLaughlin, J.L. Anal. Chem. (1983) 55, 1302-1305.

60. Cotter, R.J. Anal. Chem. (1980) 52, 1767-1770.

61. Ready, J.F. "Effects of High Power Laser Radiation"; Academic Press: New York, 1971. Pp. 157-161.

62. Ready, J.F. "Effects of High Power Laser Radiation"; Academic Press: New York, 1971. P. 82.

63. Ready, J.F. "Effects of High Power Laser Radiation"; Academic Press: New York, 1971. Pp. 67-125.

64. van der Peyl, G.J.Q.; Haverkamp, J.Q.; Kistemaker, P.G. Int. J. Mass Spectrom. Ion Phys. (1982) 42, 125-141.

65. Lincoln, K.A.; Covington, M.A. Int. J. Mass Spectrom. Ion Phys. (1975) 16, 191-208.

66. Lincoln, K.A. Int. J. Mass Spectrom. Ion Phys. (1974) 13, 45-53.

67. Knox, B.E. Dyn. Mass Spectrom. (1971) 2, 61-96.

68. Ready, J.F. "Effects of High Power Laser Radiation"; Academic Press: New York, 1971. Pp. 95-114.

69. Kovalev, I.D.; Maksimov, G.A.; Suchkov, A.I.; Larin, N.V. Int. J. Mass Spectrom. Ion Phys. (1978) 27, 101-137.

70. Furstenau, N. Fresenius' Z. Anal. Chem. (1981) 308, 201-205.

71. Scott, R.H.; Strasheim, A. Spectrochim. Acta (1970) 25b, 311-332.

72. Ready, J.F. "Effects of High Power Laser Radiation"; Academic Press: New York, 1971. P. 154.

73. Ready, J.F. "Effects of High Power Laser Radiation"; Academic Press: New York, 1971. Pp. 140-161.

74. Inghram, M.G.; Chupka, W.A. Rev. Sci. Instrum. (1953) 24, 518-520.

75. Datz, S.; Taylor, E.H. J. Phys. Chem. (1956) 25, 389-394.

76. Cotter, R.J. Anal. Chem. (1984) 56, 485A-504A.

77. Cotter, R.J.; Tabet, J.-C. Am. Biotechnol. Lab. (1984) 2, 10-20.

78. Ready, J.F. "Effects of High Power Laser Radiation"; Academic Press: New York, 1971, P. 147.

79. Bernal, E.; Ready, J.F.; Allen, F.J. J. Appl. Phys. (1974) 45, 2980-2986.

80. Hardin, E.D.; Vestal, M.L. Anal. Chem. (1981) 53, 1492-1497.

81. van der Peyl, G.J.Q.; van der Zande, W.J.; Bederski, K.; Boerboom, A.J.H.; Kistemaker, P.G. Int. J. Mass Spectrom. Ion Phys. (1983) 47, 7-10.

82. Van Breeman, R.B.; Snow, M.; Cotter, R.J. Int. J. Mass Spectrom. Ion Phys. (1983) 49, 35-50.

83. Tabet, J.-C.; Cotter, R.J. Int. J. Mass Spectrom. Ion Phys. (1983) 54, 151-158.

84. Cotter, R.J.; Tabet, J.-C. Int. J. Mass Spectrom. Ion Phys. (1983) 53, 151-166.

85. Cotter, R.J.; Snow, M.; Colvin, M. Spr. Ser. Chem. Phys. (1983) 25, 206-210.

86. Vastola, F.J.; Pirone, A.J. Adv. Mass Spectrom. (1968) 4, 107-111.

87. Vastola, F.J.; Mumma, R.D.; Pirone, A.J. Org. Mass Spectrom. (1970) 3, 101-104.

88. MacFarlane, R.D.; Torgerson, D.F. Science (1976) 191, 920-925.

89. Posthumus, M.A.; Kistemaker, P.G.; Meuzelaar, H.L.C.; Ten Noever de Brauw, M.C. Anal. Chem (1978) 50, 985-991.

90. Hunt, D.F.; Shabanowitz, J.; Botz, F.K.; Brent, D.A. Anal. Chem. (1977) 49, 1160-1163.

91. Cotter, R.J.; Fenselau, C. Biomed. Mass Spectrom. (1979) 6, 287-293.

92. Stoll, R.; Rollgen, F.W. Org. Mass Spectrom. (1979) 14, 642-645.

93. van der Peyl, G.J.Q.; Isa, K.; Haverkamp, J.; Kistemaker, P.G. Org. Mass Spectrom. (1981) 16, 416-420.

94. van der Peyl, G.J.Q.; Isa, K.; Haverkamp, J.; Kistemaker, P.G. Nucl. Inst. Meth. Phys. Res. (1982) 198, 125-130.

95. van der Peyl, G.J.Q.; Isa, K.; Haverkamp, J.; Kistemaker, P.G. Int. J. Mass Spectrom. Ion Phys. (1983) 47, 11-14.

96. Stoll, R.; Rollgen, F.W. Org. Mass Spectrom. (1981) 16, 72-75.

97. Stoll, R.; Rollgen, F.W. Z. Naturforsch. (1982) 37A, 9-14.

98. Heinen, H.J. Int. J. Mass Spectrom. Ion Phys. (1981) 38, 309-322.

99. Hillenkamp, F. Int. J. Mass Spectrom. Ion Phys. (1982) 45, 305-313.

100. Hillenkamp, F. Spr. Ser. Chem. Phys. (1983) 25, 190-205.

101. Cooks, R.G.; Busch, K.L. Int. J. Mass Spectrom. Ion Phys. (1983) 53, 111-124.

102. Cotter, R.J. Anal. Chem. (1981) 53, 719-720.

103. Heresch, F.; Schmid, E.R.; Huber, J.F.K. Anal. Chem. (1980) 52, 1803-1807.

104. McCrery, D.A.; Ledford, E.B.; Gross, M.L. Anal. Chem. (1982) 54, 1435-1437.

105. Dow, R.S.; Fernandez-Guardiola, A.; Manni, E. Electroenceph. Clin. Neurophysiol. (1962) 14, 399-407.

106. Palkovits, M.; Brownstein, M.J. In "Brain Microdissection Techniques"; Cuello, A.C., Ed.; John Wiley and Sons, Inc.: New York, 1983. Pp. 1-36.

107. Slayback, J.R.B.; Story, M.S. Ind. Res. Dev. (1981) 23(2), 128-134.

108. Kirby, H.; Sokolow, S.; Steiner, U. In "Tandem Mass Spectrometry"; McLafferty, F.W., Ed.; John Wiley and Sons, Inc.: New York, 1983. Pp. 337-352.

109. Yost, R.A.; Enke, C.G.; McGilvery, D.C.; Smith, D.; Morrison, J.D. Int. J. Mass Spectrom. Ion Phys. (1979) 30, 127-136.

110. Cotter, R.J. Anal. Chem. (1979) 51, 317-318.

111. Perchalski, R.J.; Bruni, J.: Wilder, B.J.; Willmore, L.J. J. Chromatogr. (1979) 163, 187-193.

112. Vanderborgh, N.E.; Roland-Jones, C.E. Anal. Chem. (1983) 55, 527-532.

113. Dawson, P.H.; Fulford, J.E. Int. J. Mass Spectrom. Ion Phys. (1982) 42, 194-211.

114. Dawson, P.H. In "Quadrupole Mass Spectrometry and Its Applications"; P.H. Dawson, Ed.; Elsevier: Amsterdam, 1976. Pp. 23-24.

115. Perchalski, R.J.; Yost, R.A.; Wilder, B.J. Anal. Chem. (1983) 55, 2002-2006.

116. Baldwin, M.A.; McLafferty, F.W. Org. Mass Spectrom. (1973) 7, 1353-1356.

117. Hansen, G.; Munson, B. Anal. Chem. (1978) 50, 1130-1134.

118. Rapp, U.; Dielmann, G.; Games, D.E.; Gower, J.L.; Lewis, E. Adv. Mass Spectrom. (1980) 88, 1660-1668.

119. Reinhold, V.N.; Carr, S.A. Anal. Chem. (1982) 54, 499-503.

120. Cotter, R.J. Anal. Chem. (1980) 52, 1589A-1606A.

121. Fentiman, A.F. Jr.; Foltz, R.L.; Kinzer, G.W. Anal. Chem. (1973) 45, 580-583.

122. Plattner, R.D.; Yates, S.H.; Porter, J.K. J. Agric. Food Chem. (1983) 31, 785-789.

123. Fenimore, D.C.; Whiteford, J.H.; Davis, C.M.; Zlatkis, A. J. Chromatogr. (1977) 140 9.

124. Benninghoven, A. Int. J. Mass Spectrom. Ion Phys. (1983) 53, 85-99.

125. Oehme, M. Anal. Chem. (1982) 55, 2290-2295.

126. Balasanmugam, K.; Hercules, D.M. Anal. Chem. (1983) 55, 145-146.

127. Verbueken, A.H.; VanGrieken, R.E.; Paulus, G.J.; Bruijn, W.C. Anal. Chem. (1984) 56, 1362-1370.

128. Yost, R.A.: Perchalski, R.J.: Brotherton, H.O.; Johnson, J.V.; Budd, M.B. Talanta (1984) 31, 929-935.

129. Stoll, R.G.; Harvan, D.J.; Cole, R.B.; Haas, J.R. (1984) Paper presented at the 32nd Conference on Mass Spectrometry and Allied Topics, San Antonio, May 27-June 1. Pp. 838-839.

130. Kelner, L.; Fales, H.M.; Markey, S.P. (1984) Paper presented at the 32nd Conference on Mass Spectrometry and Allied Topics, San Antonio, May 27-June 1. Pp. 850-851.

131. Busch, K.L.; Cooks, R.J. Science (1982) 218, 247-254.

132. Busch, K.L.; Unger, S.E.; Vincze, A.; Cooks, R.G.; Keough, T. J. Am. Chem. Soc. (1982) 104, 1507-1511.

133. Magee, C.W. Int. J. Mass Spectrom. Ion Phys. (1983) 49, 211-221.

134. Laser Focus Buyer's Guide (1984), 19th Ed., PennWell Publishing Co., Littleton, MA.

135. Dutta, P.K.; Talmi, Y. Anal. Chim. Acta (1981) 132, 111-118.

136. Benyon, J.H.; Cooks, R.G.; Amy, J.W.; Baitinger, W.E.; Ridley, T.Y. Anal. Chem. (1973) 45, 1023A-1031A.

137. Gross, M.L.; Russell, D.H. In "Tandem Mass Spectrometry"; F.W. McLafferty, Ed.; John Wiley and Sons, Inc.; New York, 1983. Chapter 12.

138. Todd, P.J.; McGilvery, D.C., Baldwin, M.A.; McLafferty, F.W. In "Tandem Mass Spectrometry"; F.W. McLafferty, Ed., John Wiley and Sons, Inc.: New York, 1983. Chapter 13.

139. Ciupek, J.D.; O'Lear, J.R.; Cooks, R.G.; Dobberstein, P.; Schoen, A.E. Paper presented at the 32nd Conference on Mass Spectrometry and Allied Topics, San Antonio, May 27-June 1, 1984. Pp. 378-379.

140. Bricker, D.L.; Adams, T.A., Jr.; Russell, D.H. Anal. Chem. (1983) 55, 2417-2418.

141. Stults, J.T.; Enke. C.G.; Holland, J.F. Anal. Chem. (1983) 55, 1323-1330.

142. Holland, J.F.; Enke, C.G.; Allison, J.; Stults, J.T.; Pinkston, J.D.; Newcome, B.; Watson, J.T. Anal. Chem. (1983) 55, 997A-1012A.

143. Glish, G.L.; Goeringer, D.E. Anal. Chem. (1984) 56, 2291-2294.

144. Hein, R.E.; Cody, R.B. Paper presented at the 31st Conference on Mass Spectrometry and Allied Topics, Boston, May 9-13, 1983. P. 800.

145. McIver, R.T.; Hunter, R.L.; Story, M.; Syka, J.; Labunsky, M. Paper presented at the 31st Conference on Mass Spectrometry and Allied Topics, Boston, May 9-13, 1983. Pp. 44-45.

146. Armitage, M.A.; Fulford, J.E.; Hughes, R.J.; March, R.E.; Mather, R.E.; Waldren, R.M.; Todd, J.F.J. Adv. Mass Spectrom. (1980) 8B, 1754-1763.

147. Stafford, G.C.; Kelley, P.E.; Reynolds, W.E.; Syka, J.E. Paper presented at the 31st Conference on Mass Spectrometry and Allied Topics, Boston, May 9-13, 1983. Pp. 48-49.

148. Glish, G.L. Paper presented at the 31st Conference on Mass Spectrometry and Allied Topics, Boston, May 9-13, 1983. Pp. 191-192.

BIOGRAPHICAL SKETCH

Robert John Perchalski was born in Collingdale, Pennsylvania on February 8, 1948. He graduated from Central Catholic High School in Melbourne, Florida, in June, 1965, and entered the University of Florida in September. He received the Bachelor of Science degree with a major in chemistry in June, 1969. In the fall of 1969, he entered the University of Florida graduate school and completed the course work for the Ph.D. in analytical chemistry in June, 1971. At that time, he was commissioned as a 2nd Lieutenant in the U.S. Army and served three months on active duty at Ft. Benning, Georgia.

Upon release from the Army, he accepted a position as a laboratory technologist at the University of Florida, College of Pharmacy. In August, 1972, he accepted the position of Research Chemist in the Medical Research Service at the Gainesville, Veterans Administration Medical Center. Until December, 1984, he directed the analytical research program for the Neurology Service for the investigation of the pharmacology and clinical effectiveness of new and established antiepileptic drugs. A large part of this effort involved the development of reliable methods of determining concentrations of these drugs, their metabolites, and neurologically important biomolecules in biological samples.

In March, 1975, he received the Master of Science degree in analytical chemistry from the University of Florida. In September,

1980, he returned to the University of Florida to complete work on the Ph.D. in analytical chemistry. Dr. Perchalski is now working as Head of Analytical Research and Development for Pharmatec, Inc., Alachua, Florida, a research firm specializing in the development of soft drugs and drug delivery systems, with particular emphasis on targeting drugs to specific organs. He is also Adjunct Assistant Professor in the Department of Medicinal Chemistry, College of Pharmacy, University of Florida. He has authored and co-authored a number of articles and chapters dealing with the determination of drugs in body fluids and tissues, and the pharmacology of antiepileptic drugs.

He is married and has four children.

I certify that I have read this study and that in my opinion it conforms to acceptable standards of scholarly presentation and is fully adequate, in scope and quality, as a dissertation for the degree of Doctor of Philosophy.

Richard A. Yost, Chairman
Associate Professor of Chemistry

I certify that I have read this study and that in my opinion it conforms to acceptable standards of scholarly presentation and is fully adequate, in scope and quality, as a dissertation for the degree of Doctor of Philosophy.

James D. Winefordner
Graduate Research Professor
of Chemistry

I certify that I have read this study and that in my opinion it conforms to acceptable standards of scholarly presentation and is fully adequate, in scope and quality, as a dissertation for the degree of Doctor of Philosophy.

John R. Eyler
Associate Professor of Chemistry

I certify that I have read this study and that in my opinion it conforms to acceptable standards of scholarly presentation and is fully adequate, in scope and quality, as a dissertation for the degree of Doctor of Philosophy.

John G.Dorsey
Assistant Professor of Chemistry

I certify that I have read this study and that in my opinion it conforms to acceptable standards of scholarly presentation and is fully adequate, in scope and quality, as a dissertation for the degree of Doctor of Philosophy.

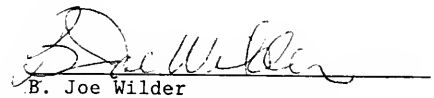

B. Joe Wilder
Professor of Neuroscience

This dissertation was submitted to the Graduate Faculty of the Department of Chemistry in the College of Liberal Arts and Sciences and to the Graduate School, and was accepted as partial fulfillment of the requirements for the degree of Doctor of Philosophy.

May, 1985

Donald R. Price
Dean for Graduate Studies
and Research